The Effects of Waves and Tidal Inundation on Sediment Deposition and Flux across a Bay-Marsh Boundary

Melissa S. Duvall
Annapolis, Maryland

B.S., Environmental Science and Policy, University of Maryland, 2010

A thesis presented to the Graduate Faculty of the
University of Virginia in Candidacy for the degree of
Master of Science

Department of Environmental Sciences

University of Virginia
August, 2014

Abstract

Sediment deposition processes acting on salt marshes adjacent to larger bodies of water, such as bays, differ from the processes acting in tidal creek marshes, but have not been well characterized by previous research. This difference in interface alters the primary controls on suspended sediment concentration (SSC), an indication of sediment availability, as well as sediment flux to and deposition on the marsh. This study was conducted along the boundary between a shallow, microtidal coastal lagoon, Hog Island Bay, and a microtidal salt marsh on the edge of Chimney Pole, a marsh island on the Eastern Shore of Virginia. This research sought to characterize the hydrologic regime at the bay-marsh boundary, determine changes in SSC due to changing wave-generated bottom shear stress, establish the effect of tides and currents on sediment transport to the marsh, and estimate changes in bottom shear stress due to relative sea level rise (RSLR) and storm surge.

Two primary differences in bay and tidal creek environments are the presence of waves and unconstrained flow. The results from this study indicate a strong correlation between wind direction and wave formation, whereby the largest waves formed when westerly winds (i.e. the direction of longest fetch) blew across Hog Island Bay at relatively high speeds (> 8 m s^{-1}). Maximum wave-generated bed shear stress on the tidal flat during times of strong westerly winds occurred at water elevations near the marsh platform height (~0.5 m above MSL), above which shear stress declined. Our findings showed that waves primarily force SSC, but the impact of wave events on sediment deposition at Chimney Pole is limited by the fact that these events typically occur when the marsh is not flooded. When the marsh is

flooded, wave height is rapidly diminished as waves propagate across the bay-marsh boundary due to vegetation and shallow water depths. Modeling changes in wave-induced bed shear stress with depth revealed that shear stress is likely approaching a maximum given present-day sea level, wind and tidal conditions. If the marsh keeps pace with RSLR, sediment deposition will be maximized by present-day conditions or slow RSLR. However, if the marsh elevation remains constant, potential deposition may increase with increasing RSLR and storm surge.

Winds also forced currents, whereby weaker, southerly winds were associated with an alternating northward flood, southward ebb current pattern, whereas strong, northerly winds pushed currents southward regardless of tidal phase. Overall, the unconstrained flow present in Hog Island Bay limited sediment deposition on Chimney Pole, because currents carried sediment towards, but also away from, the marsh during flooding conditions. High bed shear stress likely prevented sediment transported onto the marsh from depositing near the marsh edge; therefore it was deposited further into the marsh interior. Calculated (0.025 g cm^{-2}) and measured (0.028 g cm^{-2}) deposition for the March 2014 deployment showed that the marsh is accreting further away from the edge. The results indicated that bed shear stress was sufficient to remobilize sediment after it deposited, however grain size analysis revealed that this process is likely limited by bed cohesiveness at the site.

Acknowledgements

Thank you to my advisor, Pat Wiberg, and committee members, Matt Kirwan and Matt Reidenbach, for the advice and support given to me throughout my time at UVA; the Reidenbach lab for sharing instruments and wind data needed to complete this project; the boat drivers at the shore (David, Pat, and Chris) for braving the winter chill on the ride out to Chimney Pole; Ross Timmerman for instrumentation troubleshooting; Alia Al-Haj for PSA help; Amanda Timmerman for assisting with field work; grad students for their friendship and the memories; the NSF Long-Term Ecological Research Program at the Virginia Coast Reserve and the UVA Department of Environmental Sciences for financial support; God; as well as my family and Naveed for their love and encouragement in all my endeavors.

Table of Contents

List of Figures

List of Tables

Chapter 1: Introduction

Intertidal salt marshes are among the world's most biologically productive and economically valuable ecosystems (Day et al. 1989). Marshes sequester carbon, improve water quality, and protect highly populated coastal land from storm surge and erosion (Day et al. 1989). Tidal marsh loss has accelerated in recent decades on a global scale, resulting in estimated losses between a quarter to a half of total marsh area (WHO 2005). Whether marshes survive SLR depends on their ability to build elevation through the accumulation of organic material and deposition of mineral sediment (Friedrichs & Perry 2001).

Suspended sediment concentration (SSC), a common proxy for sediment availability, strongly influences marsh accretion rates (Kirwan et al. 2010). In the Virginia Coast Reserve (VCR), a barrier-lagoon-marsh system on the Atlantic side of the lower Delmarva Peninsula, creeks supply only small amounts of sediment into the system (Lawson et al. 2007). Therefore, wind waves primarily determine SSC by resuspending sediment from bay bottoms (Lawson et al. 2007) and eroding marsh edges (McLoughlin et al. 2014). Field measurements indicate significant spatial and temporal variations in SSC in shallow bays and tidal creeks (Lawson et al. 2007; Christiansen et al. 2000), driven in part by storm surge and episodically high wave conditions.

Transport of suspended sediment from bays and creeks onto marsh surfaces depends upon current magnitude and direction, and water surface elevation. Sediment deposition on marsh surfaces depends on SSC, inundation time, and sediment settling rates, as well as the effect of vegetation on flow velocity,

turbulence, and wave dissipation. This research seeks to better understand the factors influencing sediment exchange across bay-marsh boundaries and deposition rates on marsh surfaces. Through better understanding these relationships, we will improve our ability to model and predict marsh vulnerability to future increases in sea level and storminess.

1.1. Objectives

The goal of this research is to examine temporal changes in SSC over tidal flats as well as the conditions under which this sediment is deposited on bordering marsh surfaces. Marsh boundaries that differ in edge properties, such as long-term erosion rates and scarp profile, are investigated. The four overarching questions that this research addresses are:

- What is the effect of wind on wave formation and current magnitude and direction on shallow tidal flats and bordering salt marshes? (Ch. 2)
- What changes in SSC occur over tidal flats due to changing wave height and water depth during a tidal cycle? (Ch. 3)
- What is the effect of tides and currents on sediment transport from a bay to an adjacent marsh surface? (Ch. 3)
- What impact will 21st century SLR, stronger coastal storms, and accompanying changes in wave conditions have on mineral sediment deposition on marsh islands? (Ch. 4)

These objectives are addressed in the chapters listed.

1.2 Study Motivation

The long-term stability of salt marshes depends on the interaction between primary production, sediment accretion, land elevation, and sea level (Morris et al. 2002). Marshes rely on macrophytes to maintain their elevation by accumulating organic material and trapping mineral sediment. The volume of sediment trapped or deposited on the marsh surface depends partly on the amount of sediment in the water column. Threshold rates of relative sea level rise (RSLR) that trigger marsh drowning depend strongly on SSC (Kirwan et al. 2010). Therefore, it is important to understand both the amount of sediment entering the water column, its source, and the trajectory of that sediment once it is suspended.

The previous work of Christiansen et al. (2000), who characterized the factors influencing sediment deposition in a relatively low-energy tidal creek marsh (fig 1.1), provides the primary motivation for this project. Rather than focusing on tidal creek marshes, the overarching concern of this project is to understand depositional processes at a bay-marsh boundary.

In tidal creek marshes, taller and thicker vegetation along the creek bank slows flow velocities (<1 cm s^{-1}), resulting in maximum deposition at the marsh edge. Additionally, tidal creeks constrain water flow inside the channel at elevations below the marsh surface. As depth increases, water overtops the channel bank, resulting in an outward flow of water, nutrients, and sediment from the creek to the marsh surface.

Along marsh-bay boundaries, stunted vegetation at the edge is less effective at slowing velocity (fig 1.2). Additionally, waves generated in the bay episodically

increase bed shear stress and SSC on the tidal flats bordering the marsh. Waves also contribute to lateral erosion of the marsh edge and vertical erosion of the marsh surface close to the edge. Furthermore, complex patterns of tidal and wind-driven flow on the flats and marsh generate uncertainty about whether resuspended sediment on the flats is carried onto the marsh platform or out into the bay. This research seeks to better characterize sediment availability and delivery to marshes with open bay boundaries, including the wind, wave, and current conditions that maximize the flux of sediment from the bay onto the marsh.

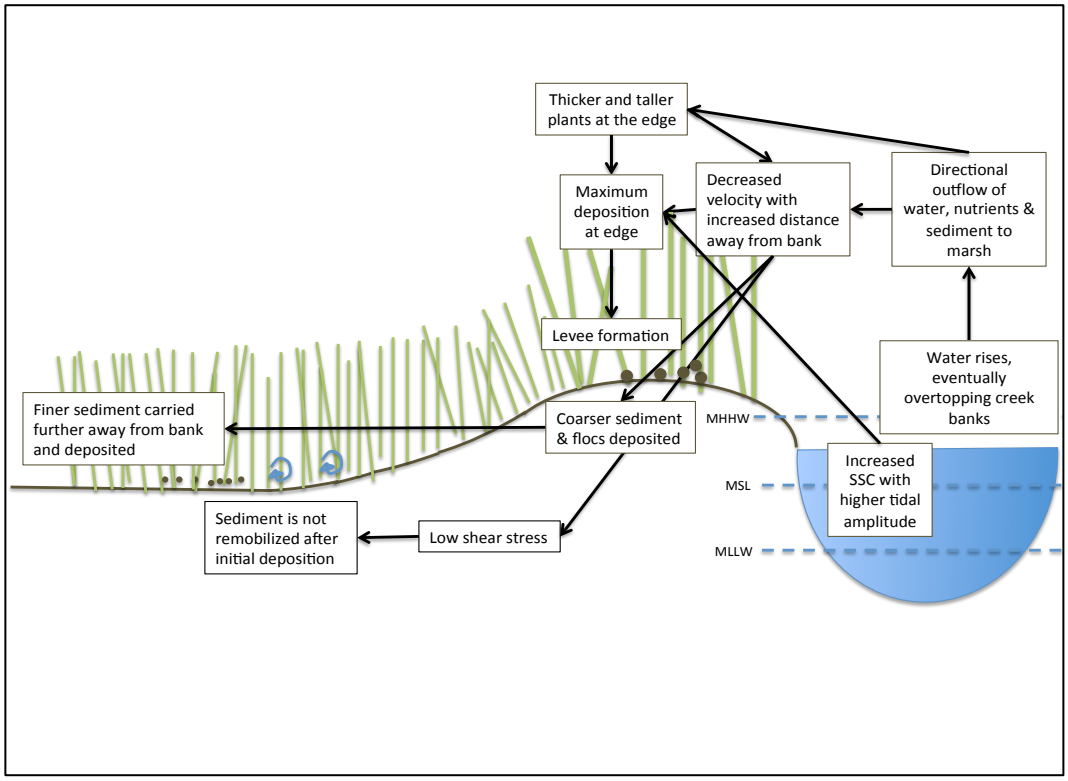

Figure 1.1: Conceptual model of processes affecting inorganic sediment deposition on a tidal creek marsh.

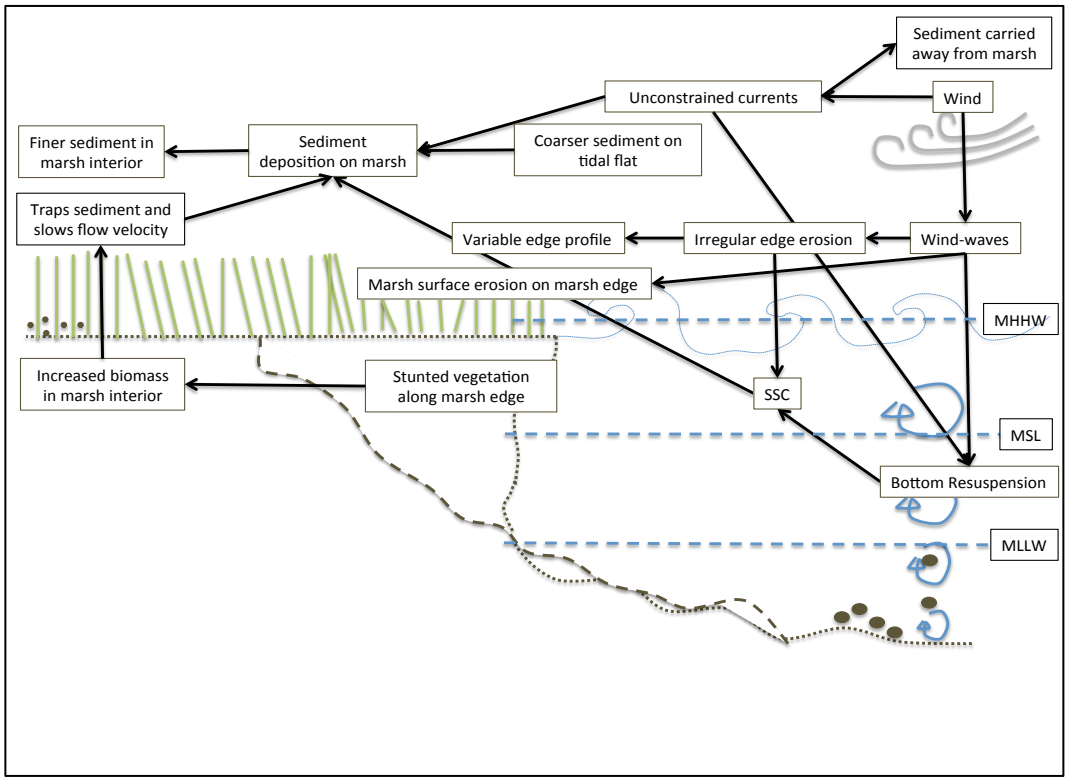

Figure 1.2: Conceptual model of processes affecting inorganic sediment deposition on a marsh island.

1.3 Background

Wind Waves

The presence of wind-generated waves on tidal flats bordering bay-marsh boundaries is the most important difference affecting the sediment dynamics of these types of marsh edges compared to tidal creek-marsh edges. Wind wave formation within shallow bays relies on energy transfer from the wind to the water surface of the bay; waves do not propagate into the coastal bays from the ocean. Wave formation depends on wind characteristics, such as duration, direction, and velocity, along with water depth and fetch (Mariotti et al. 2010). Higher wind velocities and longer wind durations typically generate larger waves. Wind direction

determines fetch, or the unobstructed distance over the water that the wind blows. Fetch determines the actual amount of energy that can be transferred from the wind to the water surface. Additionally, water depth directly controls maximum possible wave height. Thus, increasing water depth, due to tides, storm surge, or RSLR, allows larger, higher energy waves to form. Furthermore, depth indirectly controls wave height through fetch, because when dry periphery areas are wetted the surface area over which the wind can blow increases (Mariotti et al. 2010; Fagherazzi & Wiberg 2009).

Currents

Tidal currents, which may be enhanced by wind forcing and wind waves, transport sediment from the tidal flat to the marsh or out into the bay, thus further influencing entrainment and depositional processes (Carniello et al. 2012). The trajectory of suspended sediment in shallow lagoon systems is variable. Factors influencing currents include bay bottom and marsh edge morphology, as well as subtidal and intertidal vegetation. Although currents also generate bed shear stress, wave-induced bottom shear stress is primarily responsible for sediment resuspension over tidal flats (Lawson et al. 2007; Carniello et al. 2012).

Suspended Sediment Concentration

Sediment is mobilized when the bottom shear stress imparted by hydrodynamic forcing due to tidal currents, wind-induced currents, and wind-induced waves, exceeds the critical shear stress for erosion. Critical shear stress

required for erosion depends upon sediment composition and degree of bed consolidation (Mehta 1988). Critical shear stress is positively correlated with grain size, thus smaller grains are preferentially mobilized relative to larger grains, although the effects of cohesion can complicate this in muddy sediment. Sit and clay-size sediment goes directly into suspension once mobilized, therefore the threshold of motion corresponds to the threshold for suspension. Suspended sediment concentration (SSC) increases with increasing shear stress provided sediment is not supply limited (Rubin & Topping 2001), and typically decreases with height above the sediment bed, such that near-bed concentrations may be 2 or 3 orders of magnitude greater than concentrations near the surface (Mehta 1988). Additionally, Lawson et al. (2007) found a positive correlation between SSC and wind speed when winds exceeded 8 m s^{-1} in Hog Island Bay.

Shear Stress on Tidal Flats

Internal resuspension (Lawson et al. 2007) and marsh edge erosion (Day et al. 1998; McLoughlin et al. 2014) contribute to SSC within the bays and tidal creeks of the VCR. The amount of material removed from edges and tidal flats is a function of the shear stress applied. Wind waves and currents (wind-driven and tidal) determine shear stress distribution on tidal flats (Fagherazzi & Wiberg 2009; Carniello et al. 2011). The combination of wave and current stresses enhances the actual bed shear stress beyond the sum of both factors (Mariotti et al. 2010), due to the interaction between wave and current boundary layers (Carniello et al. 2011). In general, tides generate insufficient bed shear stresses to resuspend sediment, such

that most resuspension occurs during wind events that produce relatively large surface waves, wind-driven currents, and storm surge (Lawson et al. 2007). Wave-generated bed shear stress is a function of water depth as well as wave height and period. For given wave conditions, as water depth increases, wave-generated shear stress decreases. However, increasing water depth allows for the formation of larger waves in depth-limited systems like the bays of the VCR. Therefore, the relationship between increasing water depth and bed shear stress is not straightforward (Fagherazzi & Wiberg 2009).

Bottom shear stresses are strongly influenced by the morphology of the intertidal landscape (Fagherazzi et al. 2006; Defina et al. 2007). Although wave height and fetch increase with water depth, greater depths can reduce the shear stress exerted on the bed by waves. Fagherazzi and Wiberg (2009) identified four bottom shear stress regimes acting on tidal flats that vary as a function of water depth, wave height, and fetch. At tidal elevations below Mean Lower Low Water (MLLW), increased fetch and wave height coincide with increased water depth. Since these forces counteract one another, bottom shear stress does not change significantly. As water rises from MLLW to Mean Sea Level (MSL) (i.e. common tidal flat elevation range), water depth reduces shear stress despite slight increases in wave height and fetch. The greatest average shear stress is associated with tide levels ranging from MSL to MHHW (i.e. common tidal salt marsh elevation range). This is because fetch increases due to marsh platform inundation, and wave height increases more quickly than depth. Finally, above MHHW, wave height increases

more slowly than water depth. Greater depths reduce the frictional force exerted by surface waves on the bottom, thus lowering shear stress.

Edge Erosion

Wind waves are the primary cause of lateral edge erosion along many marsh shorelines, including those within the VCR (Möller et al. 1996, 1999). Wave energy dissipation occurs when waves impinge upon the marsh boundary, thus scouring and eroding the edge (Tonelli et al. 2010). Erosion of marsh edges provides a potentially significant source of sediment for bays and marshes (Mariotti & Carr 2014). When previously intact sediment detaches from the edge due to wave scouring it can increase the amount of sediment in the water column. Currents transport this newly added sediment either back onto the marsh surface or further away to other areas within the bay.

Edge profile influences wave energy dissipation along a bay-marsh boundary. For a given tidal height, wave thrust is maximum along a vertical scarp and minimum along a terraced scarp (Tonelli et al. 2010). However, for a given scarp thrust varies based on water depth. For a vertical edge profile, as tide level increases, wave thrust increases to a maximum at an elevation just below the marsh platform height. For depths greater than the platform height (i.e. when the marsh is inundated), wave thrust rapidly decreases with increasing tidal elevation until a depth at which the waves and the bank do not interact (Tonelli et al. 2010). For terraced scarps, during lower tidal elevations most wave energy is dissipated on the lower terrace. During tidal elevations close to the platform elevation, energy is

distributed upon both upper and lower terraces (Tonelli et al. 2010). Therefore, at a given location along a marsh boundary, erosion potential varies from the bottom to the top of the edge.

Aboveground Marsh Vegetation

Aboveground marsh vegetation dissipates waves (Möller et al. 1999) and currents, as well as associated bed shear stresses. This allows for highly efficient inorganic sediment trapping (Mudd et al. 2010), while dampening the potential for sediment remobilization. The effectiveness of vegetation at attenuating energy depends upon both shoot density, which affects horizontal friction, as well as vegetation height, which influences the depth of the boundary layer (Möller 2006).

Sea Level Rise & Changing Waves

Increased depth due to RSLR and strengthened winds will likely result in larger wind waves. From 1985 to 2008, both mean and 90th percentile wind speeds in the North Atlantic increased by approximately 0.04 m s^{-1} each year (Young et al. 2011). Given the current rates, within the next half century both median and 90th percentile wind speed will increase by 2 m s^{-1}. Larger waves *may* increase the amount of sediment resuspended from tidal flats. On one hand, larger waves generate greater bottom shear stresses at any given water depth. On the other hand, deeper water decreases the bottom shear stress for a given wave height and period. In either case, increased accretion due to increased erosion and resuspension will only occur if currents transport sediment onto the marsh instead of along the marsh

edge or further out into the bay. This has not been accounted for in most marsh models, which may overestimate surface accretion rates on marshes bordering shallow bays.

In addition, larger waves may increase rates of lateral erosion. Edge erosion elevates sediment supply on the tidal flat, which may subsequently be transported back onto the marsh and increase surface accretion. This would create a stabilizing mechanism whereby enhanced edge erosion decreases the potential for surface drowning (Mariotti & Carr 2014). However, this mechanism relies on currents to carry sediment to the marsh platform, which is uncertain given the unconstrained flow environment present at marsh-bay boundaries.

1.4 Site Description

The study site is located along a section of the edge of Chimney Pole Marsh, a marsh island bordering Hog Island Bay, a shallow, microtidal coastal bay near the southern end of the Delmarva Peninsula (fig 1.3,1.4). Hog Island Bay is part of the VCR, a barrier-lagoon-marsh system extending over 100 km along the Atlantic side of the peninsula. The bay is approximately 100 km^2, and about 50% of the bay is less than 1 m deep at mean low tide. Tides within the bay are semidiurnal, with a mean tidal range of ~1.2 m (Oertel 2001, Lawson et al. 2007, Mariotti & Fagherazzi 2013). Additionally, RSLR along the Delmarva coast is approximately 4 mm yr^{-1} (Zervas 2001).

In the VCR, creeks input only small amounts of sediment into the system. Therefore, most sediment processes occur via redistribution of sediment by

currents between the shallow lagoons, barrier islands, and tidal salt marshes that comprise this ecosystem (Mariotti & Fagherazzi 2010). SSC does not exhibit periodicity on tidal time scales, signaling non-periodic forcing, such as wind-driven waves (Lawson et al. 2007). Due to the low population and human development both within and near the VCR, sediment processes are minimally impacted by human activity.

The elevation of the marsh surface at the study sites ranges from ~ 0.4 to 0.65 m above MSL (McLoughlin 2010). Surface elevation decreases from the marsh edge to the marsh interior, which slopes downward towards a large tidal channel behind the study site. Given its elevation, the study site does not flood every tidal cycle during neap tides. Long-term lateral edge erosion rates range from less than 0.5 m yr^{-1} to greater than 2 m yr^{-1} (McLoughlin et al. 2014). On the marsh, *Spartina alterniflora* biomass increases from the marsh edge to the interior. Additionally, McLoughlin (2010) found that median and mean grain sizes on Chimney Pole marsh decrease from the edge (49.4 μm and 64.3 μm, respectively) to the interior (42.8 μm and 55.7 μm). There is a high abundance of periwinkle snails (150-225 per m^2) and large, interconnected crab burrows in the study area, which reduce sediment shear strength, thereby promoting erosion of the marsh edge (McLoughlin 2010).

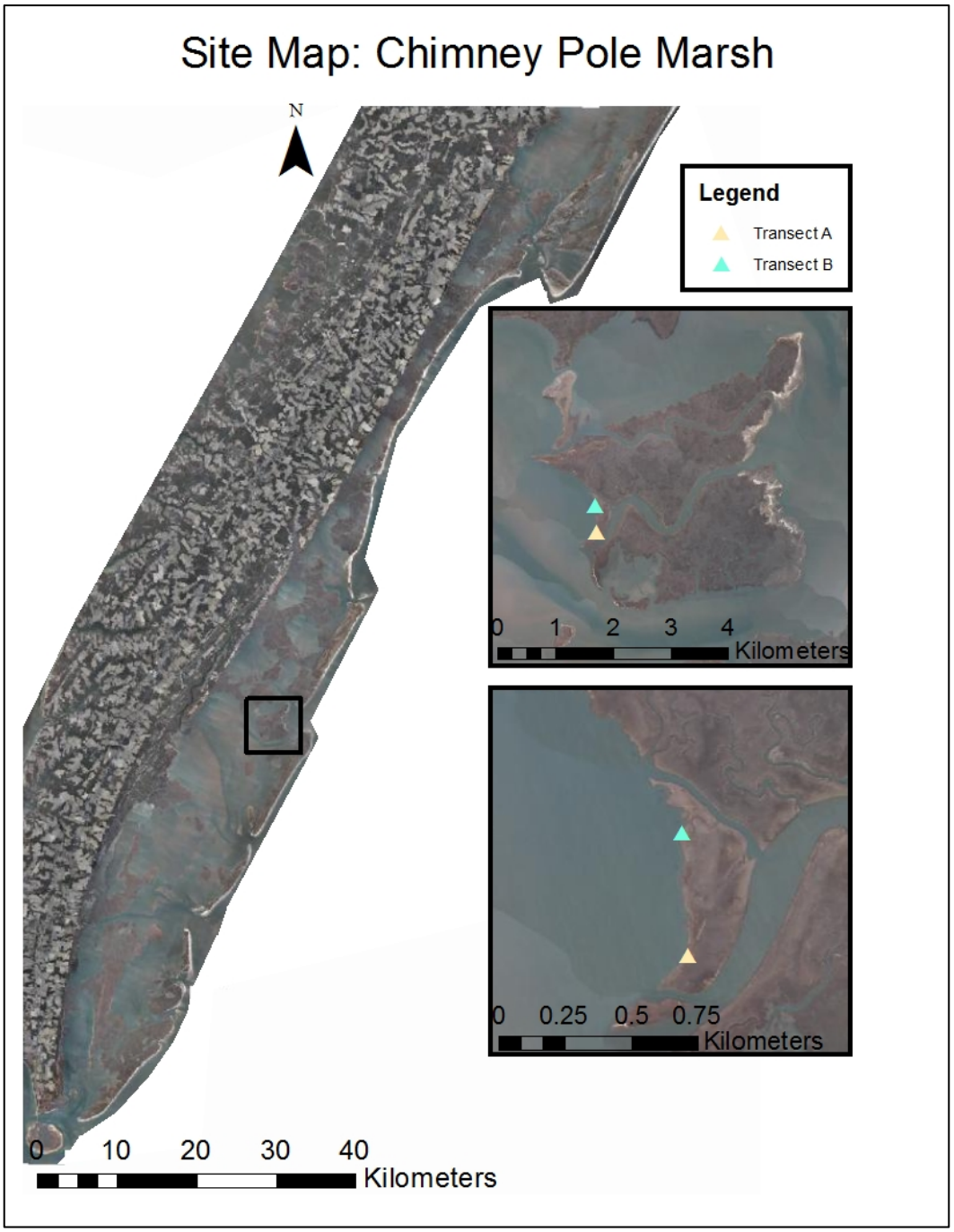

Figure 1.3: Maps showing location of Chimney Pole Marsh inside Hog Island Bay, as well as the location of transects A and B.

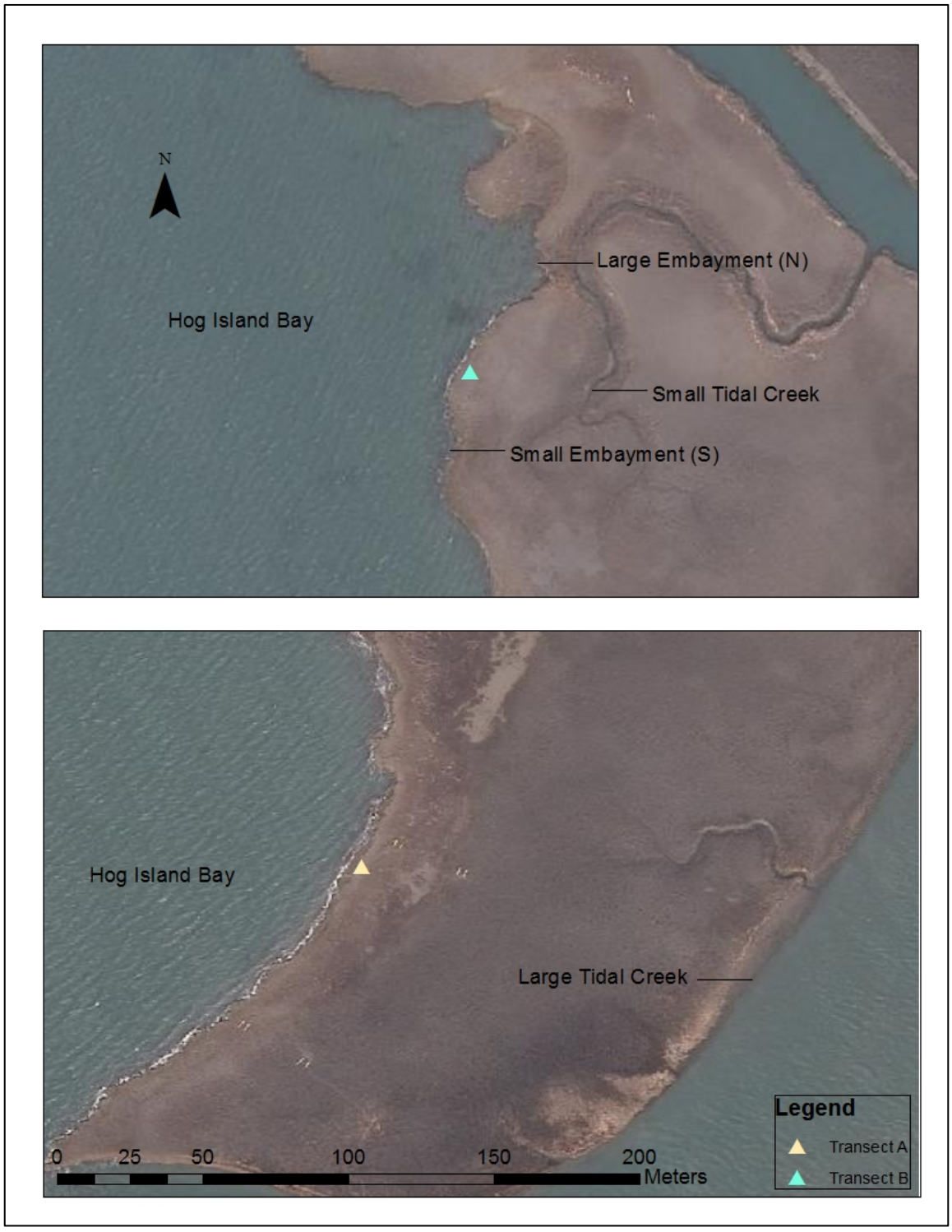

Figure 1.4: Zoomed-in site map of transect A and B detailing important landscape features.

1.5 Approach

For this study, we established two transects (A & B) that crossed variably eroding edges and extended from the lagoon to the marsh interior (~22 m long). Transect A crosses a gently sloped, slowing eroding (0.5 m yr^{-1}) edge, and transect B crosses a quickly eroding (1.5 to 2 m yr^{-1}) cliff scarp. At both transects, the edge orientation is northeast (~30°) to southwest (~210°)

Current, wave, and turbidity measurements were taken at 4 monitoring stations (i.e. lagoon, tidal flat, marsh edge, and marsh interior) that varied in distance from the bay-marsh boundary. Measurements were taken at either transect A or B, or at both transects, during 4 separate deployments (i.e. Feb-Mar 2013, May-Jun 2013, Nov-Dec 2013, and Mar 2014) (fig 1.5). Multiple deployments allowed us to capture seasonal trends in winds, hydrodynamics, and SSC. The first two deployments focused primarily on transect A, whereas the last two deployments focused on transect B. Simultaneous recording at both stations was limited by the number of instruments available for deployment. Additionally, along both transects, biomass was measured at 3 marsh stations (i.e. marsh edge, middle marsh, and marsh interior) and sediment characteristics at 4 stations (i.e. the 3 marsh stations and the tidal flat). Sediment deposition was also measured along transect B at the same 3 marsh stations.

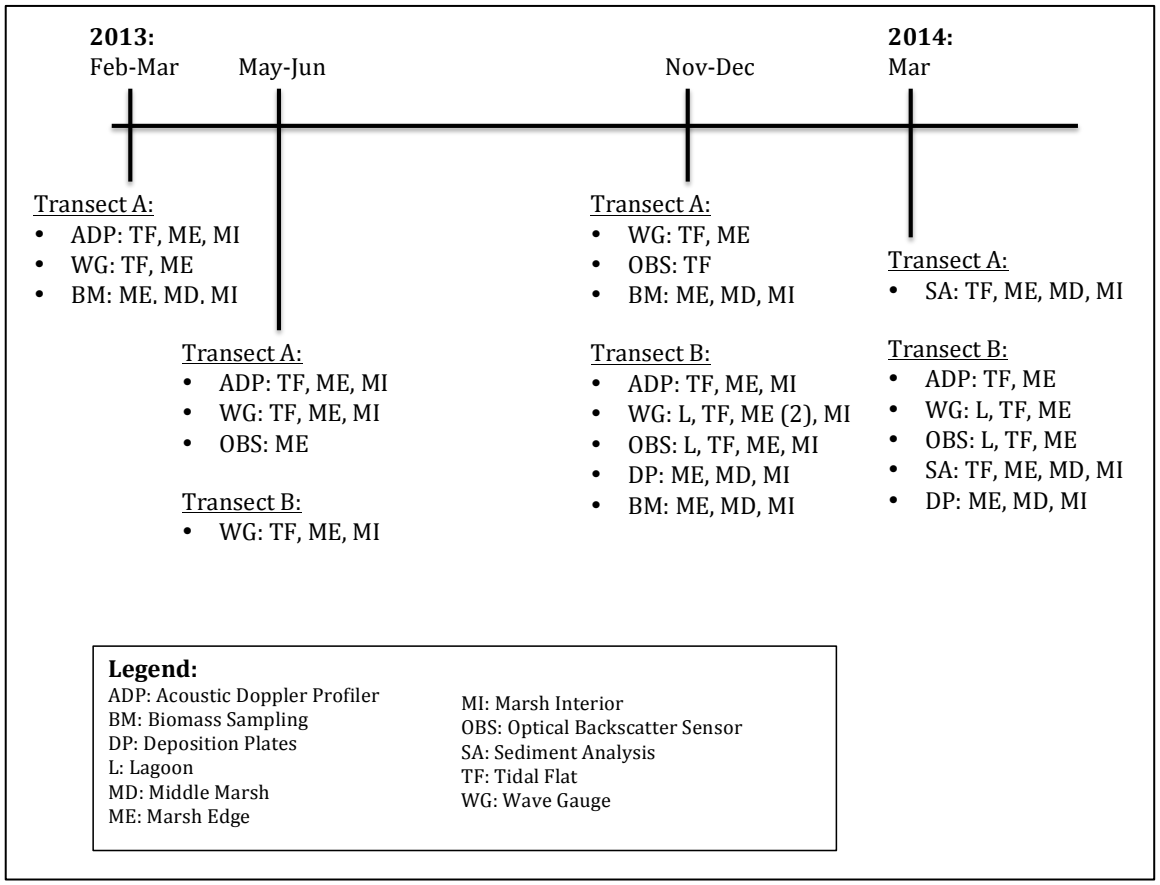

Figure 1.5: Deployment timeline detailing instrument type and location, as well as other measurements that were taken.

Chapter 2: Effect of Wind on Currents and Waves

2.1 Objectives

A main objective of this study is: What is the effect of wind on wave formation and current magnitude and direction on shallow tidal flats and bordering salt marshes? We compared wind speed and direction data from nearby meteorological stations to current and wave measurements taken along tidal flat-to-marsh transects during several deployments. This allowed us to determine a relationship between the variables, as well as identify any seasonal trends. In developing these relationships, we also investigated the influence of factors such as marsh edge morphology and bay bathymetry on current direction and wave propagation.

2.2 Methods—Data Collection and Analysis

Water depth, waves and currents were recorded at sites along Transect A and B (see fig 1.5) as described below. The sampling locations on each transect included the tidal flat, marsh edge, and marsh interior (table 2.1). Additional sites were sampled during some but not all deployments.

Transect	Station	Acronym	Latitude	Longitude	Elevation
A	Tidal Flat	TAF	37°27'46.73"N	75°42'58.44"W	-0.45 m
A	Edge	TAE	37°27'46.56"N	75°42'57.96"W	0.65 m
A	Interior	TAI	37°27'46.32"N	75°42'56.88"W	0.56 m
B	Tidal Flat	TBF	37°27'58.62"N	75°42'58.26"W	-0.5 m
B	Edge	TBE	37°27'58.56"N	75°42'58.11"W	0.55 m
B	Interior	TBI			0.40 m

Table 2.1: Latitude, longitude, and elevation for tidal flat, edge, and interior measuring stations at transects A and B. Elevations are given relative to MSL.

Water Depth & Storm Surge

Two types of instruments, acoustic Doppler profilers (ADPs) and wave-tide gauges, recorded depth at 15-minute intervals during each deployment. Depth was determined from pressure records that were corrected for fluctuations in atmospheric pressure and referenced to mean sea level (MSL) datum recorded at the Wachapreague, VA NOAA tide station. In addition, storm surge was estimated as the difference between predicted and observed tides recorded at the Wachapreague VA station.

Currents

Nortek AS Aquadopp© ADPs measured horizontal and vertical velocities (i.e. East, North, Up) every 15-minutes at specified intervals (e.g. 0.1m cells) above a given blanking distance. The blanking distance (e.g. 0.1 or 0.2m) is the distance above the ADP sensor head below which the instrument cannot reliably record. The ADPs also output signal strength, a proxy for SSC. As SSC increases, the strength of the acoustic return signal also increases.

We deployed ADPs for 3 to 4 weeks at different times of the year (see fig 1.5), which allowed us to identify seasonal trends. During a given deployment, multiple ADPs recorded along one transect, providing simultaneous current measurements on the tidal flat, at the marsh edge, and in the marsh interior. We attached the upward-looking ADPs to metal frames and used either stakes (marsh) or dive screws (tidal flat) to secure the frames to the ground.

The data collected from the instrument were analyzed in Matlab®. The data were filtered to remove false readings due to the reflection of the beam off the water surface during times of shallow water. Filtering the data by depth ensured that the height of the cells containing values did not exceed the water depth at a given time. On the marsh, readings were averaged over the whole current profile. On the tidal flat, measurements were averaged at various elevations to analyze currents both above and below the marsh platform elevation.

Wind Waves

RBR, Ltd. wave-tide gauges were deployed simultaneously with the ADPs (see fig 1.5). Pressure readings from the gauges were further processed with RBR's Ruskin software to obtain both depth and wave statistics, such as significant wave height and peak period. The gauges were programmed to sample at either 4 or 6 Hz every 15 minutes.

Multiple wave-tide gauges simultaneously recorded waves along a given transect, which allowed us to resolve wave propagation from the bay to the marsh interior. On the marsh, the gauges were attached to metal frames, which were staked to prevent the frames from moving. On the tidal flat and in the bay, the gauges were attached to 10 foot, 0.75 inch-diameter PVC pipes. The pipes were pushed approximately 3 feet into the ground until the bottom of the gauge was flush with the bed surface.

2.3 Methods—Calculations

Current-generated Bottom Shear Stress

After the data were processed, current-generated bed shear stress were calculated using the expression:

$$\tau_{curr} = C_d \rho u^2 \quad \text{(Eq. 2.1)}$$

where ρ=1020 kg/m^3 is water density, u is current speed and C_d is the drag coefficient. The drag coefficient was estimated as:

$$C_d = \frac{gn^2}{h^{\frac{1}{3}}} \quad \text{(Eq. 2.2)}$$

where n is the roughness coefficient

$$n = \left[\frac{2\sqrt{8g}}{h^{\frac{1}{6}}} \times log_{10}\left(\frac{h}{D_{84}}\right) + 1\right]^{-1} \quad \text{(Eq. 2.3)}$$

(Hornberger et al. 1998; Lawson et al. 2007), h is the water depth, g=9.81 m/s^2, and D_{84} is the 84th percentile of the grain size distribution.

Wave-generated Bottom Shear Stress

Wave-induced bottom orbital velocity was calculated using linear wave theory:

$$u_b = \frac{\pi H_s}{T sinh(kh)} \quad \text{(Eq. 2.4)}$$

and wave-generated bed shear stress was estimated as:

$$\tau_{wave} = \frac{1}{2} f_w \rho u_b^2 \quad \text{(Eq. 2.5)}$$

where

$$f_w = 0.04 \left[\frac{u_b T}{2\pi k_b} \right]^{-0.25} \quad \text{(Eq. 2.6)}$$

H_s is significant wave height, T is wave period, k is wave number ($2\pi/L$), L is wave length, f_w is the friction factor, and k_b=3D_{84} is the roughness length scale of the bed (Fredsoe & Deigaard 1992). The wave number k is calculated using the dispersion equation derived from linear wave theory

$$\sigma = \sqrt{gk\tanh(kh)} \quad \text{(Eq. 2.7)}$$

where $\sigma = 2\pi/T$.

2.4 Results

Water Depth & Storm Surge

Depth data provide an indication of the elevations of sampling locations relative to MSL (tbl 2.1). Depth measurements indicate that TBE (0.55 m) is lower in elevation than the TAE (0.65 m), and that the marsh interior (0.4 m and 0.56 m) is lower than the marsh edge at both sites (fig 2.1, 2.2). As a result, site B floods more frequently that site A. When the marsh is flooded the water is deeper in the interior than along the edge, and the interior remains inundated with water for longer periods of time (tbl 2.4).

A comparison of measured tides to predicted tides recorded at the Wachapreague, VA NOAA station provides evidence of storm surge in the coastal bays (tbl 2.2). The highest mean surge occurred during the early spring (0.2291 m and 0.2426m), whereas the mean surge in the summertime was much lower (0.0933

m). This is unsurprising given that strong winds (>8 m s^{-1}) from the north that force storm surge (Fagherazzi et al 2010; Mariotti et al. 2010) are more prevalent in the winter (fig 2.3; fig 2.18).

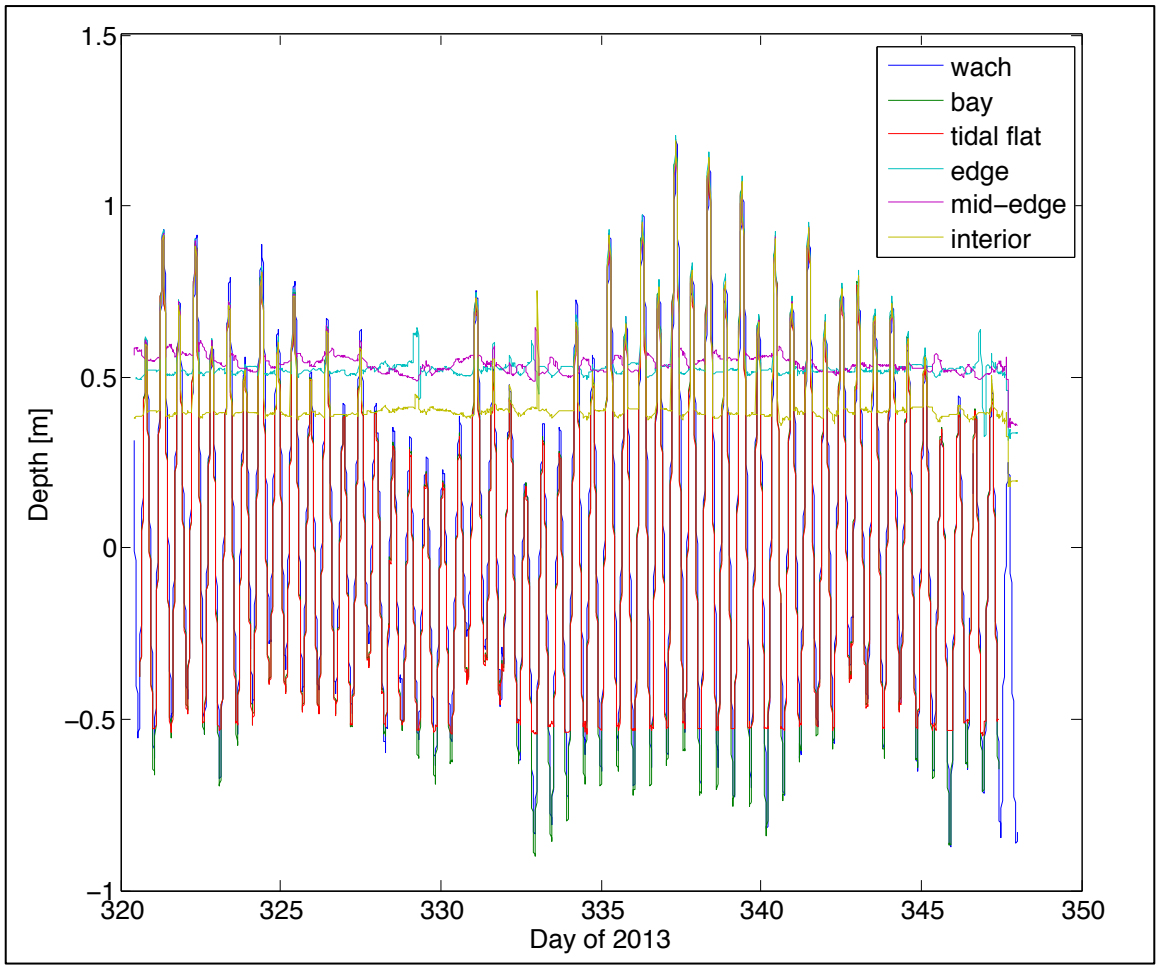

Figure 2.1: Water depth (m) relative to MSL(m) recorded at transect B during November and December 2013; the line labeled "wach" shows the measure tide at the nearby NOAA Wachapreague tide gauge.

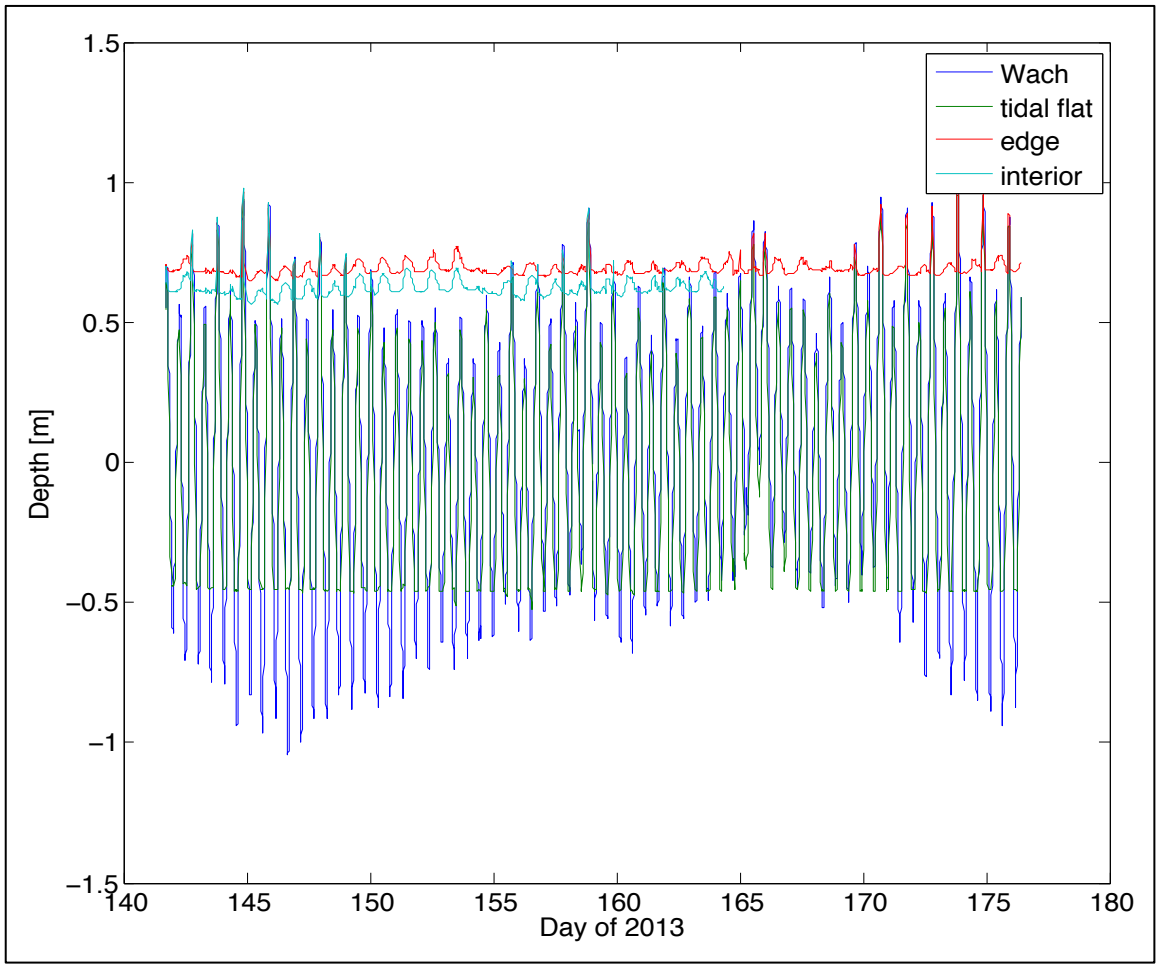

Figure 2.2: Water depth (m) relative to MSL recorded at transect A during May and June 2013; the line labeled "wach" shows the measure tide at the nearby NOAA Wachapreague tide gauge.

Deployment	**$HT_m > HT_p$**	**Average Surge**
Feb-Mar 2013	43.6%	0.2291 m
May-Jun 2013	46.2%	0.0933 m
Nov-Dec 2013	73.5%	0.1642 m
Mar 2014	77.3%	0.2426 m

Table 2.2: Storm surge calculated as the difference between measured high tide (HT_m) and predicted high tide (HT_p). $HT_m > HT_p$ indicates the number of times that measured high tide exceeded the predicted high tide, relative to the total number of high tides in the deployment.

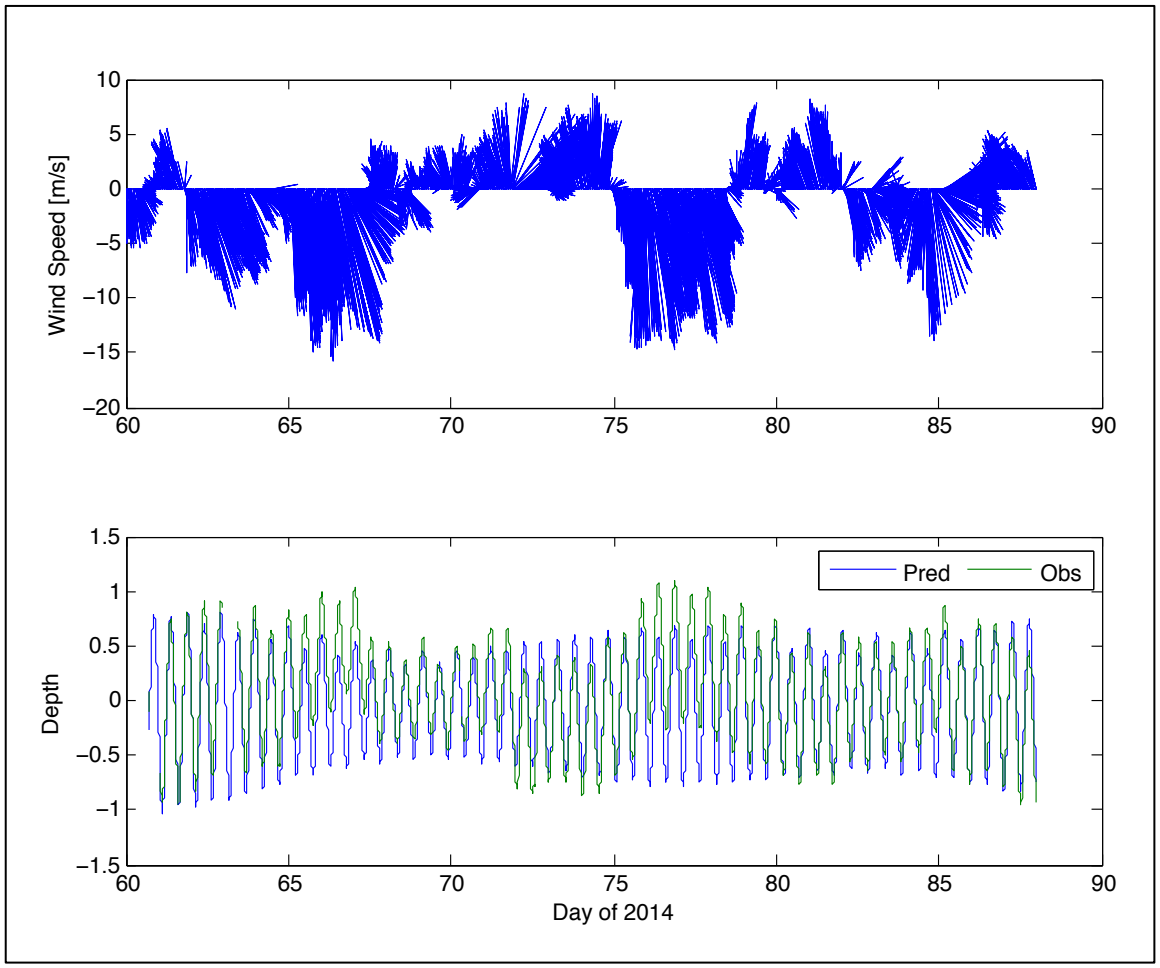

Figure 2.3: Top: wind speed (m/s) recorded at the South Bay station and plotted as the direction towards which the wind is blowing. Bottom: Depth (m) relative to MSL of predicted and observed tides recorded at the Wachapreague, VA NOAA station during March 2014.

Currents (Transect A)

In the Virginia coastal bays, southerly winds are more common relative to northerly winds, particularly during the summertime. Winds influence the magnitude and direction of tidal currents. Figure 2.4 compares wind patterns to mean current magnitude and direction averaged over the entire water column at TAF. Southerly winds correspond with an alternating northward flood, southward ebb current pattern. Conversely, in the presence of stronger northerly winds,

currents flow towards the south, regardless of tidal phase though with tidally varying speeds. Average current speeds during times of weaker southerly winds were less than half (<5 cm/s) the speeds during periods of stronger northerly winds (>10 cm/s). As discussed below, current speeds also increased during spring tide.

Current magnitude and direction recorded on TAF at water elevations exceeding the marsh elevation, as well as currents recorded at TAE and TAI, are presented in figure 2.5. On the tidal flat, tides flowed towards the northeast during flood tide, and towards the southwest during ebb tide (fig 2.5a, b). The dominant axis of water movement (NE-SW) paralleled the marsh edge (NE-SW). On the marsh platform, water flooded the marsh from Hog Island Bay and ebbed towards the large tidal creek behind the site (fig 2.5c,d,e,f; see fig 1.4). It is important to note that data collected from the marsh were limited by infrequent flooding during the deployment, as well as the ADP blanking distance. The marsh currents displayed in figure 2.5 occurred over multiple tidal cycles during spring tide.

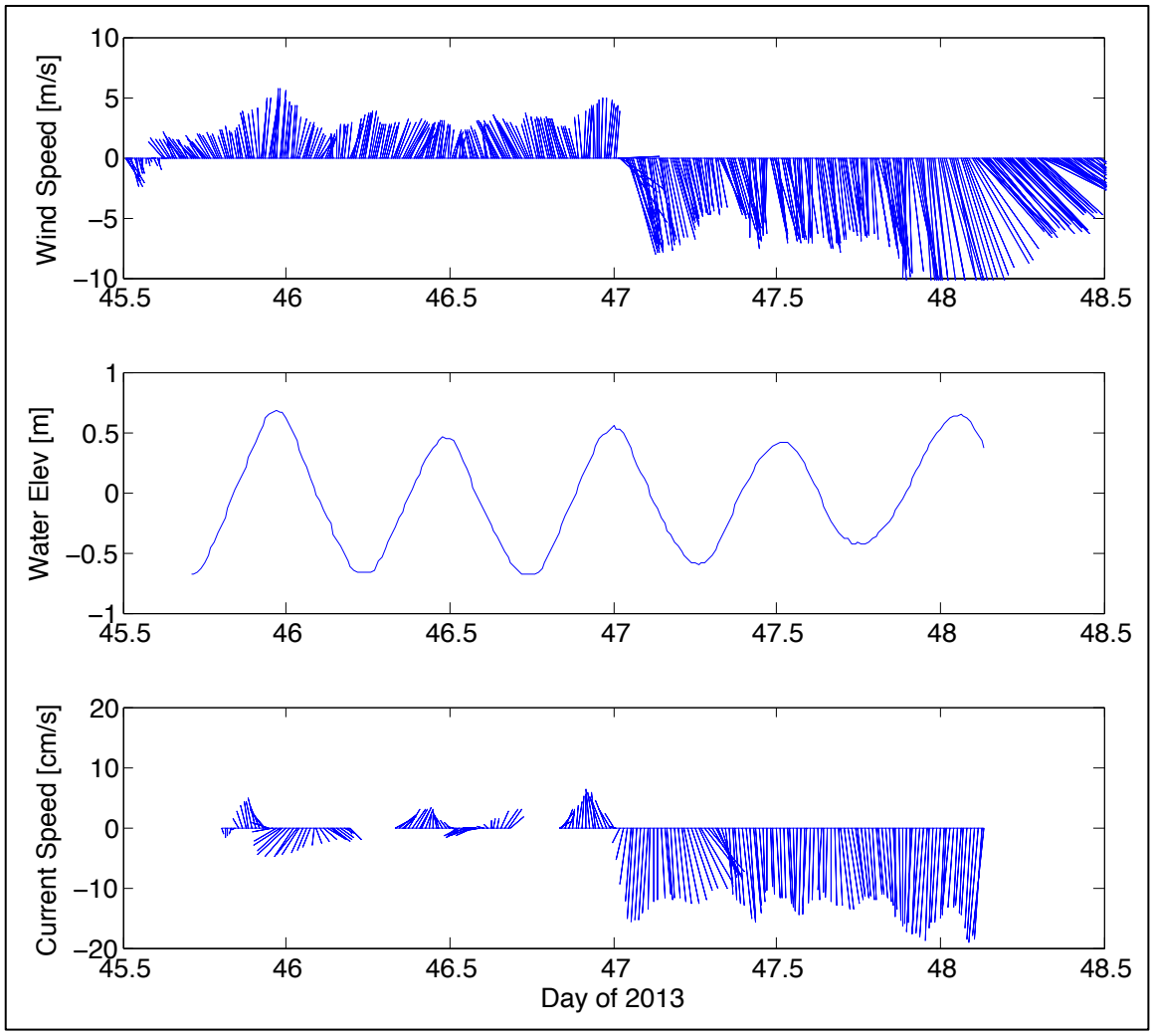

Figure 2.4: From top to bottom: wind speed (m/s) recorded at the South Bay station and plotted as the direction towards which the wind is blowing, depth (m) relative to MSL, and current magnitude (cm/s) plotted as the direction towards which the water is flowing. Currents were averaged over the entire height of the water column and recorded at TAF during February-March 2013.

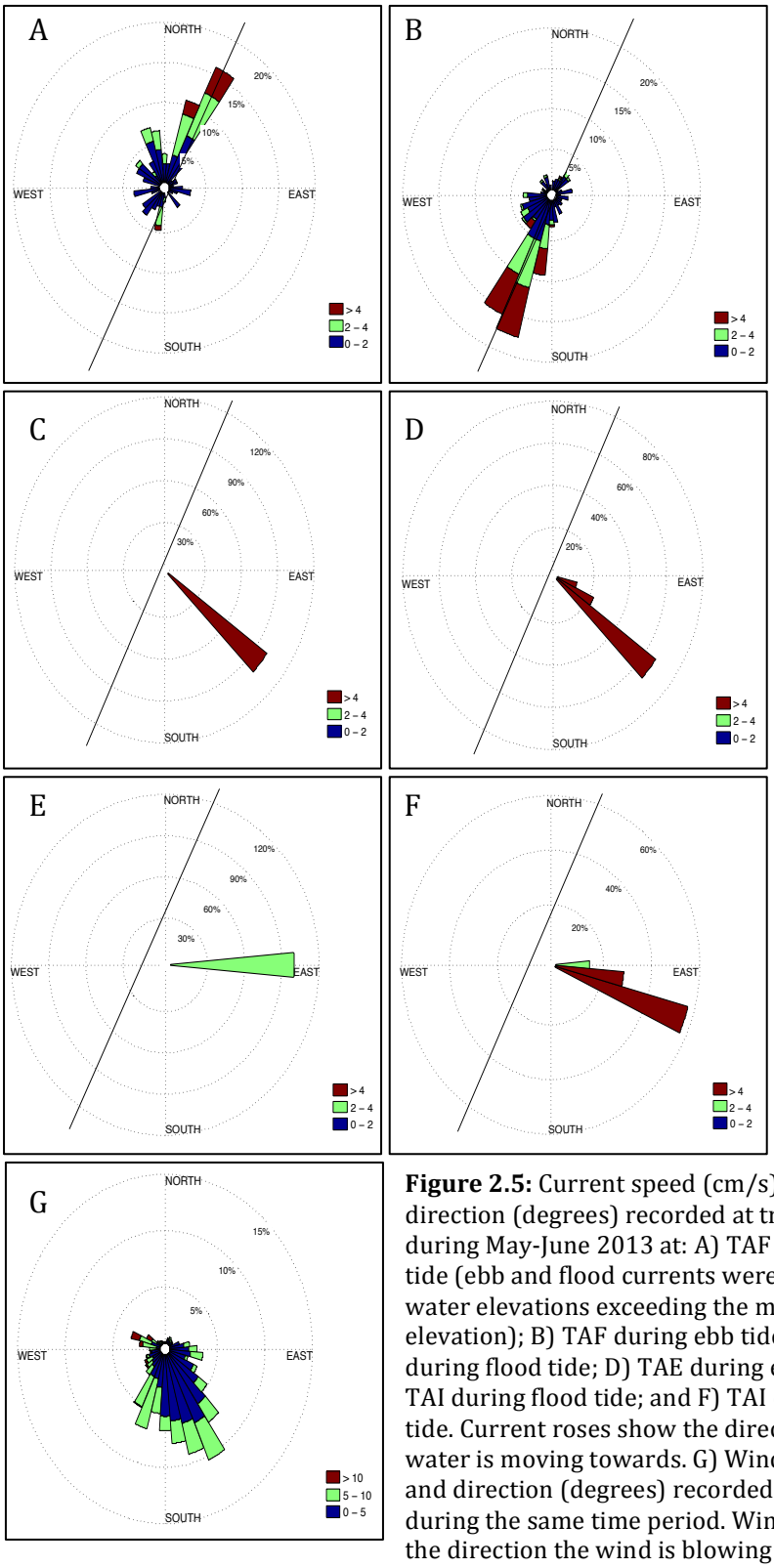

Figure 2.5: Current speed (cm/s) and direction (degrees) recorded at transect A during May-June 2013 at: A) TAF during flood tide (ebb and flood currents were measured at water elevations exceeding the marsh elevation); B) TAF during ebb tide; C) TAE during flood tide; D) TAE during ebb tide; E) TAI during flood tide; and F) TAI during ebb tide. Current roses show the direction the water is moving towards. G) Wind speed (m/s) and direction (degrees) recorded in South Bay during the same time period. Wind rose shows the direction the wind is blowing from.

Currents (Transect B)

At TBF, currents primarily flowed towards the southwest, parallel to the orientation of the marsh edge (NE-SW), when measurements were averaged over the entire water column (fig 2.6). The southward flow was forced by prevailing winds from the north during the March 2014 deployment.

Figure 2.7 shows current patterns at transect B on the marsh surface. Water floods the marsh edge from the marsh interior and from the large embayment north of site B (fig 2.7c). Water ebbs off the marsh edge into Hog Island Bay as well as southward towards site A (fig 2.7d). In the marsh interior, water floods from Hog Island Bay and ebbs towards the small tidal creek behind site B (fig 2.7e,f). The dominant south-southeast flow direction in the interior was similar to the current pattern recorded at site A, but also coincided with strong winds from the north-northwest during November and December 2013.

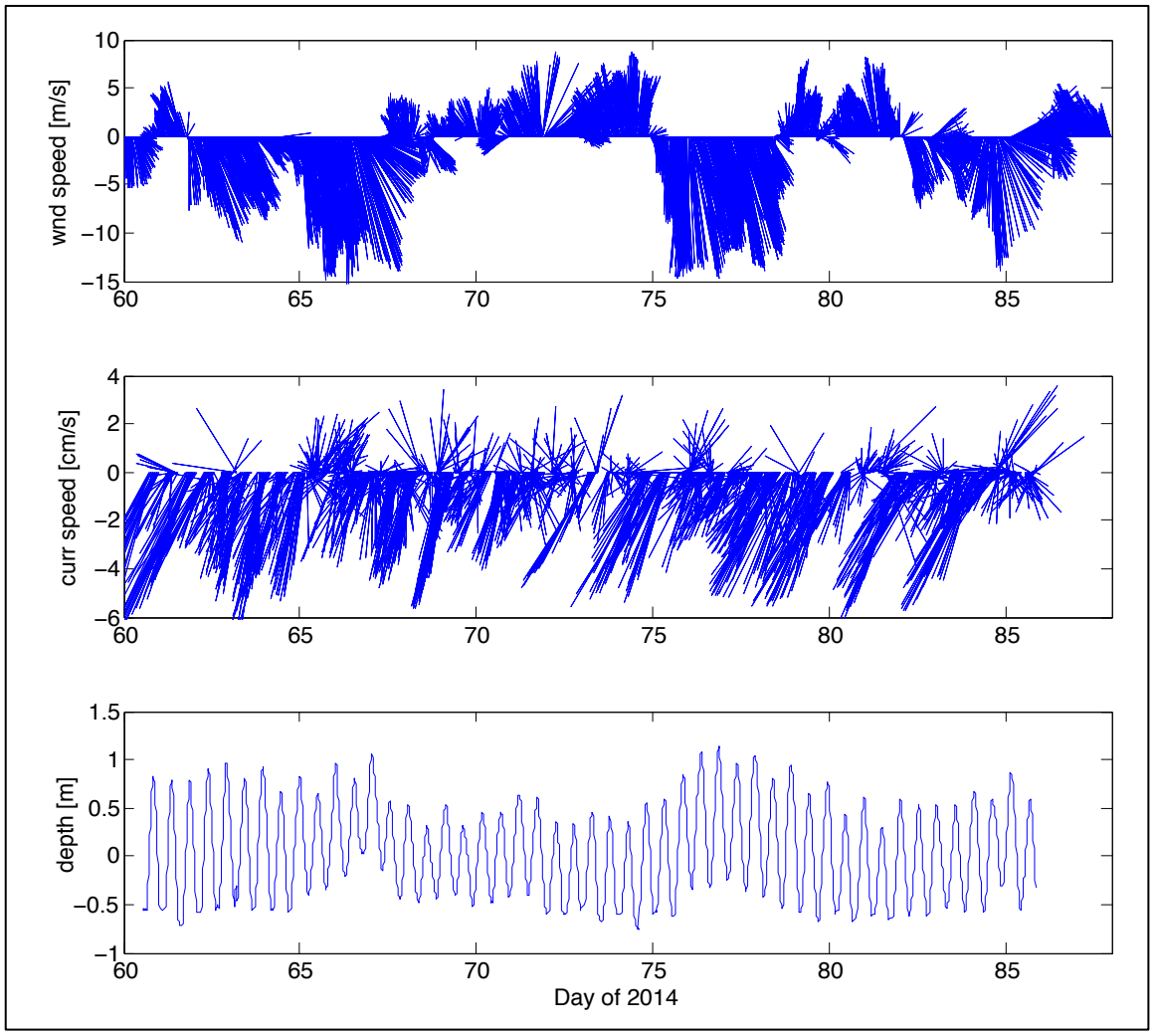

Figure 2.6: From top to bottom: wind speed (m/s) recorded at the South Bay station and plotted as the direction towards which the wind is blowing, current magnitude (cm/s) plotted as the direction towards which the water is flowing, and depth (m) relative to MSL. Currents were averaged over the entire height of the water column and recorded at TBF during March 2014.

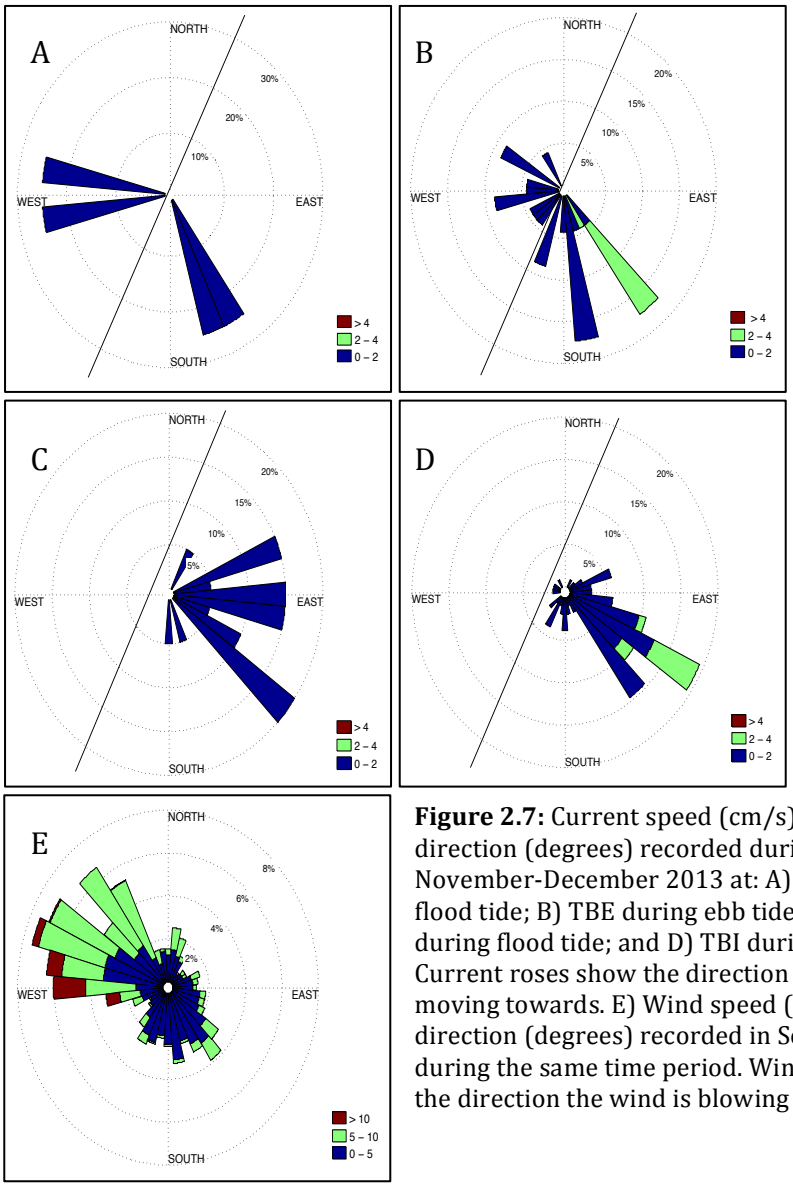

Figure 2.7: Current speed (cm/s) and direction (degrees) recorded during November-December 2013 at: A) TBE during flood tide; B) TBE during ebb tide; C) TBI during flood tide; and D) TBI during ebb tide. Current roses show the direction the water is moving towards. E) Wind speed (m/s) and direction (degrees) recorded in South Bay during the same time period. Wind rose shows the direction the wind is blowing from.

Effect of Edge Morphology on Currents

The marsh edge is a morphological influence on flow. At TAF, when water depth was both above (2.8a) and below the marsh elevation (2.8b), currents primarily flowed towards the northeast and southwest, which parallels the orientation of the edge. Although the variability in flow direction increased at water depths higher than the marsh elevation, it was not as remarkable as at TBF. When water depth was below the marsh elevation at TBF, currents almost exclusively flowed towards the southwest (2.8d), which also parallels the orientation of the edge. Little northward flow was recorded due to the prevalence of northerly winds. When depth exceeded the marsh elevation at TBF, water either moved onto the marsh or further out into the bay as unconstrained flow (2.8e).

‘

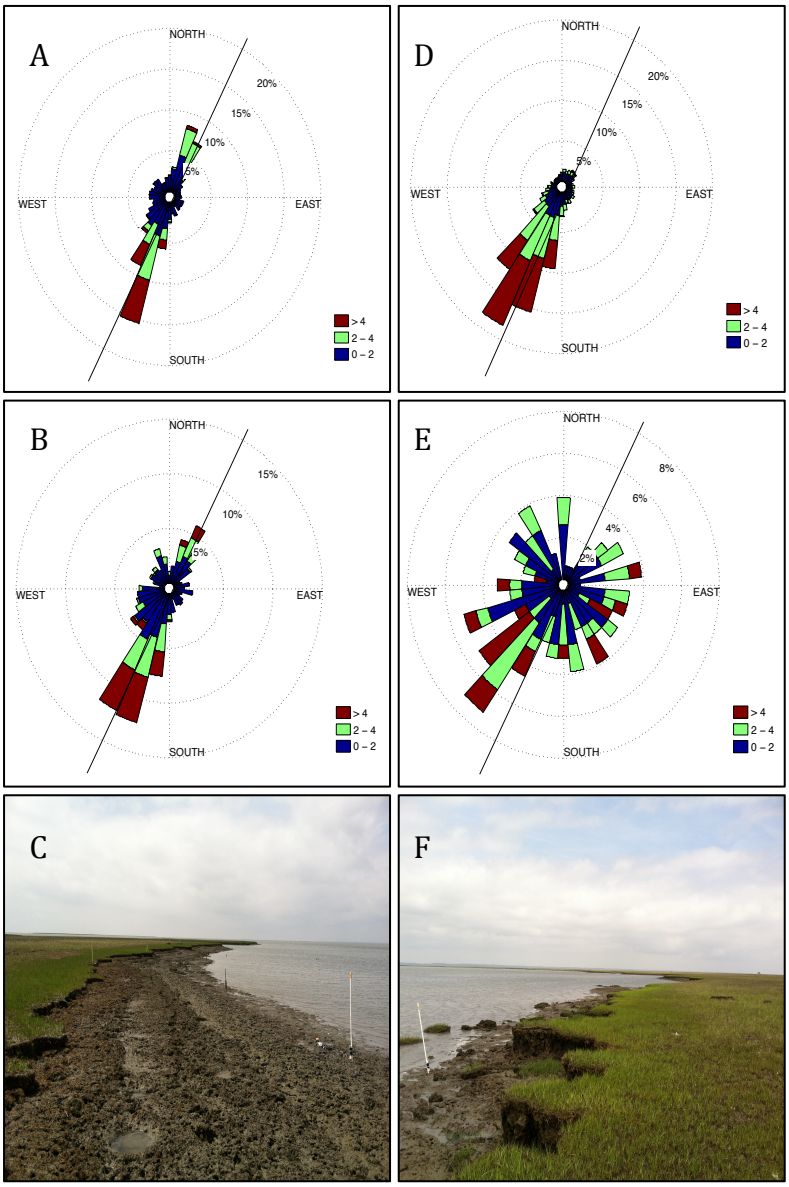

Figure 2.8: Current speed (cm/s) and direction (degrees) recorded at: A & D) water elevations below the marsh surface elevation at TAF and TBF, respectively; and B & E) water elevations exceeding the marsh surface elevation at TAF and TBF, respectively. C) Picture of edge at transect A. F) Picture of edge at transect B. Currents at TAF were recorded during May-June 2013 and currents at TBF were recorded during March 2014.

Wind Waves (Transects A & B)

Figure 2.9 shows significant wave height separated by wind speed and direction. Westerly winds (180°- 360°) blowing across Hog Island Bay produce the

largest waves, because the fetch generated is sufficient for wave formation (fig 2.9). On the other hand, easterly winds (<180°) from the Atlantic blow across barrier islands (e.g. Hog Island) and Chimney Pole, thus inhibiting wave formation due to insufficient fetch, particularly for sites bordering the marsh. In addition to direction, high wind speeds (> 8 m s^{-1}) force larger waves relative to lower wind speeds (< 8 m s^{-1}). Mean wave heights for each wind direction group were up to 3.2 times higher under high wind speed conditions compared to low wind speed conditions. At Chimney Pole, winds blowing from the west-northwest (~295°) (i.e. the direction of longest fetch) at high wind speeds generated the highest waves (median=0.25 m) (fig 2.9).

Figure 2.10 also illustrates the influence of wind direction and wind speed on wave height on the tidal flat. When winds blew across Hog Island Bay at high speeds (> 8 m s^{-1}) the largest waves formed, which occurred on days 328 and 332. However, when westerly winds coincided with low wind speeds, either small or no waves formed, which occurred on day 337.

Figure 2.11 shows wave transformation at transect B between the bay (~15 m offshore of the marsh edge) and marsh interior. As waves propagated from the bay up onto the tidal flat, wave height increased by 33% (fig. 2.11). Subsequently, as the waves crossed the marsh edge their height rapidly diminished. Wave height recorded in the bay was reduced by 67, 78, and 83% at the marsh edge, middle and interior, respectively.

Wave heights at the transect B Bay (TBB) and TBF are more similar to each other than to waves at TAF (fig. 2.12). Waves at TBB have a 96% correlation with

waves at TBF and an 85% correlation with waves at TAF. Waves at TBF have a 91% correlation with waves at TAF. Waves are 33% larger at TBF than at TBB, and are 6% larger at TBF compared to TAF. However, slightly higher waves at TBF than TAF are likely attributable to deeper depths due to the instrument's location at a lower elevation.

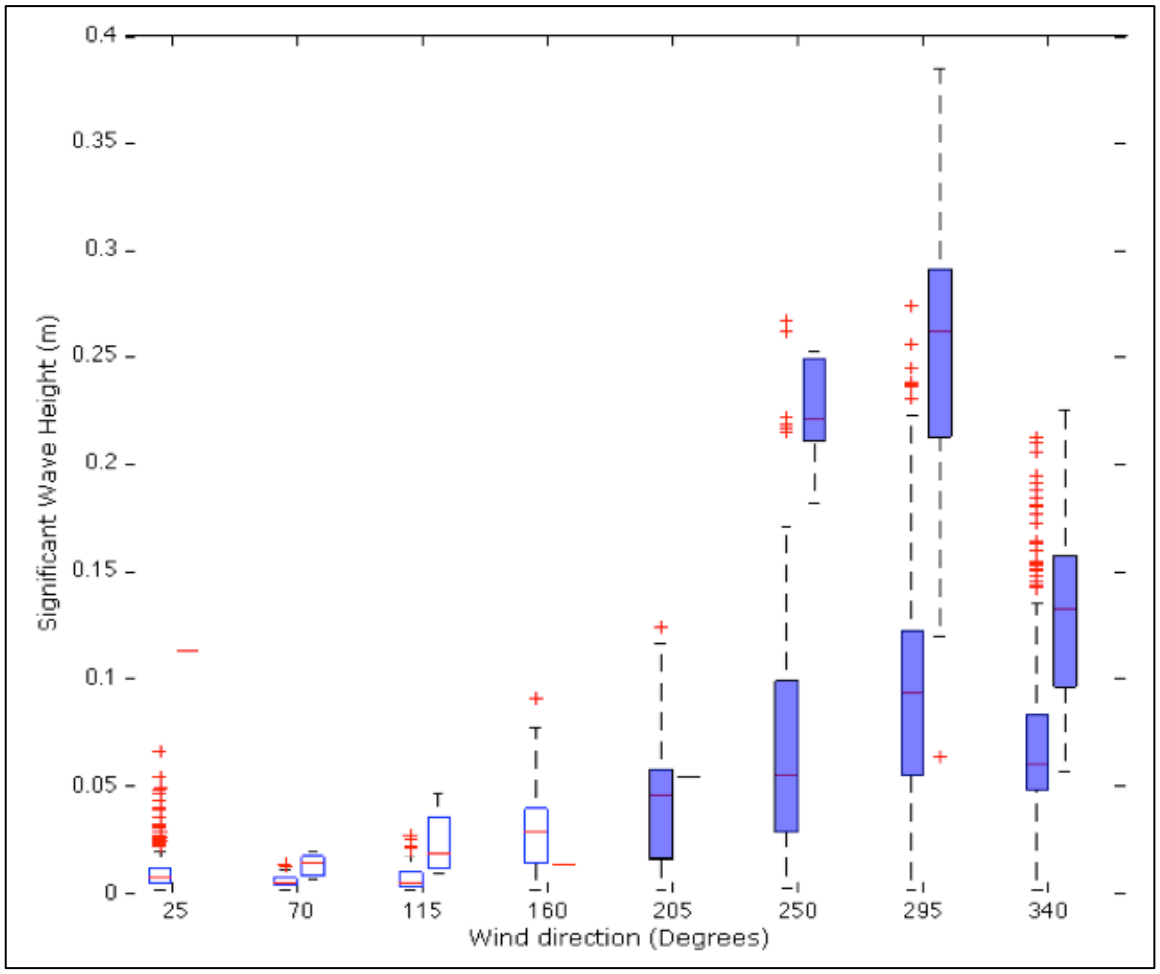

Figure 2.9: Significant wave height compared to wind direction for low (left; <8 m s^{-1}) and high (right; >8 m s^{-1}) wind speeds. Blue shading indicates westerly winds blowing across Hog Island Bay. Data were recorded in February-March 2013 at TAF. Wind speeds did not exceed 8 m s^{-1} for the 25°, 160°, and 205° wind direction groups, therefore there are no data.

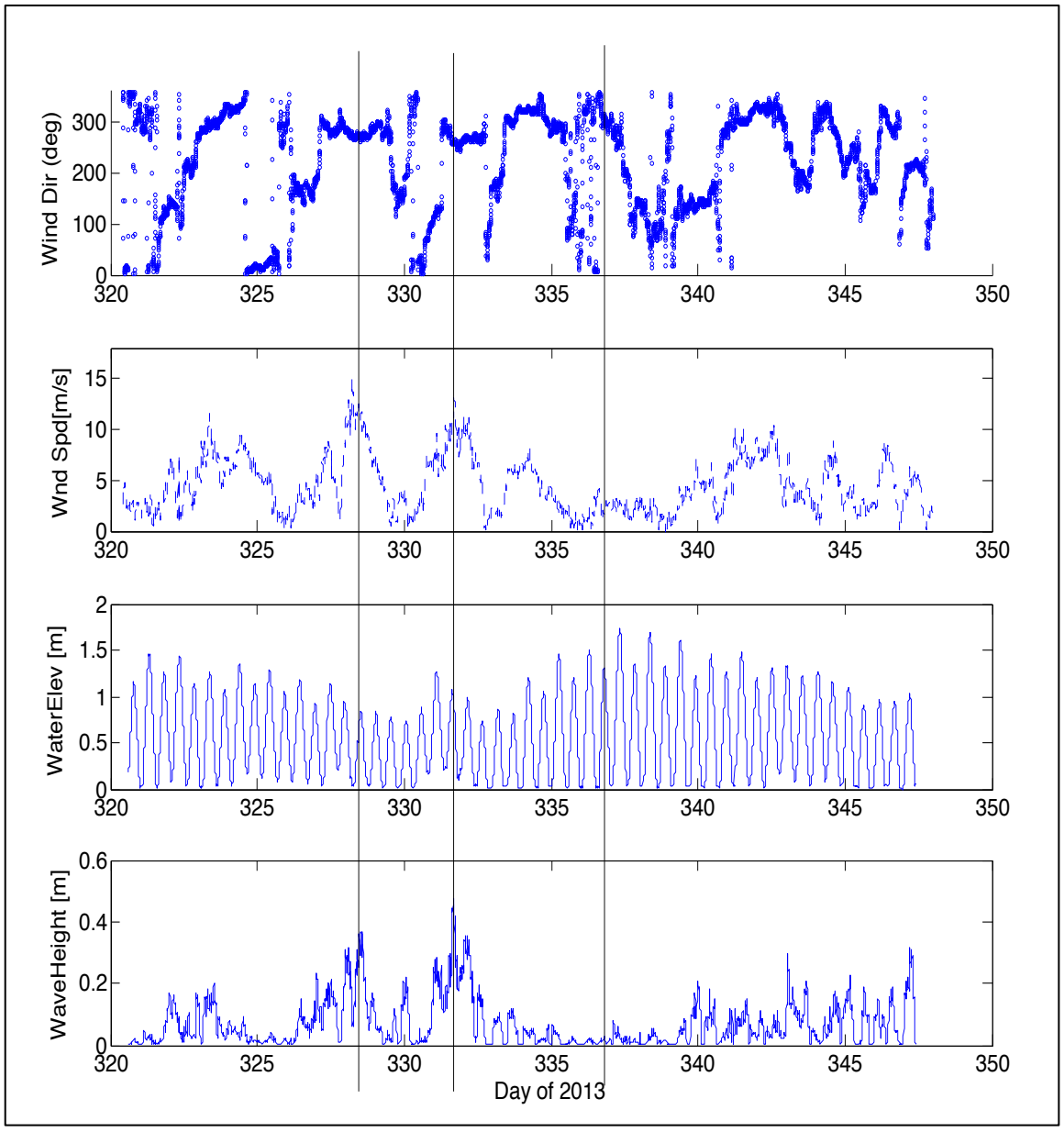

Figure 2.10: From top to bottom: wind direction (degrees) and wind speed (m/s) recorded in South Bay; water depth (m); and significant wave height (m) recorded at TBF during November-December 2013.

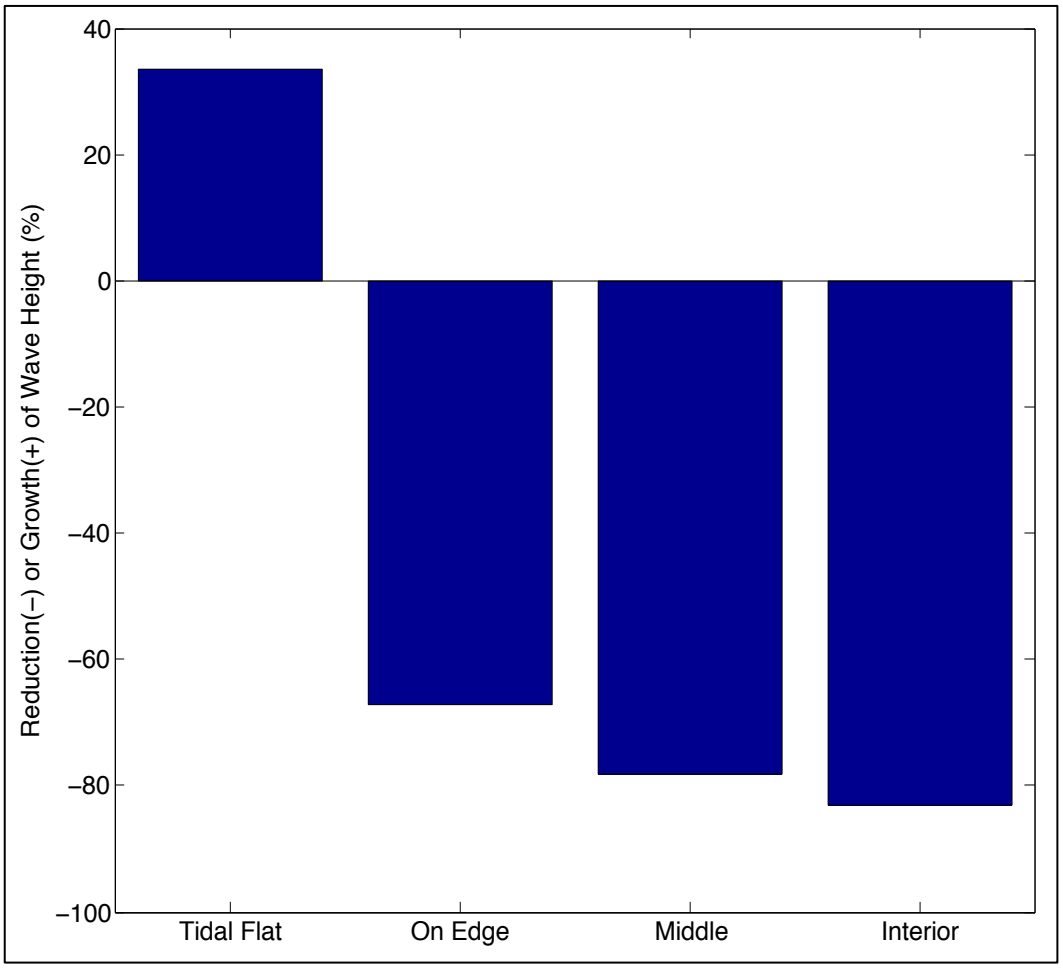

Figure 2.11: Average growth or reduction (%) in significant wave height as waves propagated from the bay to the marsh interior, shown as a percentage of the initial height recorded at TBB. Data were recorded during November-December 2013 at transect B.

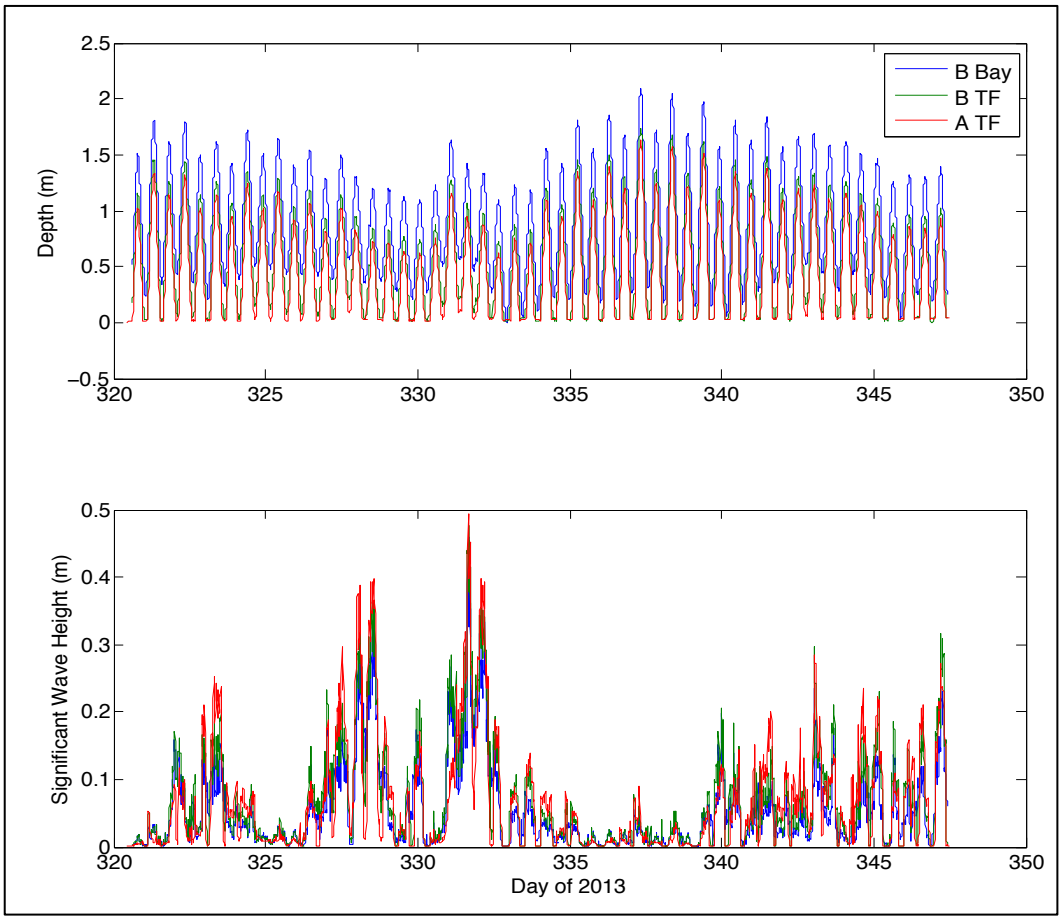

Figure 2.12: Top: Depth (m) recorded at TBB, TBF, and TAF. Bottom: Significant wave height (m) recorded at the same stations. Data were recorded during the November-December 2013 deployment.

Shear Stress Regimes

Waves account for the largest proportion of total bed shear stress (fig 2.13, 2.14). During large storms, wave-generated bed shear stress on the tidal flat was 2 orders of magnitude larger than current-induced bed shear stress. Current shear stress on the tidal flat increased as tidal range increased (fig 2.16), such that the highest shear stress occurred during spring tide (fig 2.13).

On the marsh, mean wave-induced bed shear stress is 17% higher at the edge than the interior. Wave and current bed shear stress on the marsh never exceeded

0.35 Pa and 0.005 Pa, respectively. Total shear stress on the marsh only exceeded 0.07 Pa, the critical threshold for suspension, 4.9% of the time at TBE and 3.6% of the time at TBI during November and December 2013 (fig 2.15). On the tidal flat, total shear stress was greater than 0.07 Pa for 27% of the time.

Figure 2.17 shows total shear stress (waves + currents) on TBF as a function of depth and wind speed for times when the wind blew from a west-northwest direction (i.e. the direction of longest fetch). When wind speeds are less than 8 m s^{-1}, total bottom shear stress does not differ significantly among depth groups due to little wave formation. For every depth group, median total shear stress under low wind speed conditions (range=0-0.06 Pa) was lower than under high wind speed conditions (range=0.09-0.35 Pa). When wind speed exceeded 8 m s^{-1}, maximum shear stresses occurred at water elevations just below MHHW (~0.7 m), above which shear stress declined with increasing depth. A wind threshold for significant wave generation of 8 m s^{-1} was a previously determined value from Lawson et al. (2007).

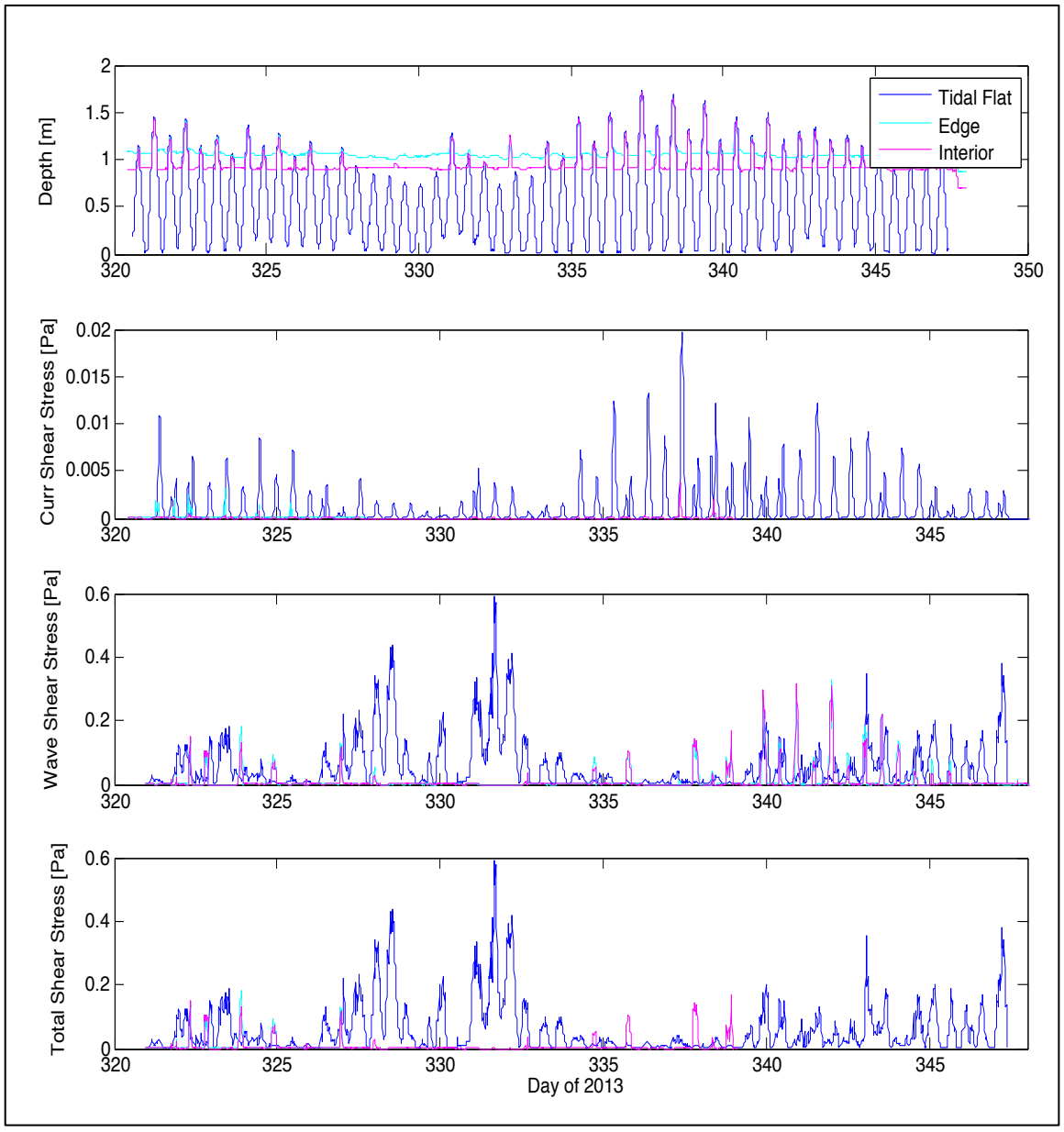

Figure 2.13: From top to bottom: depth (m), current shear stress (Pa), wave shear stress (Pa), and total shear stress (Pa) generated by both currents and waves recorded at TBF, TBE, and TBI during Nov-Dec 2013.

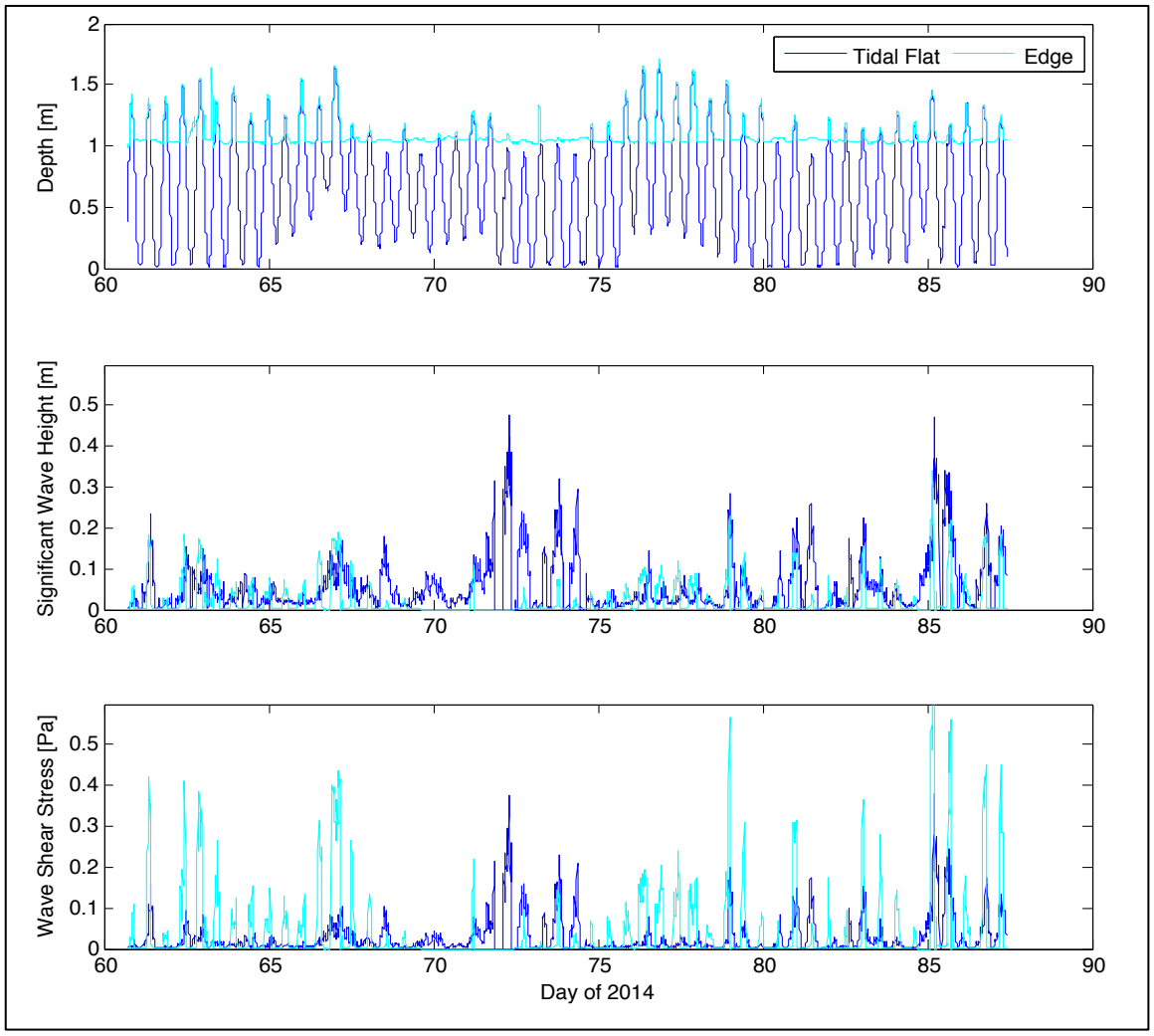

Figure 2.14: Depth (m), significant wave height (m), and wave shear stress (Pa) recorded in March 2014 at TBF and TBE. Note: the instrument located at TBE during this deployment was closer to the edge than during the Nov-Dec 2013 deployment (2.13).

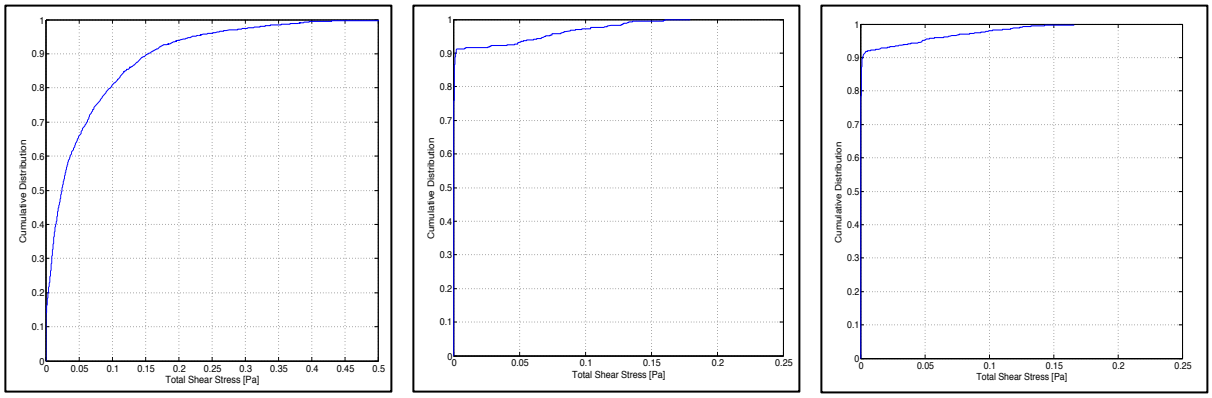

Figure 2.15: Cumulative distribution of total shear stress at TBF, TBE, and TBI during November-December 2013.

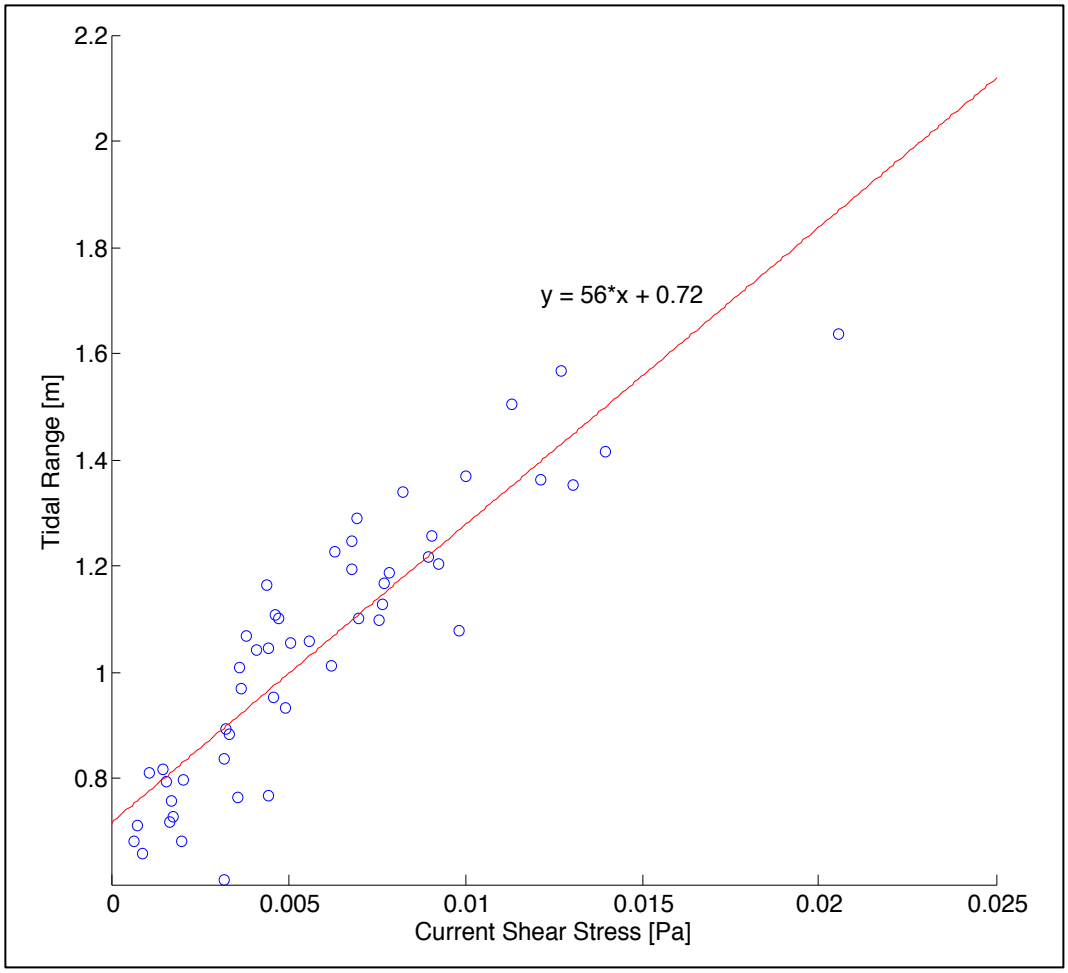

Figure 2.16: Peak current shear stress (Pa) during each tidal cycle compared to tidal range, calculated as the difference between high and low tide. Data were recorded at TBF during November-December 2013.

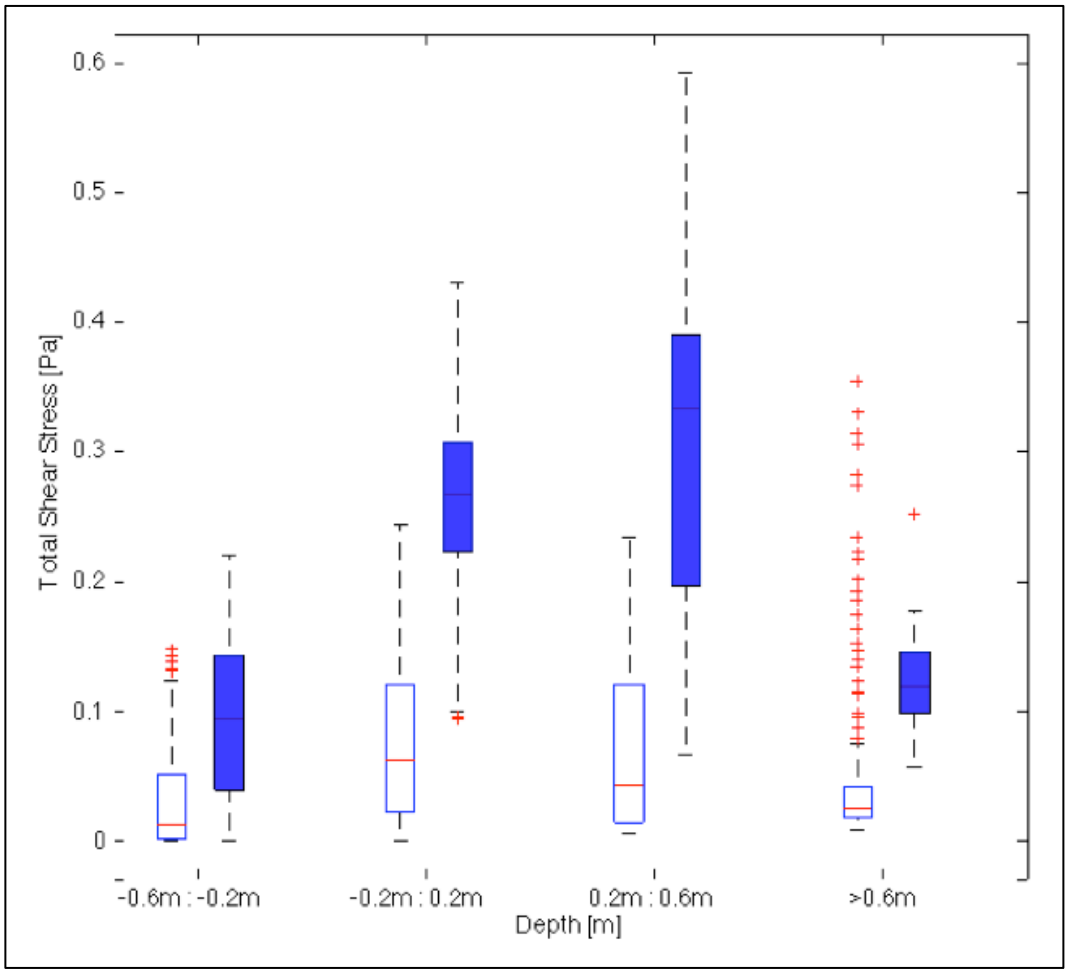

Figure 2.17: Total shear stress (Pa) as a function of water depth (m) at times when wind blew across the bay from a W-NW direction (240-305 degrees). Data are separated into low (<8 m/s; white boxes) and high (>8 m/s, blue boxes) wind speed groups. Data were recorded at TBF in November-December 2013.

Seasonal Variations in Wind & Waves

Wind speed and direction displayed seasonality in the study area. From late fall to early spring, northerly winds prevailed (2.18 a, c, d). Northerly winds during winter months were typically stronger than the southerly winds that prevailed during the early summer (2.18b). Wind speeds exceeded 8 m s^{-1} only 5% of the time during the May-June 2013 deployment compared to 12%, 11%, and 31% of the time during the February-March 2013, November-December 2013, and March 2014

deployments, respectively. Although 50th percentile wave heights did not vary much among different seasons, 95th and 98th percentile wave heights in the winter were up to 12 cm higher than summer wave heights (tbl 2.3).

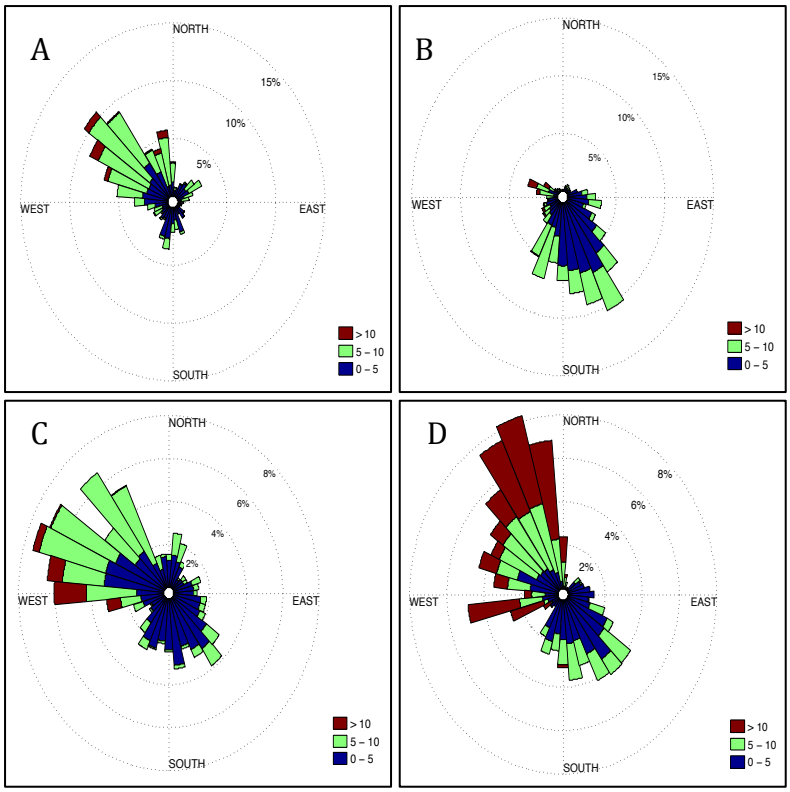

Figure 2.18: Wind Direction recorded in South Bay during A) February- March 2013; B) May-June 2013; C) November-December 2013; and D) March 2014.

Deployment	50th	75th	95th	98th
Feb-Mar 2013	0.0585	0.1118	0.2456	0.3048
May-Jun 2013	0.0303	0.0737	0.1513	0.1936
Nov-Dec 2013	0.0297	0.0890	0.2263	0.3208
Mar 2014	0.0301	0.0729	0.1900	0.2666

Table 2.3: 50th, 75th, 95th, and 98th percentile significant wave heights (m) given for all 4 deployments.

	Site A			Site B			
	TAF	**TAE**	**TAI**	**TBB**	**TBF**	**TBE**	**TBI**
Edge erosion rate	<0.5 m yr^{-1}			1.5-2 m yr^{-1}			
Scarp slope	low			high			
Depth	-0.5	0.65	0.56		-0.5	0.55	0.4
Est. inundation Freq (days/mo)	25.5	2.7	4.2	30	25.5	5.1	6.9
Flood curr. dir. when marsh is flooded	Along edge (NE)	On-marsh (SE)	On-marsh (E)	X	None (uncon-strained)	On & off-marsh (SE, W)	On-marsh (E, SE)
Ebb curr. dir. when marsh is flooded	Along edge (SW)	On-marsh (SE)	On-marsh (ESE)	X	None (uncon-strained)	On & off-marsh (SE, W)	On-marsh (SE)
90th Percentile H_s (m) (May-Jun 2013)	0.1331	0.0007	0.0007	X	0.1690	0.0247	0.0267
90th Percentile H_s (m) (Nov-Dec 2013)	0.1832	0.0017	X	0.1333	0.1702	0.0215	0.0122
90th Percentile τ_{wav} (Pa) (May-Jun 2103)	0.0947	0.0007	0.0004	X	0.1164	0.0210	0.0135
90th Percentile τ_{wav} (Pa) (Nov-Dec 2013)	0.1199	0.0018	X	0.1489	0.1533	0.0058	0.0099

Table 2.4: Summary of key findings and results. X indicates no data available.

2.5 Discussion

Water Depth & Storm Surge

Marsh surface topography strongly influences the frequency and duration of marsh flooding (Cahoon & Reed 1995). Deeper water and prolonged inundation occurred at site B due to its lower elevation relative to site A. Given this, accretion rates at site B may be higher than at site A.

Storm surge strongly affects water level in the Virginia coastal bays (Mariotti et al. 2010). Evidence of storm surge in Hog Island Bay was found during each

season, but was highest during the late winter to early spring. Storm surge enhances the potential for sediment delivery to open boundary marshes due to prolonged inundation. This is particularly true when storm surge coincides with a spring tide (Stumpf 1983).

Storm surge allows for the formation of larger waves, which generate greater bottom shear stresses for any given depth. Our data did not capture larger waves during storm surge events, possibly due to unfavorable wind conditions. For example, strong winds from the northeast produce the largest storm surge in the Virginia coastal bays (Mariotti et al. 2010), but generate little wave fetch at our site. As discussed below, storm surge coincided with decreased wave-induced bed shear stress on the tidal flat and increased bed shear stress at the marsh edge.

There is a positive correlation between current speed and tidal range (Fagherazzi et al. 2013). The tidal prism, the amount of water that enters and exits the lagoon during a tidal cycle, can be approximated as the product of tidal range and the area of the bay flooded by the tide. Given that storm surge increases flooded area and therefore tidal prism, storm surge likely increases current magnitude.

Currents (Transect A)

When southerly winds are present, there is an alternating northward flood, southward ebb current pattern at TAF and TBF. Southerly winds likely help push flood tides northward, whereas tidal slope likely influences the southward ebb tide. On the other hand, the southward flood and ebb current pattern that exists in the presence of stronger northerly winds is attributable to wind forcing.

The transport of water between the marsh and the lagoon occurs as a shallow sheet flow in the absence of tidal creeks (French et al. 1995; Temmerman et al. 2005). On the marsh, water flows from the bay towards the large tidal creek during flood and ebb tide. Faster draining of the large tidal creek behind site A could create a water surface slope in the direction of the creek. Furthermore, behind TAI the surface slopes sharply downward towards the creek (McLoughlin 2010), which may increase current magnitude in that direction. The large creek is also present behind site B, but it is further away and therefore less influential.

Currents (Transect B)

Dominant flood and ebb currents moved along the edge towards the southwest at TBF when measurements were averaged over the entire water column for the March 2014 deployment. This is likely due to prevailing winds from the north during that time period, which pushed currents southward. We recorded a northward flood, southward ebb pattern during a few instances when southerly winds were present, which agrees with the current pattern recorded at TAF.

At the marsh edge, water moves from the marsh interior towards Hog Island Bay. This may be influenced by a faster response of the bay to ebbing tide relative to the marsh interior, causing the setup of a tidal slope. Water also moves from the large embayment north of site B (see fig 1.4) southward towards site A. The irregular edge morphology likely influences the variable current patterns at TBE. In the marsh interior, flood and ebb tides move towards the small tidal creek behind the site (see fig 1.4). Faster draining of the small creek, as well as the steep

downward slope of the marsh surface behind TBI, likely force currents towards that direction. Furthermore, the prevalence of winds from the north-northwest during November and December 2013 likely helped push currents on the marsh towards the south-southeast.

Effect of Edge Morphology on Currents

Edge profile acts as a morphological influence on current direction. The edge at transect A is relatively straight, whereas the transect B edge is jagged, consisting of wave gullies and embayments. Our results indicate that at elevations below the marsh platform height, the edge steered currents along the marsh boundary at both transects. At elevations above the marsh platform, the edge had little to no effect on current direction and sediment transport. Unconstrained flow at elevations above the marsh platform may facilitate the transport of the material that is in the water column onto the marsh. Furthermore, the high variability in current direction at water depths greater than the marsh platform height may be influenced by slack water at high tide.

Sediment Advection onto the Marsh

Sediment deposition on the marsh platform relies on currents to transport sediment across the bay-marsh boundary. Overall, the data reveal that currents do transport sediment from the bay to the marsh surface, but not exclusively. Currents also move sediment along the edge and further out into the bay. Tidal creeks that cut through the marsh further complicate current patterns. Given dominant flow

directions, it is unlikely that the tidal creeks provide sediment to our sites. However, the smallest sediment grains with low settling velocities may be transported across the marsh to the creek without depositing. The higher current velocities moving towards that direction would aid this process. Given the complex hydrodynamics, models predicting sediment deposition on marsh islands should not assume that the amount of sediment deposited on the marsh is proportional to the amount resuspended from the tidal flat.

Wind Waves

In the Virginia coastal bays, wave height is forced by wind direction and wind speed. Winds blowing from the west-northwest (i.e. the direction of longest fetch) at speeds greater than 8 m s^{-1} generated the highest waves at the study site. Typically, these conditions occurred during winter storms.

As waves propagated from Hog Island Bay onto the tidal flat, wave height increased. This may be attributable to processes such as wave shoaling or refraction. For any given depth, increased wave height increased wave shear stress on the tidal flat, thus increasing resuspension and erosion potential. Due to the tidal flat's higher elevation relative to the lagoon, water depths are shallower. The combined influence of higher waves and shallower depths increased total bed shear stress on the tidal flat compared to the lagoon.

As waves propagated from the tidal flat across the marsh platform, they quickly dissipated due to shallow water depths and the presence of marsh vegetation (Möller et al. 1999). At site A, shallower depths (tbl 2.4) and higher

biomass density (tbl 3.2) resulted in greater wave dissipation relative to site B, despite similar wave conditions recorded at TAF and TBF.

Shear Stress Regimes

When winds blew from a W-NW direction at speeds exceeding 8 m s^{-1}, maximum bed shear stresses coincide with water elevations between MSL and MHHW, the range associated with stable marsh platforms (Fagherazzi & Wiberg 2009). Above MHHW, elevations typically associated with storm surge, bed shear stress declined with increasing depth. These findings agree with Fagherazzi & Wiberg's (2009) model. However, their model showed a decline in total shear stress between MLLW and MSL due to higher depths reducing shear stress despite slight increases in wave height. Our data did not reveal a decline in total shear stress between MLLW and MSL.

A trade off exists between elevated SSC on the tidal flat and prolonged marsh inundation. At Chimney Pole, the highest bed shear stress on the tidal flat was produced by wave events that occurred during neap tide when the marsh barely flooded (fig. 2.13, 2.14). These events also produced the highest SSC, although very little sediment reached the marsh platform due to infrequent flooding. Similar wind conditions during spring tide or storm surge events did not produce as high bottom shear stress.

The highest bed shear stress on the tidal flat and on marsh edge did not overlap. Whereas bed shear stress on the tidal flat was greatest during neap tide, bed shear stress on the marsh edge was greatest during spring tide when water

depths were sufficient to sustain wave energy as waves propagated across the bay-marsh boundary. Therefore, at the marsh edge, surface erosion and sediment remobilization are most likely during spring tide and/or large storm surge events.

Chapter 3: Effects of Tides, Waves and Currents on Sediment Resuspension, Flux, and Deposition

3.1 Objectives

Wave-induced bed shear stress is a primary control of SSC on tidal flats. One objective of this study is: What changes in SSC occur over tidal flats due to changing wave height and water depth during a tidal cycle? In this chapter, we discuss the relationship between SSC, tidal elevation and wave height both on the tidal flat and the marsh platform.

The transport of sediment onto the marsh depends upon current magnitude and direction, and water surface elevation. A second objective is: What is the effect of tides and currents on sediment transport from a bay to an adjacent marsh surface? We estimate SSC near the water surface using a Rouse profile and then calculate sediment flux to determine the amount of sediment moving across the bay-marsh boundary. We also relate spatial deposition patterns to biomass density, sediment properties, and long-term surface elevation table (SET) records.

3.2 Methods—Data Collection and Analysis

Measured Sediment Deposition

To measure sediment deposition, 9 ceramic tiles were placed flush on the marsh surface at 3 distances away (i.e. 3 replicates per station) from the marsh edge at transect B. The ceramic tiles remained on the marsh for the duration of the November and March deployments. A metal straight edge was used to scrape off the

sediment that had deposited on the tiles and then the sediment was dried and weighed it.

Sediment Characteristics

Sediment collected from sampling stations along both transects was analyzed to determine water content, organic content, and grain size distributions. Sediment was extracted from the top 2 cm of the marsh platform and tidal flat using a plastic tube with a plunger approximately 5 in. long with a 1 in. diameter. Six samples were gathered from each station (i.e. tidal flat, marsh edge, mid-marsh, and marsh interior) at both transects for a total of 48 samples.

Using 3 of the samples from each station, water content was calculated as the weight of the sample lost when dried (i.e. wet weight-dry weight). Organic content was calculated as the weight of the sample lost on ignition (i.e. dry weight-ashed weight).

With the remaining 3 samples, grain size distribution was determined using a laser diffraction particle size analyzer (Beckman Coulter LS I3 320). First, any large organic matter in the sample was removed using a 2 mm sieve. Then, the remaining organic matter was dissolved using hydrogen peroxide. After the samples were prepped, the PSA was used to analyze 3 subsamples of each sample (i.e. 9 samples per station), and then the results were averaged.

Biomass Sampling

Aboveground biomass was sampled at 3 stations (marsh edge, middle, and interior) at sites A and B in November 2013. Six replicates were taken at each station. Three samples were taken to the left of each station at 6 m intervals, and 3 samples were taken to the right. A 1 ft^2 quadrangle was used to mark the sample area, and stems inside the quadrangle were clipped at the sediment surface and put into plastic bags. The samples were brought back to the lab where they were dried and weighed to determine biomass weight.

Sediment Resuspension

Two types of optical backscatter sensors (OBS) were used to measure SSC both on and off the marsh platform. On the marsh, Campbell Scientific® OBS-3+ attached to external dataloggers were deployed. Each datalogger was placed inside a dry box, which was mounted onto two 6-ft. 0.75-in. diameter steel rods approximately 1.5 m above the marsh surface. A metal frame was staked to the marsh surface and the OBS was attached at a 45° angle to limit sediment settling on the sensor face, which can interfere with light transmission.

On the tidal flat and in the bay, submersible RBR *Virtuoso* dataloggers with attachable Seapoint Sensors, Inc. auto-ranging OBS were utilized. To deploy the instruments, we attached two 10-ft. 0.75-in. diameter PVC pipes to each other, and then attached the logger. The pipes were pushed approximately 3 ft. into the tidal flat and bay bottom so that the end of the logger was flush with the ground. The sensor was approximately 0.35 m above the sediment surface.

Data from both instruments was filtered by depth to remove false measurements recorded above the water surface and during times when the water was so shallow that the water surface interfered with the return signal. A comparison between SSC and total shear stress allowed for the determination of the threshold shear stress when SSC exceeded 65 mg L^{-1}, approximately the background concentration.

OBS Calibration

The OBS measured turbidity in nephelometric turbidity units (NTUs). The instruments must be independently calibrated with sediment from the site to yield suspended sediment concentration. To do this, first sediment was collected from the tidal flat and mixed with water to create a slurry. A tank was filled with 20 L of water and aquarium salt was added to create an environment similar to ocean salinity (35 ppt). Next, the OBS was attached to a 2-ft. PVC pipe so that it could be maneuvered while in the tank. Sediment was added in small increments, and after each addition the tank was stirred and a 45 mL water sample was taken. The instrument recorded for at least 1 minute after each sediment addition. For every OBS calibration a total of 20 to 25 water samples were collected

We followed the filtration method outlined in Guy (1969) to determine concentration. First, glass microfiber filters were dried and weighed to obtain a dry filter weight. Then, using vacuum filtration, the sediment was transferred from the water sample onto the filter. The filters were dried and weighed a second time, and then the initial filter weight was subtracted to obtain the sediment weight. The

sediment weight was divided by the water volume filtered (45mL) to yield concentration. Finally, NTUs were plotted against sediment concentration to determine a conversion curve (Fig 3.1, Appx. 1).

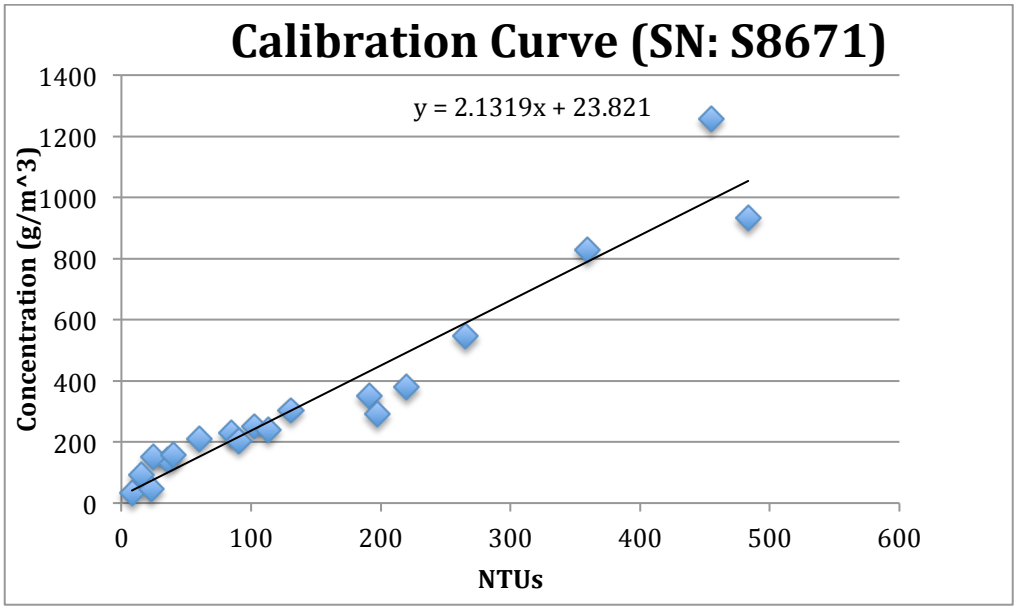

Figure 3.1: Example of calibration curve.

3.3 Methods—Calculations

Settling Velocity

The relationship between grain size and settling velocity was determined using Stoke's Law:

$$w_s = \frac{(\rho_s - \rho_f) g D^2}{18 \rho_f \nu} \qquad \text{(Eq. 3.1)}$$

where ρ_s is particle density, ρ_f is fluid density, D is particle size, and ν is kinematic viscosity of the fluid. Stokes' law was chosen because it is valid for slowly moving, very small grains with a particle Reynold's number (R_D= uD/ ν) less than 0.5. When

this rule was tested using approximate settling velocity (~3.18 x 10^{-4} m s^{-1}) and the largest median grain size (21.64 μm), R_D=0.005, which suggests Stokes' law is applicable at our Chimney Pole sites.

SSC Profile

The OBS provide SSC at 0.35 m above the bed (mab). To estimate SSC through the full water column, the Rouse Equation was applied (Rouse 1937) to 3 grain size fractions *i* given by

$$C_{si} = C_a \left(\frac{z \times (h - z_a)}{z_a \times (h - z)} \right)^{r_i} \quad \text{(Eq. 3.2)}$$

where r_i= -w_{si}/(κ$u_{\star c}$) is the Rouse parameter for each grain size fraction, w_{si} is the particle settling velocity, $u_{\star c}$ is current shear velocity (=$\sqrt{\tau_{curr}/\rho}$), κ is von Karman's constant (0.41), h is water depth, z is the height in the water column at which C_{si} is being estimated. C_a is the reference concentration at the reference height z_a =3D_{50}, where D_{50} is the median grain size. The reference concentration (C_a) was calculated using Smith and McLean's (1977) equation:

$$C_a = C_{bed} \frac{\gamma S}{1 + \gamma S} \quad \text{(Eq. 3.3)}$$

where S=(τ_b – τ_{cr})/ τ_{cr} is the excess shear stress determined from τ_b, the wave-current (or total) bed shear stress. Critical shear stress was determined to be τ_{cr} =0.07 Pa by examining relationship between SSC and total shear stress. This value agrees with threshold for motion curves (Shields 1936; Miller et al. 1977). A value of γ=5e^{-4}, the resuspension coefficient, was chosen by adjusting the peaks in estimated

SSC to match the peaks in measured SSC. Field and laboratory studies have shown large variation in values of γ , ranging from 10^{-2} to 10^{-5} (e.g. Smith and McLean 1977; Wiberg and Smith 1983; Sternberg et al. 1986; Hill et al. 1988; Drake and Cacchione 1989). A value of C_{bed}=0.3, the bed concentration of the sediment, was used in Eq. 3.3.

SSC profiles calculated with Eq. 3.1 were used to estimate SSC in the upper portion of the water column when water depths exceeded the surface elevation of the marsh. This was necessary in order to accurately represent the amount of sediment advected across the bay-marsh boundary. In addition, total sediment mass within the water column was approximated by integrating the profile obtained using Eq. 3.1 for each time step (15 min, to conform to the measurement interval for waves, currents, and SSC). Total mass provided a way to account for sediment retained in suspension (i.e. not redeposited) between time steps in addition to accounting for sediment resuspension. This is important because sediment at our sites is very fine and settles slowly. Using three size fractions with varying settling velocities was used to provide a better estimate of the amount of material retained in suspension compared to a single size fraction.

Sediment Flux and Calculated Deposition

Sediment flux was calculated using the equation:

$$Q_s = \int_0^h U C_s dz \qquad \text{(Eq. 3.4)}$$

where U is average horizontal sediment velocity, assumed to be equal to fluid velocity, Cs is sediment mass concentration, and h is water depth. Measured current velocity and modeled SSC near the surface were used to approximate the amount of material crossing the bay-marsh boundary. For flux and deposition, currents and SSC were averaged over the depth of water flooding the marsh at each time step, such that one flux value was calculated at each time step. Flux differences were used to determine sediment deposition between the marsh edge and marsh interior. It was assumed that all sediment in suspension was deposited evenly over the marsh in the area between the marsh edge and marsh interior, roughly 15 m away. Deposition was calculated for 15 minute intervals, which was the length of time over which the flux difference was calculated. To estimate total deposition over the length of the 4 week deployment, average deposition per 15 minutes was multiplied by the total time the current direction was approximately perpendicular to the marsh edge (i.e. orientation of the sediment plates).

3.4 Results

Measured Sediment Deposition

At our Chimney Pole sites, no sediment deposited on the marsh surface near the edge (tbl 3.1). Maximum deposition occurred at the mid-marsh sediment plates (~8 m from the edge), and there was also some deposition further into the marsh interior (~15 m from the edge).

	Sediment Deposition (g cm^{-2})	
Location (Distance from edge)	**Nov-Dec 2013**	**March 2014**
Edge (~2 m)	0 ± 0	0 ± 0
Middle (~8 m)	0.024 ± 0.015	0.036 ± 0.009
Interior (~15 m)	0.001 ± 0.001	0.019 ± 0.01

Table 3.1: Average sediment deposited (g cm^{-2}) at three distances away from the bay-marsh boundary at transect B during the November-December 2013 and March 2014 deployments.

Sediment Characteristics

Grain size analysis revealed an overall decrease in mean particle size from the tidal flat to the marsh interior at site A, however this decrease was not linear. We recorded larger D_{16}, D_{50}, and D_{84} particle sizes at both the edge and mid-marsh relative to the tidal flat and interior (tbl 3.2, fig 3.2). At site B, grain size increased from the tidal flat to the marsh interior for the 3 size classes.

At all stations, approximately 16% of the bed is clay (<4 μm). At least 84% of the bed is silt (< 63 μm) or smaller at all stations except for the transect B middle and interior stations, where silt accounted for slightly less of the bed composition (> 75%). The remaining sediment was very fine-grained sand.

Sediment on the tidal flat has 7-9 % higher water and is composed of 1-3% more organic matter than sediment in the marsh interior (tbl. 3.3). Biomass was lower on the marsh edge and highest in the marsh interior at our sites. Low biomass at the edge coincided with low allochthonous sediment deposition.

Transect	Stations	D_{16}	D_{50}	w_s (m s^{-1}) for D_{50}	D_{84}
A	Tidal Flat	2.13 ± 0.26	12.56 ±2.82	1.07×10^{-4}	36.77 ±7.47
A	Marsh Edge	2.74 ± 0.66	18.73 ± 5.66	2.38×10^{-4}	51.08 ± 12.13
A	Marsh Middle	3.015 ± 0.54	21.51 ± 3.75	3.14×10^{-4}	57.72 ±12.13
A	Marsh Interior	1.68 ± 0.47	9.53 ± 4.74	6.17×10^{-5}	31.62 ± 14.67
B	Tidal Flat	2.10 ± 0.13	11.42 ± 1.22	8.86×10^{-5}	33.41 ± 5.95
B	Marsh Edge	2.19 ± 0.21	14.10 ±2.23	1.35×10^{-4}	44.01 ± 6.14
B	Marsh Middle	2.80 ± 0.57	21.64 ± 3.39	3.18×10^{-4}	67.26 ± 8.63
B	Marsh Interior	3.11 ± 0.50	21.64 ± 3.39	3.18×10^{-4}	67.26 ± 8.63

Table 3.2: Grain size (μm) averaged over 3 samples (9 subsamples) taken at each station. Values given are for the 16th, 50th, and 84th percentiles. Settling velocity (w_s) was estimated for D_{50} using Stokes' law

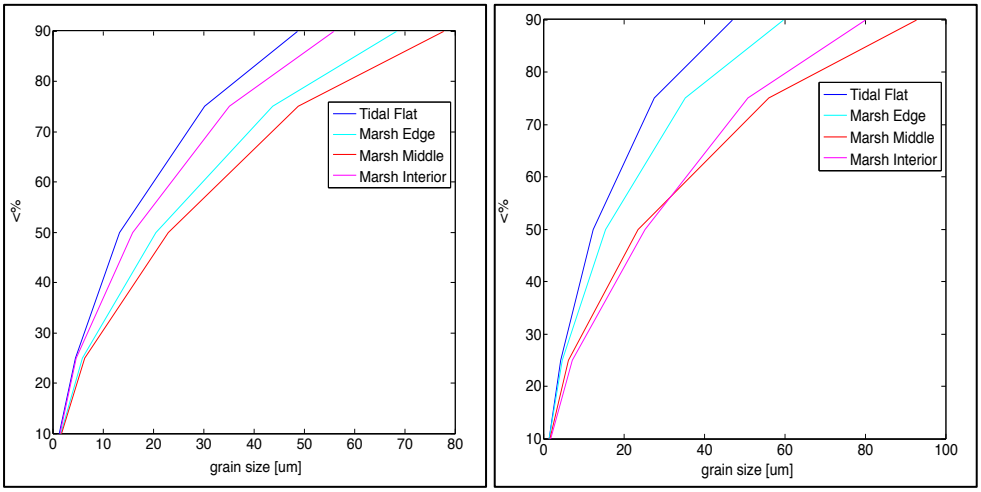

Figure 3.2: Percentage of sample less than a given grain size. Samples were taken from 4 stations along transect A (left) and transect B (right)

Site	Station	Water (%)	Organic Matter (%)	Biomass (g ft^{-2})
A	Tidal Flat	51.15 ± 3.58	8.18 ± 1.46	n/a
A	Edge	48.96 ± 4.48	11.24 ± 2.96	4.87 ± 1.11
A	Middle	49.28 ± 4.80	9.63 ± 1.77	6.16 ± 2.49
A	Interior	44.04 ± 1.24	5.97 ± 0.48	7.59 ± 3.83
B	Tidal Flat	47.66 ± 3.34	6.15 ± 1.81	n/a
B	Edge	44.39 ± 3.27	6.73 ± 1.02	4.05 ± 2.49
B	Middle	31.53 ± 4.36	3.32 ± 0.96	2.98 ± 0.49
B	Interior	38.47 ± 3.21	4.47 ± 5.2	6.37 ± 2.38

Table 3.3: Average water fraction (%) and average organic matter fraction (%) of sediment samples taken from each stations along transects A and B. Vegetation was sampled in November to yield average biomass (g ft^{-2}).

Sediment Resuspension

Tidally averaged SSC obtained from the OBS (0.35 mab) was positively correlated with tidally averaged significant wave height when waves exceeded 0.1 m (fig 3.3). In general, the relationship between SSC and wave height was similar at TAF, TBF, and TBB.

Measured SSC at all sites varied overtime in response to changing bottom shear stress (fig 3.4). On the tidal flat, SSC near the bed (0.35 mab) was 3 to 5 times higher than the background concentration (~65 mg L^{-1}) when relatively large wave events occurred during neap tide cycles. Background concentration depicted is slightly variable due to differences in instrumentation and calibration error, however background SSC ranged from 50 to 80 mg L^{-1}. On the tidal flat the correlation between SSC and wave-induced shear stress was 67%, whereas the correlation between SSC and current-generated shear stress was only 2%. Further away from the marsh edge in the bay (TBB), the correlation between SSC and wave shear stress was 51%. There were no current measurements taken at TBB.

Figure 3.5 shows the relationship between near-bed SSC and wave-generated shear stress at TBB and TBF. There was a positive correlation between SSC and wave-induced shear stress at TBF and TBB. The relationship between SSC and bottom shear stress is complicated by the fact that SSC remains elevated even after bed shear stress declines due to low settling velocities and changing tidal stage.

During large wave events in November, SSC on the tidal flat was 16-19% higher at TBF than TBB.

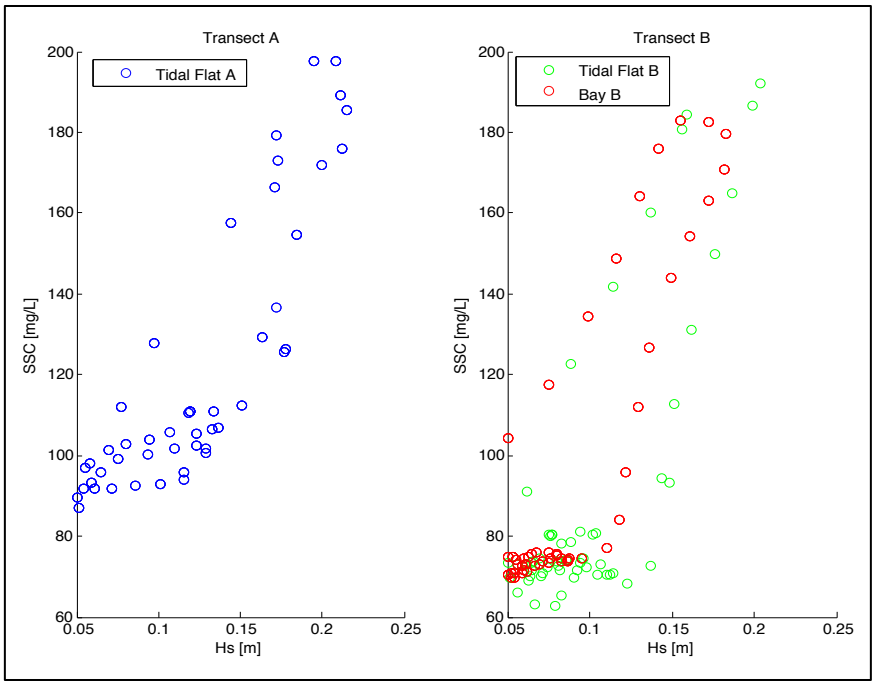

Figure 3.3: Relationship between tidally averaged significant wave height (m) and SSC (mg/L) recorded at TAF (left) and at TBB and TBF (right) during November-December 2013.

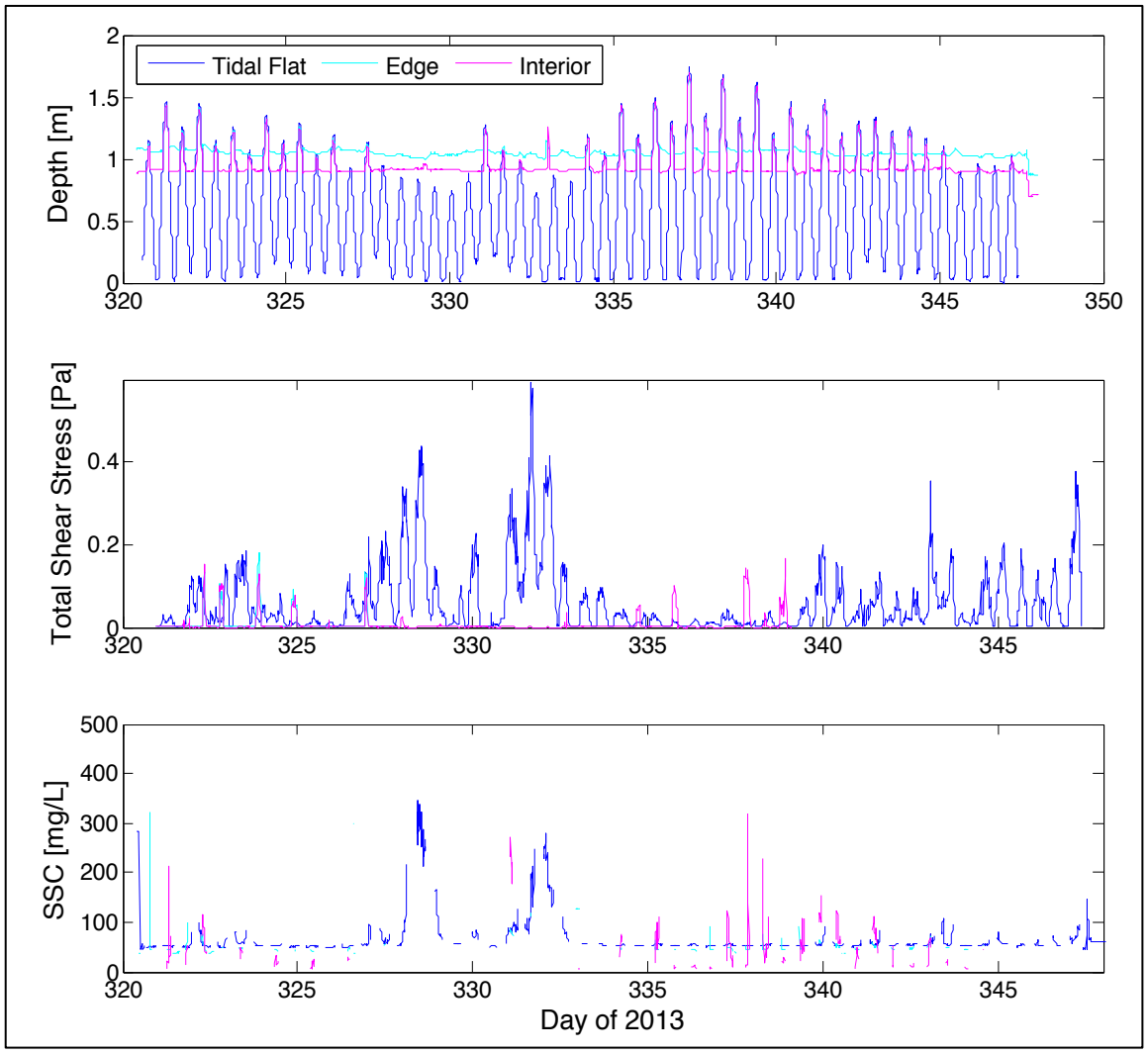

Figure 3.4: From top to bottom: depth (m), total shear stress (Pa) generated by both currents and waves, and SSC (mg L^{-1}) recorded at TBF, TBE, TBI during November-December 2013.

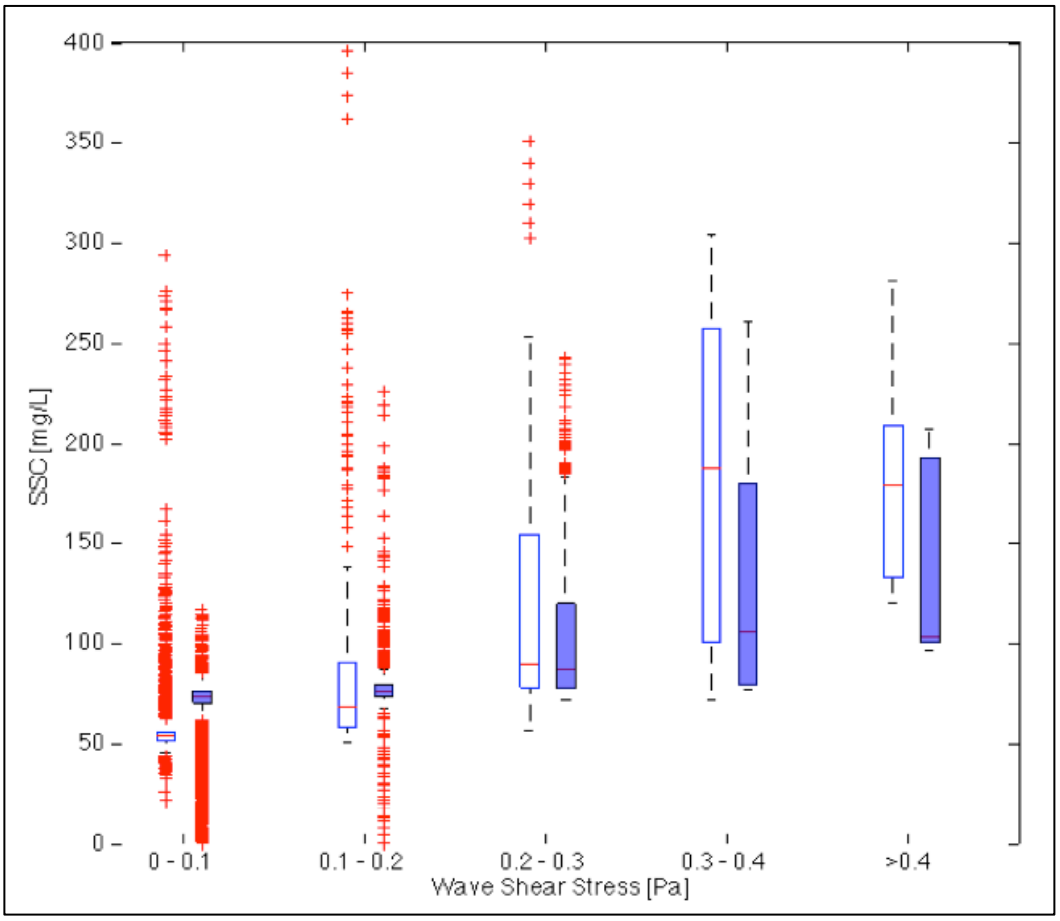

Figure 3.5: SSC (mg L^{-1}) as a function of wave shear stress (Pa) recorded at TBF (white) and TBB (blue) during November-December 2013.

SSC on the Marsh

The largest wave events did not elevate SSC over the marsh because the events occurred during neap tide when the marsh rarely flooded. During periods of marsh inundation, SSC recorded on the marsh was similar to the background concentration recorded on the tidal flat (fig. 3.4). SSC at the marsh edge was about 45% higher than SSC in the interior at transect B in November-December 2013. However, interior SSC was more variable (5-207 mg L^{-1}) than edge SSC (40-120 mg L^{-1}). Average sediment mass (= SSC x depth) was higher in the interior (30 g m^{-2}) than near the edge (19 g m^{-2}) in November-December 2013. At the edge and the

interior, the correlation between current and wave-generated bed shear stresses and SSC was less than 25%. The correlation between SSC at the edge and interior and current shear stress on the tidal flat is 27% and 16%, respectively. The correlation between SSC at the edge and interior and wave shear stress on the tidal flat is less than 1% and 7%, respectively.

Sediment Flux and Calculated Deposition

Sediment transport across the bay-marsh boundary relies on tidal inundation and advection by currents of SSC-bearing water from the flats to the marsh. In order to estimate sediment transport to the marsh, we must be able to adequately estimate SSC in the water flooding the marsh. Figures 3.6 and 3.7 show changes in recorded and calculated SSC in response to changing bottom shear stress at TBF and TAF. Overall, there was approximately a 50% correlation between recorded SSC and calculated SSC at 0.35 mab for both the 1 and 3 grain size fractions (fig 3.6). As indicated by the Rouse equation (Eq 3.1), SSC decreases with height above the bed at a rate dictated by the ratio of particle settling velocity to current shear velocity.

During neap tide the marsh does not flood unless there is a storm surge event (fig 3.8, 3.9). For example the marsh only flooded for approximately 6% and 15% of the May-June 2013 and March 2014 deployments, respectively. For the March deployment, of the 30 tidal cycles when the marsh flooded, 19 occurred during spring tide. During the May-June deployment, the marsh flooded during 9 tidal cycles, all of which occurred during spring tide.

SSC estimated near the water surface at TBF during March 2014 (3.8) and TAF during May-June 2013 (fig 3.9) were similar. Average sediment flux across the bay-marsh edge was comparable during May- June 2013 at TAF (2.9 g m^{-2} s^{-1}) and March 2014 at TBF (3 g m^{-2} s^{-1}) (fig 3.8, 3.9). Average sediment deposition was calculated to be 0.0019 ± 0.003 g cm^{-2} and 0.0083 ± 0.005 g cm^{-2} per 15 minutes that the flow was from the edge to the interior (tbl 3.4). Total calculated deposition for the 4 weeks was 0.032 g cm^{-2} for May and 0.025 g cm^{-2} for March.

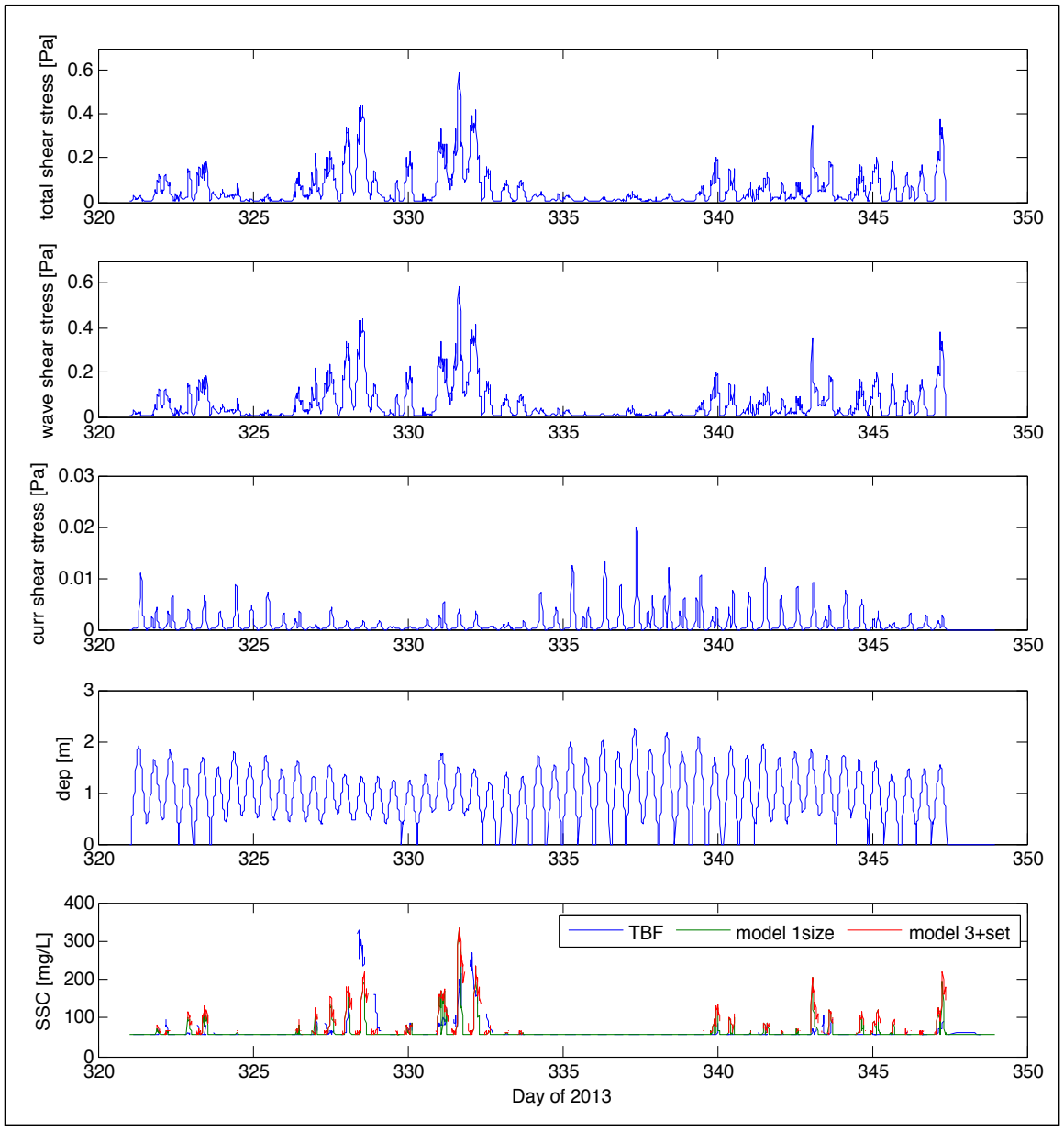

Figure 3.6: From top to bottom: total shear stress (Pa), wave shear stress (Pa), current shear stress (Pa), water depth (m), and SSC(mg L^{-1}) recorded and modeled at 0.35 mab. SSC was modeled using 1 grain size and 3 grain sizes. For the 3 grain size model, sediment settling between time steps was accounted for. Data were recorded at TBF during November-December 2013.

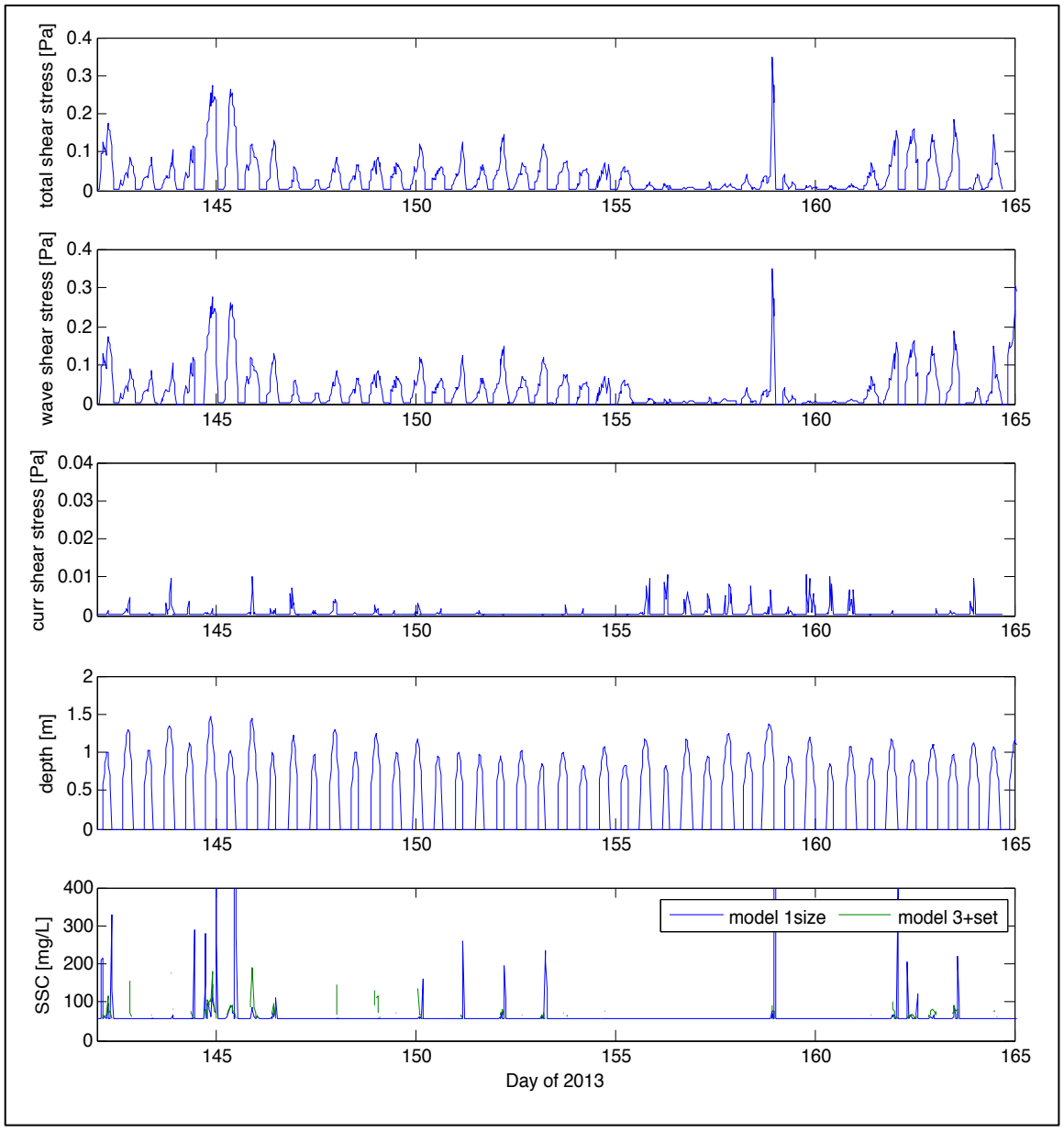

Figure 3.7: From top to bottom: total shear stress (Pa), wave shear stress (Pa), current shear stress (Pa), water depth (m), and modeled SSC (mg L^{-1}) at 0.35 mab. SSC was modeled using 1 grain size and 3 grain sizes. For the 3 grain size model, sediment settling between time steps was accounted for. Data were recorded at TAF during May-June 2013.

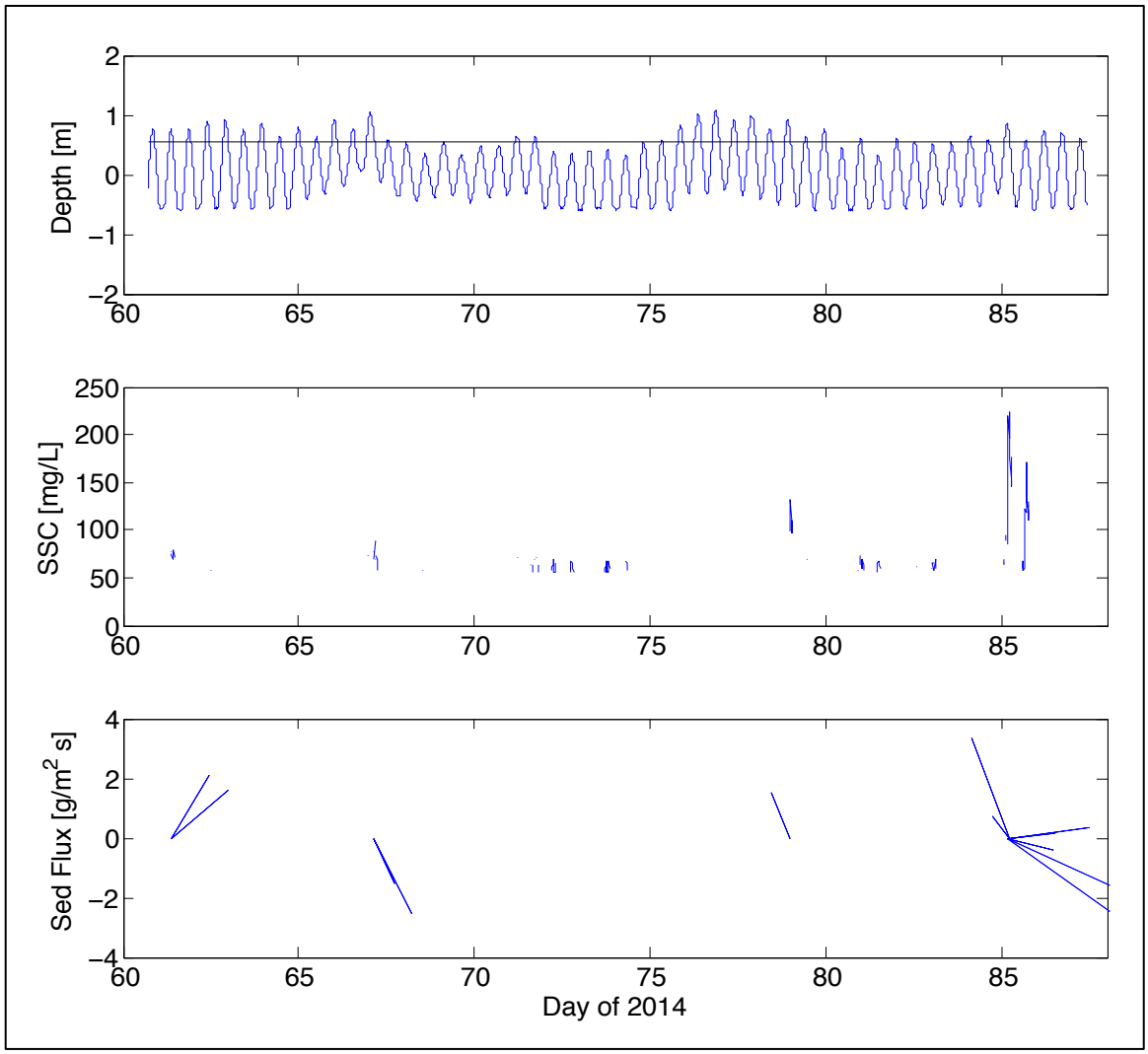

Figure 3.8: From top to bottom: Depth (m), SSC (mg L^{-1}) estimated at the top of the water column, and sediment flux (g m^{-2} s^{-1}) above the marsh platform height at TBF during March 2014. Flux shown is total flux in all directions.

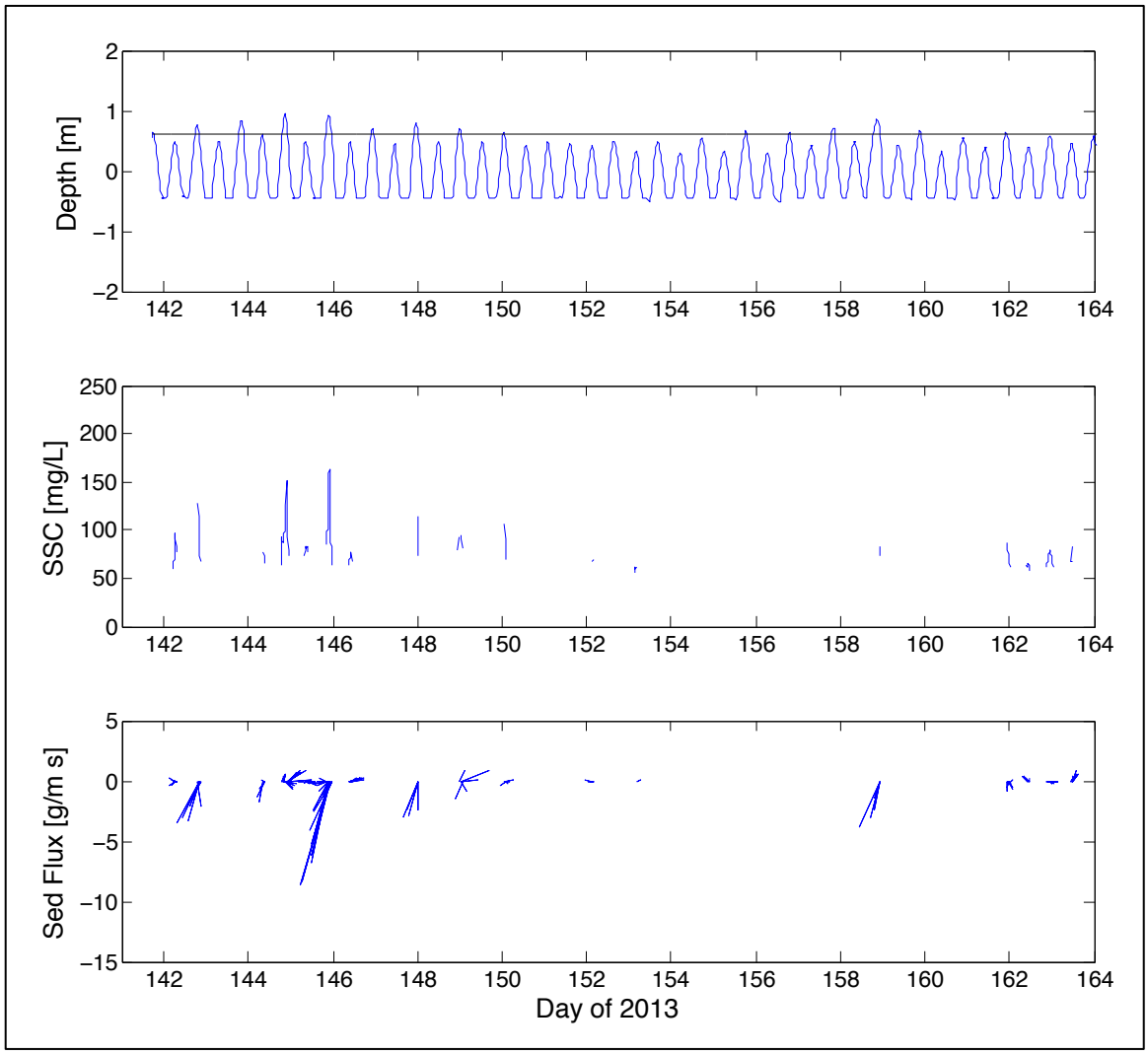

Figure 3.9: From top to bottom: Depth (m), SSC (mg L^{-1}) estimated at the top of the water column, and sediment flux (g m^{-2} s^{-1}) above the marsh platform height at TAF during the May-June 2013. Flux shown is total flux in all directions.

Deployment	Flux From:	Avg. Sed. Dep. (g cm^{-2}) per 15 min.	Avg. Sed. Dep. (g cm^{-2}) per 4 weeks
May 2013	TAF	0.0019 ± 0.003	0.025
March 2014	TBF	0.0083 ± 0.005	0.032

Table 3.4: Average sediment deposition calculated from sediment flux across the bay-marsh boundary at TBF and TAF. Assumes equal deposition from the edge to the interior.

3.5 Discussion

Sediment Deposition

In tidal creek marshes, maximum vegetation densities near the creek bank trap sediment and slow flow velocities, thus promoting sediment deposition. Maximum deposition in most tidal creek marshes occurs along the creek-marsh edge (Christiansen 1998), whereas maximum deposition at our site B occurred approximately 8 m away from the bay-marsh edge, with additional deposition further into the interior (tbl 3.5). Given that the dominant current direction on the marsh is southeast at TAI, TAE, and TBI, aligning the sediment plates in this direction rather than perpendicular to the edge might have allowed us to capture more sediment.

No deposition was recorded near the marsh edge during two separate deployments at transect B. Sediment deposition was not measured at transect A, however long-term SET records at transect A also indicate surface erosion along the marsh edge near Transect A (P.L. Wiberg, personal communication). Both sparse vegetation and the presence of wave action on the marsh surface near the edge likely inhibit sediment deposition or permit resuspension of any sediment that does deposit. As a result, currents carry sediment further into the marsh interior until a point where particles are able to settle onto the surface.

As shown in table 3.5, the amount of sediment deposited along the creek bank in Phillips creek marsh is similar to the amount deposited ~8 m away from the edge on Chimney Pole. However, the deposition occurred during two weeks at

Phillips Creek and during 4 weeks at Chimney Pole. Therefore, maximum deposition rates at Phillips Creek appear to be higher than at Chimney Pole.

Site:	Chimney Pole		Phillips Creek (Christiansen 1998)	
Measurement Interval	4 weeks		2 weeks	
Timing of Measurement	Nov 2013	Mar 2014	Feb 1998	May-Jul 1997
Deposition (g/cm^2) at edge	0	0	0.04	0.004-0.024
Deposition 7-8 m from edge	0.024	0.036	0.015	0.002-0.009

Table 3.5: Comparison of measured total deposition at Phillips Creek Marsh and Chimney Pole Marsh.

Sediment Characteristics

Organic matter lowers the bulk density of the sediment (Feagan et al. 2009), thereby increasing porosity. At the tidal flat and the interior, increased porosity due to higher organic content may have resulted in increased water content. Lawson (2004) and McLoughlin (2010) found a positive relationship between median grain size and organic content at Bay and Marsh sites in Hog Island Bay. However, our results do not confirm this. The dense upper layer of root mat at Chimney Pole complicated sediment collection at the edge and marsh middle stations.

At transect A, D_{16}, D_{50}, D_{84} sediment sizes increased from the marsh edge to the middle marsh, then decreased from the middle marsh to the interior. At transect B, $D_{16,}$ $D_{50,}$ and D_{84} sediment sizes increased from the edge to the interior. This is opposite to the trends found in tidal creek marshes, where grain size decreases with distance away from the creek bank due to larger particles settling out of suspension first.

At the marsh edge, wave shear stress exceeded threshold shear stress (0.07 Pa) 3% in May-June 2013 (TAE), 5% in November-December 2013 (TBE), and 16%

in March 2014 (TBE). In the marsh interior, wave shear stress exceeded threshold shear stress 1% in May-June 2013 (TAI) and 5% in November-December 2013 (TBI). It is possible that high shear stresses near the edge prevent particles from settling out of suspension. As a result, grains settle further into the marsh interior.

Based on shear stress alone, sediment remobilization on the marsh is possible, unlike tidal creek marshes where surface shear stresses are below the threshold of motion (Christiansen et al. 2000). However, if at least 7.5% of the bed sediment is clay-sized (< 4 μm), the bed typically behaves cohesively (van Ledden et al. 2004), which can increase the critical shear stress (Parchure & Mehta 1985; Mitchener & Torfs 1996) and alter size-selective particle entrainment from the bed (Law et al. 2013). On Chimney Pole, 16% of the bed was less than 4 μm at all sampling locations. Wave action on the marsh surface near the edge may also increase bed compaction and alter sediment strength. In addition, the marsh surface has a dense root system, which increases sediment shear strength and erosion resistance (Pestrong 1969). Together, these factors lower the likelihood of sediment remobilization on the marsh surface.

Sediment Resuspension

The amount of sediment in suspension depends on total bed shear stress due to waves and currents, shear velocity in the water column, and sediment characteristics of the bed (e.g. critical shear stress, porosity, and settling velocity). On the tidal flat, SSC and wave-induced shear stress are well correlated (67%), whereas SSC is not correlated with current shear stress (2%). In comparison to tidal

creek marshes where tides moving in and out of the creek are the primary mechanism of resuspension (Christiansen et al. 2000), waves primarily force resuspension in open-boundary marshes.

The highest SSC on the tidal flat and in the bay coincided with relatively large wave events generated by strong winds from the northwest. Although the waves produced SSCs in excess of 300 mg L^{-1}, very little sediment reached the marsh platform because the events occurred during neap tide cycle when the marsh flooded infrequently. As discussed in chapter 1, our results (in agreement with Fagherazzi & Wiberg 2013) show that bottom shear stress declines at elevation greater than 0.6 m, approximately the height of the marsh. Therefore, sediment delivery is likely low during large wave events when SSC is high. This is important for estimating the effect that such events have on marsh sediment accretion and is explored further in Chapter 4.

For wave shear stress greater than 0.1 Pa, SSC on the tidal flat is higher than SSC further out in the bay. This suggests that the critical shear stress required to move the bed is lower on the tidal flat than in bay. This may be attributable to differences in bed properties, which were not measured at TBB.

SSC on the Marsh

Similar to Chimney Pole, the marsh at Phillips Creek does not flood every tidal cycle. At Phillips Creek, maximum SSC recorded on the creek bank over a tidal cycle was generally between 20-110 mg L^{-1} (Christiansen 1998). SSC on the marsh edge of Chimney Pole falls within this range, as it is similar to the background

concentration in the bay (~65 mg L^{-1}). At Phillips Creek, variability in SSC decreased with distance away from the edge. Concentrations were between 20-50 mg L^{-1} at 7-8 m from the creek bank. At Chimney Pole, interior SSC was more variable (5-207 mg L^{-1}) than SSC at the edge (40-120 mg L^{-1}), which was typically higher than interior SSC when the marsh was flooded. Measurements suggest that SSC on the marsh is not well correlated with wave and current-generated bed shear stress on the tidal flat.

Sediment Flux and Calculated Deposition

Correlation between measured and modeled SSC for November-December 2013 (fig 3.6) was similar for both the 1 and 3 grain size calculations at 0.35 mab (~50%). Therefore, estimating SSC using multiple grain sizes and accounting for settling did not significantly improve correlation with recorded SSC near the bed. However, average estimated SSC near the surface is much lower for the 1 grain size model (62 mg L^{-1}) than the 3 grain size model (93 mg L^{-1}).

Average sediment flux across the boundary was similar during May and March. Calculated deposition for the May and March deployments was of the same order of magnitude as measured deposition. During March, the average sediment deposited between the marsh middle and interior was 0.028 g cm^{-2} measured by sediment plates and was 0.025 g cm^{-2} measured by flux. Deposition measurements were not made during May 2013 at transect A. Although calculated deposition for May was similar to recorded deposition in November and March, it may be over- or underestimating actual sediment deposition during May at site A. Lower flooding

frequency during May would have reduced deposition on the marsh, whereas higher biomass density during the summer would have promoted deposition. Also, the higher frequency of on-marsh currents moving sediment across the marsh edge at site A in May would have promoted sediment deposition. Overall, if current direction and SSC near the surface are accounted for, calculating sediment deposition from flux seems to provide a reasonable estimate of actual deposition on open-boundary marshes.

Chapter 4: Estimating Changes in Potential Deposition due to Sea-Level Rise & Storm Surge

4.1 Objectives

RSLR and storm surge increase water depth, thereby allowing larger waves to form. An objective of this research is: What impact will 21st century sea-level rise, stronger coastal storms, and accompanying changes in wave conditions have on mineral sediment deposition on marsh islands? To address this question, we implemented and evaluated a model for wind-wave generation in shallow water, and the results were used to calculate changes in wave-generated bottom shear stress with changing depth. We hypothesize that as water level and wave height increase over the tidal flat, bottom shear stress also increases up to a point where an optimum combination of water depth and wave height maximize wave-generated bottom shear stress. For water depths and wave heights higher than optimum, we predict that bottom shear stress declines. Calculations of wave-generated bottom shear stress were then combined with estimates of current shear velocity based on observations to calculate near-surface SSC using the methods outlined in Chapter 3. This allowed us to estimate potential deposition on the marsh under a range of wind and depth conditions.

4.2 Methods—Calculations

Wave Conditions

Data from meteorological and tidal stations allows for an estimation of

significant wave height and peak period using the Young-Verhagen (1996a, 1996b) parametric model for finite depth, fetch-limited wave growth. The nondimensional wave energy $\varepsilon = g^2E/U^4$ and the nondimensional peak frequency $\nu = fU/g$ are related to the nondimensional fetch $\chi = gx/U^2$ and the nondimensional water depth $\delta = gh/U^2$ through the expressions:

$$\varepsilon = 3.64x10^{-3}\left\{tanhA_1 tanh\left[\frac{B_1}{tanhA_1}\right]\right\}^{1.74} \quad \text{Eq. (4.1)}$$

where E is wave energy, U is wind speed at 10 m above the surface, f is wave frequency, x is fetch, h is water depth along the fetch, and

$$A_1 = 0.493\delta^{0.75} \quad \text{Eq. (4.2)}$$

$$B_1 = 3.13x10^{-3}\chi^{0.57} \quad \text{Eq. (4.3)}$$

and

$$\nu = 0.133\left\{tanhA_2 tanh\left[\frac{B_2}{tanhA_2}\right]\right\}^{-0.37} \quad \text{Eq. (4.4)}$$

where

$$A_2 = 0.331\delta^{1.01} \quad \text{Eq. (4.5)}$$

$$B_2 = 5.215x10^{-4}\chi^{0.73} \quad \text{Eq. (4.6)}$$

From this significant wave height H_s and peak period T can be calculated:

$$H_s = 4\sqrt{\frac{\varepsilon U^4}{g^2}} \quad \text{Eq. (4.7)}$$

$$T = \frac{1}{\frac{gv}{U}} \qquad \text{Eq. (4.8)}$$

The parameters that must be specified to carry out the wave height and peak period calculations are wind speed, water depth, and depth along the fetch. Waves are assumed to propagate in the direction of the wind. Wind direction and a digital elevation model (DEM) of Hog Island Bay and its surrounding area were used to calculate fetch and average depth along the fetch (Fagherazzi & Wiberg 2009; McLoughlin et al. 2014).

South Bay wind data and Wachapreague, VA tide data were used to calculate wave height and period during time periods overlapping with our observations. Tides measured at Wachapreague were multiplied by a previously determined factor of 1.1 to better represent conditions at Chimney Pole (McLoughlin et al. 2014). Wind data from South Bay were used because the station captured the most likely wind conditions in Hog Island Bay. The wind data were not multiplied by a scaling factor even though the gauge is situated at an elevation less than 10 m (~6-7 m). This is because calculated wave heights were best correlated with recorded wave heights when an adjustment factor was not used.

Bottom Orbital Velocity and Wave Shear Stress

Output from the Young-Verhagen model was used to estimate wave-induced bed shear stress. First, a full wave spectrum was estimated based on Hs, T, and the Donelan spectrum (Donelan et al. 1985), a modified form of the JONSWAP spectrum

(Wiberg & Sherwood 2008). Second, wave-generated orbital velocity was calculated for each frequency band *i* of the surface wave spectrum S_n as (Wiberg & Sherwood 2008):

$$u_b^2 = 2\sum_i S_{u,i}\Delta f_i \qquad \text{Eq. (4.9)}$$

where

$$S_{u,i} = \frac{4\pi^2}{T_i^2 sinh^2(k_i h)} S_{n,i} \qquad \text{Eq. (4.10)}$$

and *f* is frequency (=1/*T*), *h* is depth, and *k* is wave number. Wave-generated bed shear stress was calculated from orbital velocity using Eq. 2.5.

Currents

Currents were estimated at TAF and TBF using the relationship between recorded wind and currents, and accounting for the effect of edge orientation on current direction. Time series of observed depths and currents were divided into individual tidal cycles and separated by wind direction, and then overlaid. This allowed for the determination of variation in current velocity throughout a tidal cycle given either northerly winds or southerly winds. Current direction was rotated by 25° at TAF and TBF to account for the effect of edge orientation on current direction. South Bay winds and Wachapreague depth data were used in the approximation. Given the less variable nature of currents at TAF, we have greater confidence in our estimate of current velocity and direction at that site.

SSC

To evaluate SSC in shallow water, modeled waves and modeled currents were used to calculate total shear stress and current shear velocity (Eq. 2.1 & 2.5). These calculations were inputted into the Rouse equation (Eq. 3.2), which allows for an estimation of SSC at times when direct observations are unavailable.

To estimate potential deposition under a range of wind and depth conditions, average values of current shear stress (= 9.4 x 10^{-4} Pa) and shear velocity (= 8.1 x 10^{-4} m s^{-1}) were calculated for our sites during the period of observation. These values were inputted into the Rouse equation, along with wave shear stress, in order to estimate SSC. Total sediment mass in the upper water column was approximated by integrating the Rouse profile at water elevations above the marsh height. This provided an estimation of mass available for potential deposition on the marsh.

4.3 Results

Wave Conditions

There is a 77% and 71% correlation between modeled and recorded wave heights at TAF (fig. 4.1) and TBF (fig. 4.2), respectively. For wind speeds greater than 5 m s^{-1}, at both sites the model slightly overestimates waves when the wind blows from the west and north (225°-360° & 0°-45°), and underestimates waves when the wind blows from the east and south (90°-225°) (fig 4.3, 4.4). During the two large resuspension events that occurred in November-December 2013, recorded wave heights were 19% lower around day 328 and 5% higher around day 332 than estimated wave heights at TBF. At TAF, recorded wave heights were 16%

lower around day 328 and less than 1% lower around day 332 than estimated wave heights.

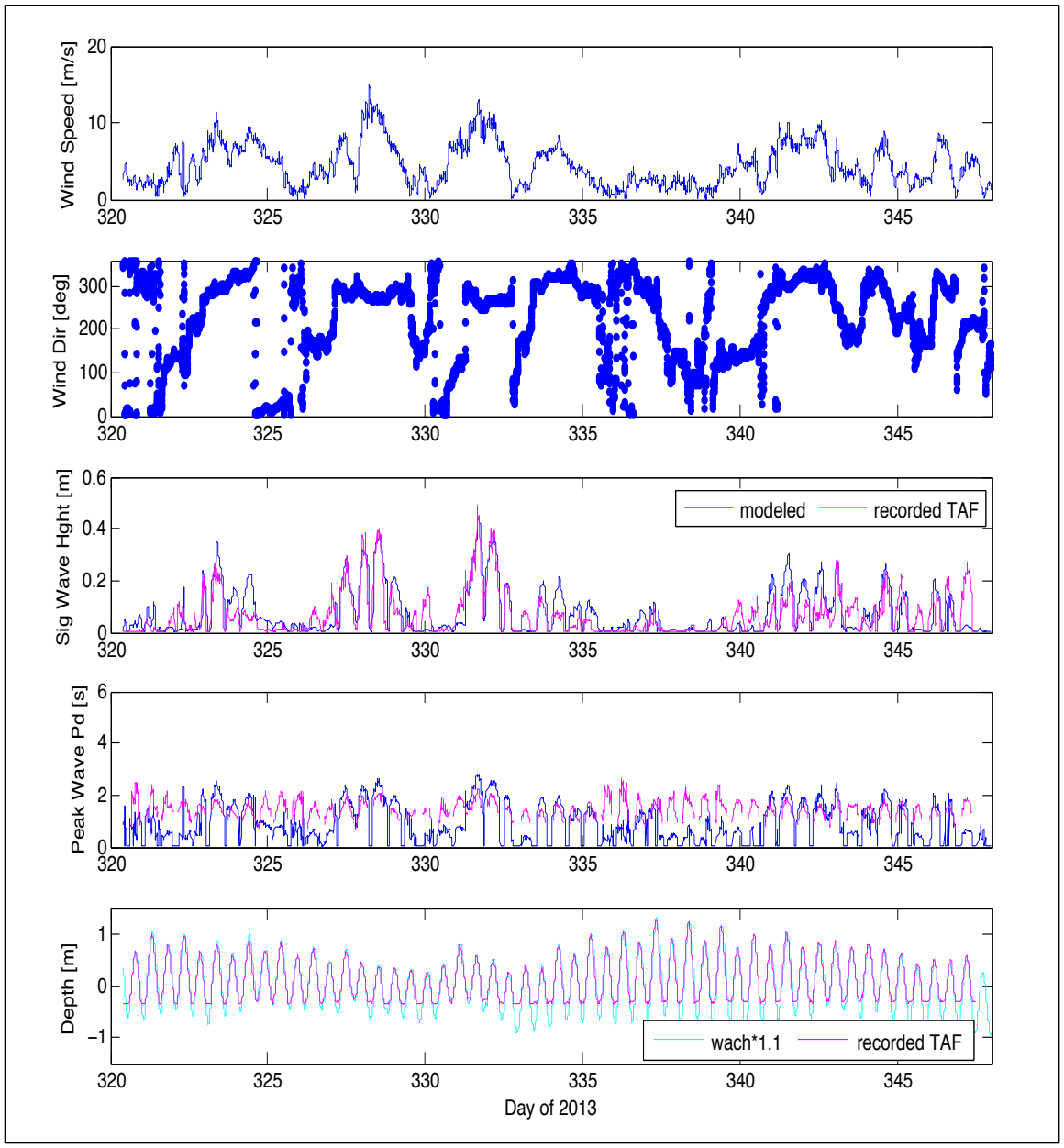

Figure 4.1: From top to bottom: wind speed (m s^{-1}) and wind direction (degrees) recorded in South Bay; significant wave height (m) and peak period (s) recorded at TAF and predicted using the Young-Verhagen model, and depth (m) relative to MSL recorded at TAF and at Wachapreague (multiplied by a scaling factor of 1.1).

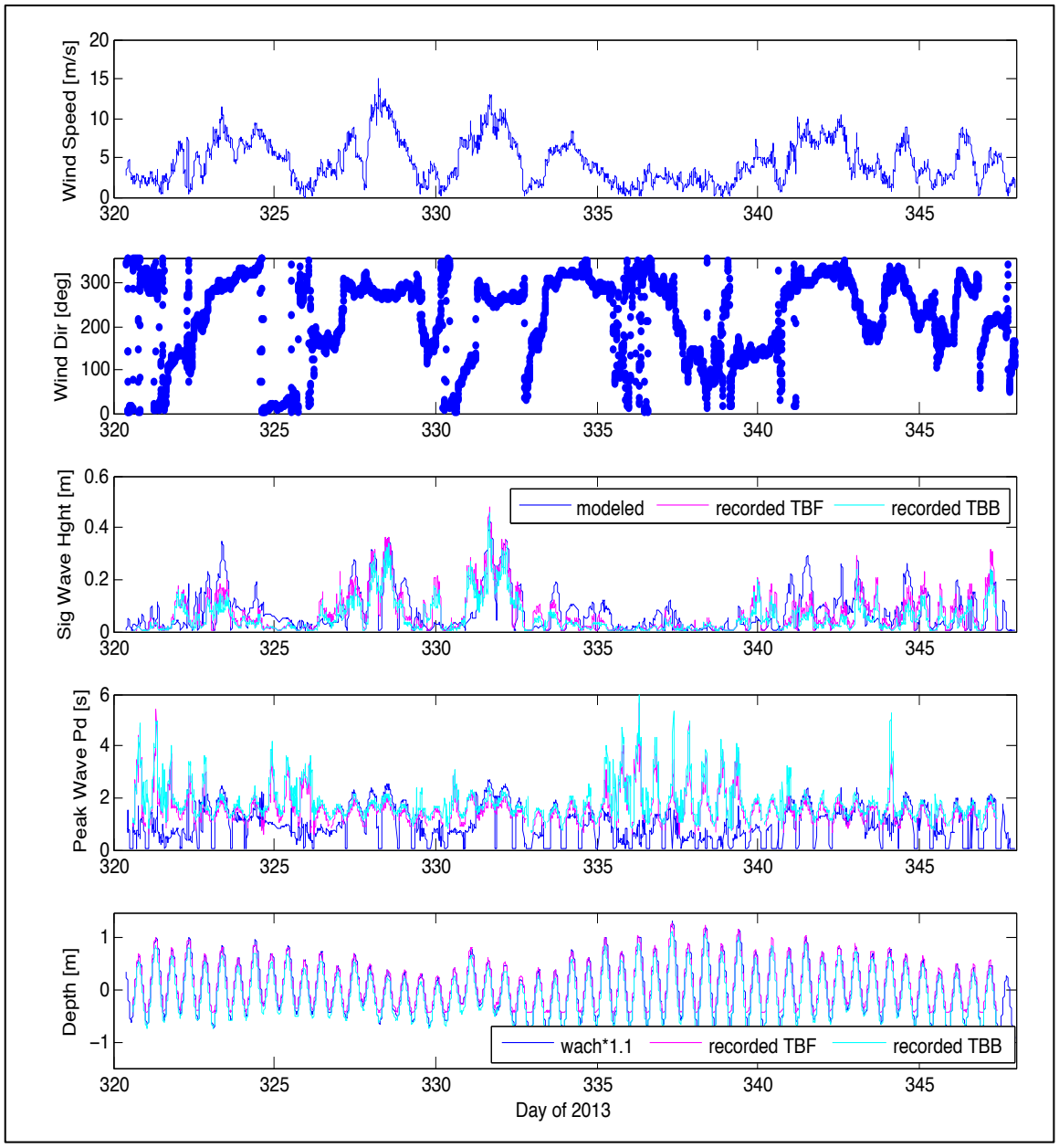

Figure 4.2: From top to bottom: wind speed (m s^{-1}) and wind direction (degrees) recorded in South Bay; significant wave height (m) and peak period (s) recorded at TBF, TBB and predicted using the Young-Verhagen model, and depth (m) relative to MSL recorded at TBF, TBB and at Wachapreague (multiplied by a scaling factor of 1.1).

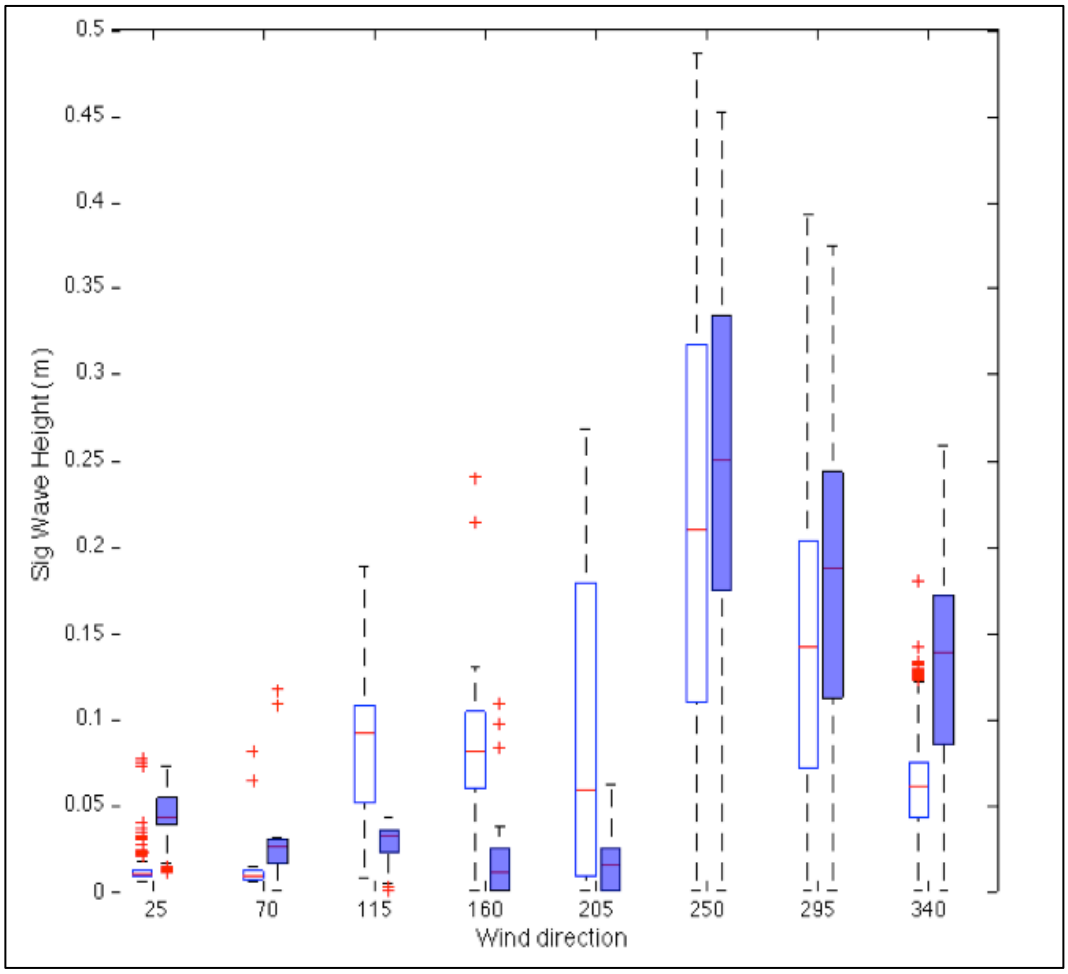

Figure 4.3: Comparison of modeled (blue) and recorded (white) significant wave height at TAF for times when wind speed exceeds 5 m s^{-1} during November-December 2013.

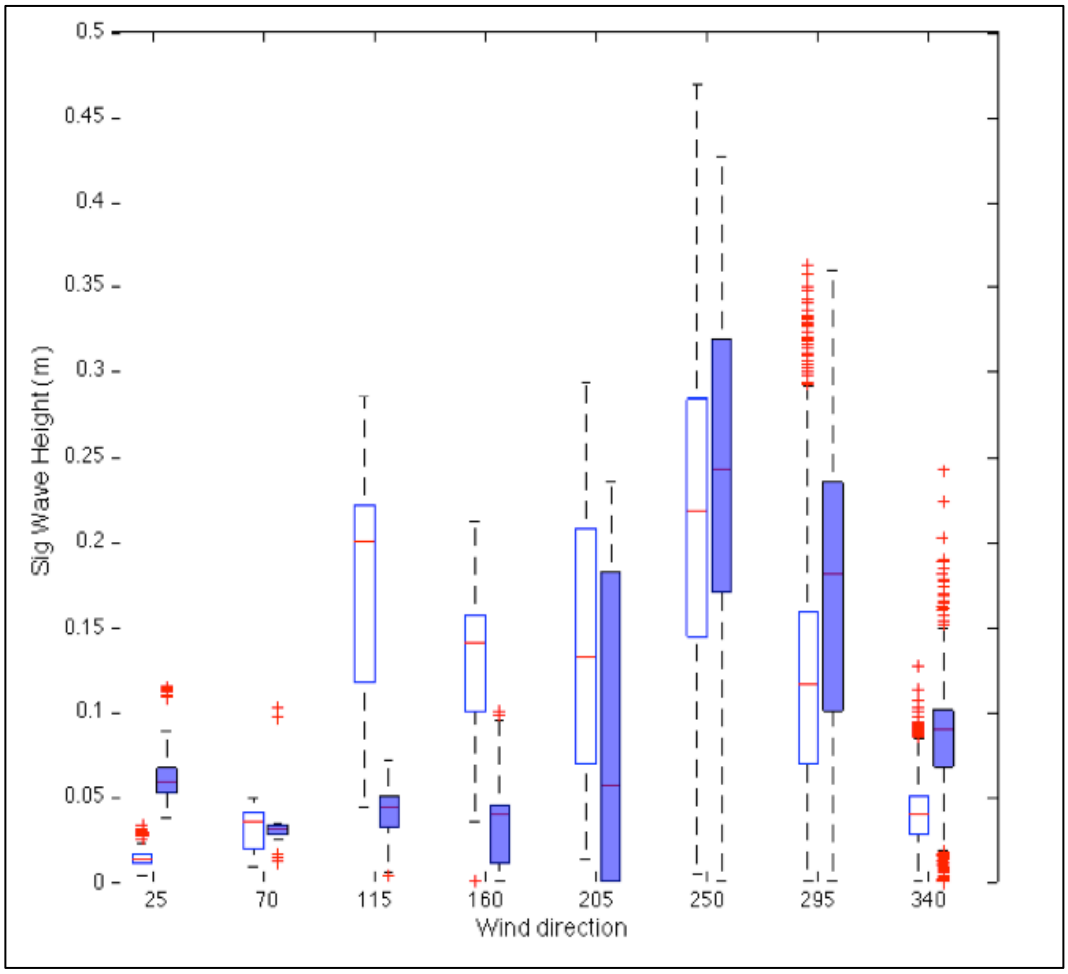

Figure 4.4: Comparison of modeled (blue) and recorded (white) significant wave height at TBF for times when wind speed exceeds 5 m s^{-1} during November-December 2013.

Currents

Fig 4.5 shows recorded and modeled currents at TAF for the May-June 2013 deployment. There is a 75% correlation between recorded and modeled currents during times of southerly winds and the approximately the same correlation during periods of northerly winds. Currents at the site follow an alternating northward flood, southward ebb pattern in the presence of southerly winds, but flow southward in the presence of northerly winds.

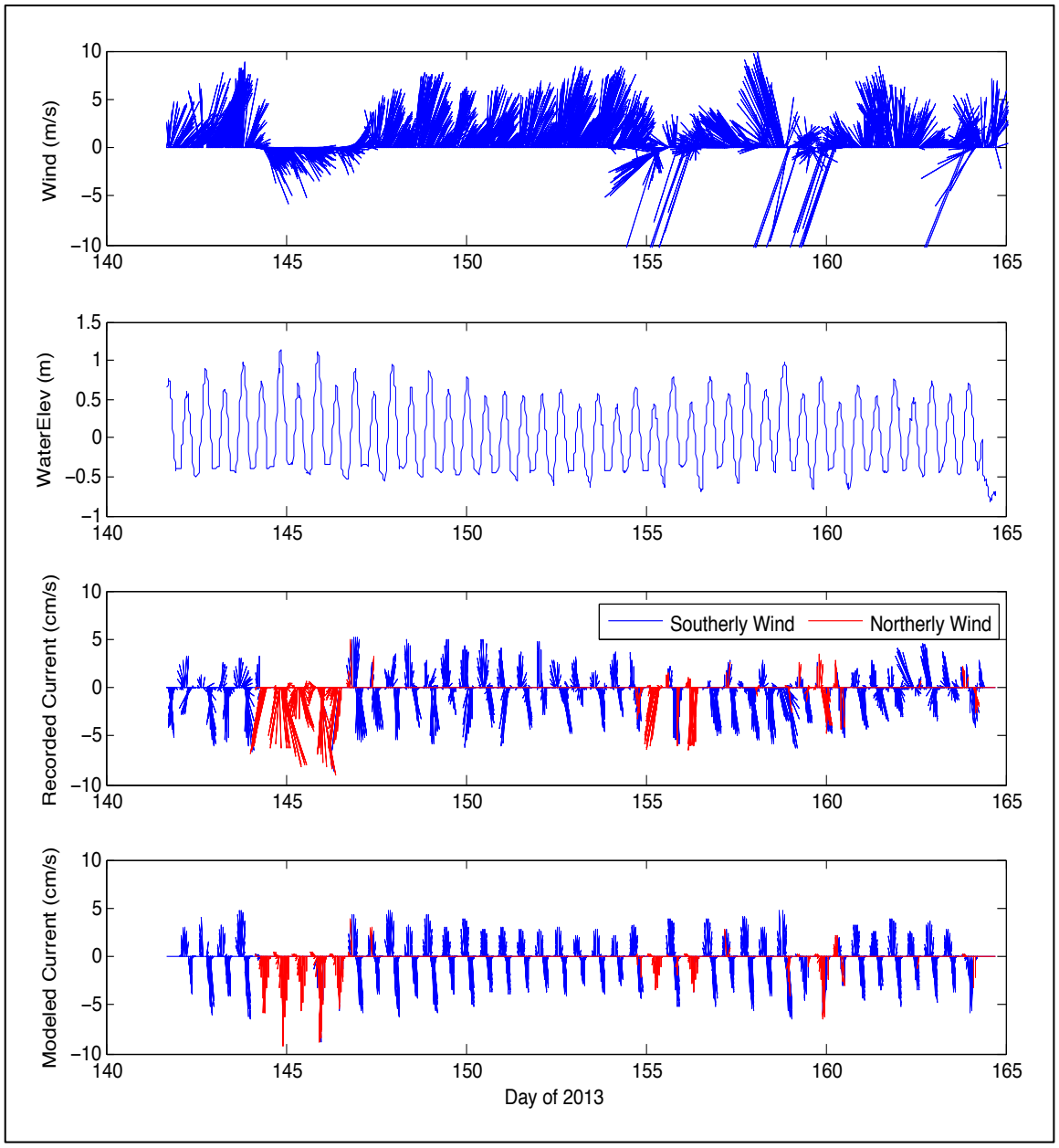

Figure 4.5: From top to bottom: wind speed (m s^{-1}) recorded in South Bay and plotted as the direction towards which the wind is blowing; depth (m) relative to MSL recorded at Wachapreague; and recorded and modeled current speed (cm s^{-1}) plotted as the direction the water is flowing towards and separated by wind direction. Currents were recorded at TAF during May-June 2013 and were modeled for the same site.

SSC

Using the Rouse equation, SSC was estimated from modeled waves and modeled currents (fig 4.6). Overall, there was a 39% correlation between recorded SSC at TBF and modeled SSC for the 3 grain size model at 0.35 mab.

On day 328, wave-generated shear stress calculated from recorded waves was 13% higher than wave shear stress calculated from modeled waves, despite lower recorded wave heights. As discussed below, this is likely attributable to longer recorded wave period. On day 332, wave shear stress calculated using recorded waves was 33% higher than wave shear stress calculated for modeled waves. Recorded SSC was 10-20% higher (at 0.35 mab) than estimated SSC during these two events likely due to higher bed shear stress (fig 4.6). However, mean SSC near the surface estimated using measured waves and currents was roughly the same as mean SSC estimated using modeled waves and currents (~93 mg L^{-1}), and the correlation between the two variables was 68%.

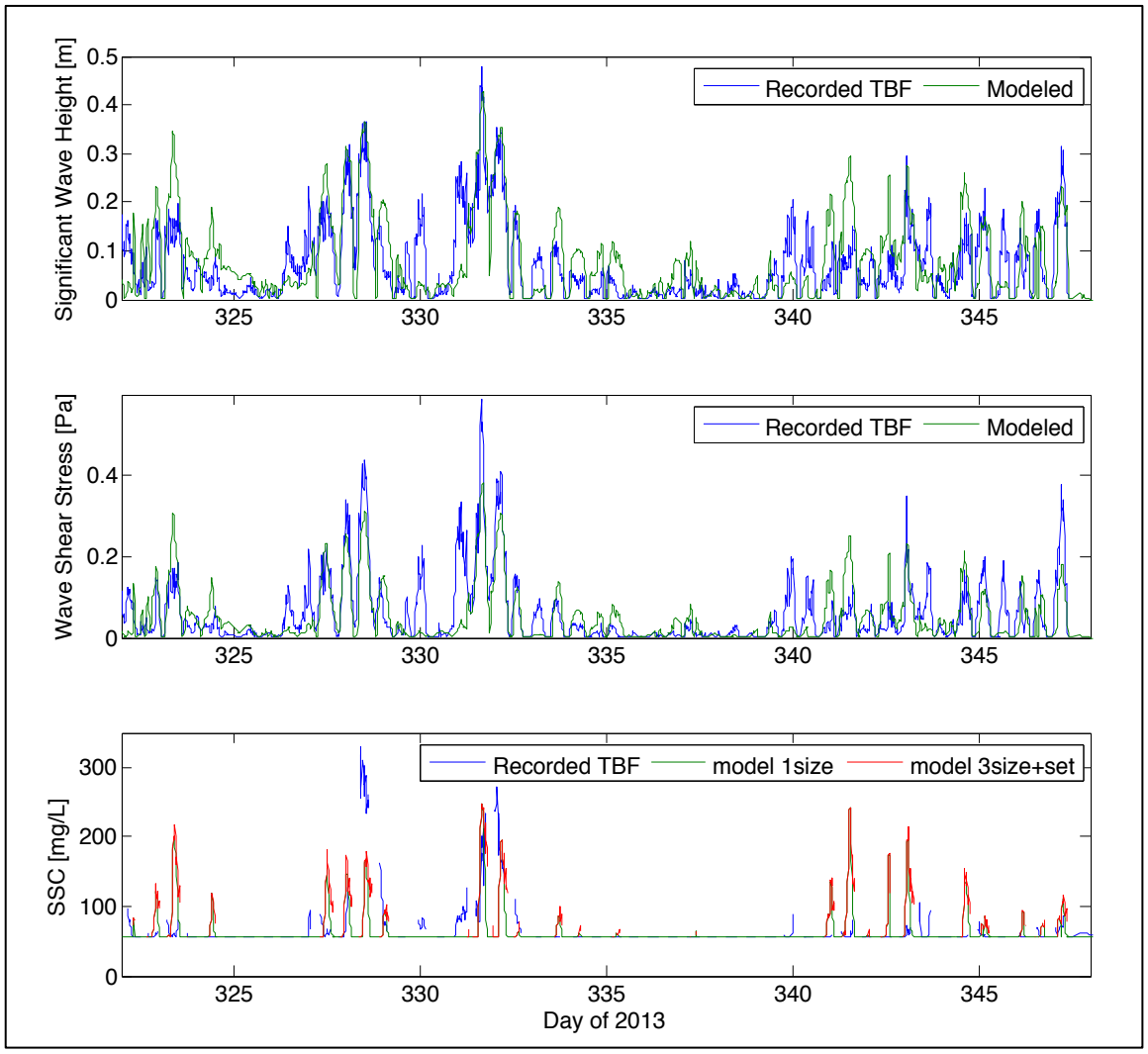

Figure 4.6: Top panel: Significant wave height (m) recorded at TBF and estimated using the Young-Verhagen model. Middle panel: Wave shear stress (Pa) calculated using recorded waves at TBF and estimated waves. Bottom panel: SSC at 0.35 mab recorded at TBF and estimated using modeled waves and modeled currents. SSC was calculated using either 1 or 3 grain sizes. For the 3 grain size model, sediment settling between time steps was also accounted for.

Effect of Water Depth on Wave-Generated Bed Shear Stress.

Figure 4.7 shows predicted changes in wave shear stress under elevated depth conditions, which could be due to storm surge or RSLR. Wave shear stress was estimated using a 10 km fetch (consistent with the fetch for winds from the west and northwest) and 3 wind speeds (5 m s^{-1}, 10 m s^{-1}, and 15 m s^{-1}). For a given

depth, wave shear stress is highest for the high wind speed group and lowest for the low wind speed group. As wind speed increases, the depth at which wave shear stress is maximized also increases. Maximum wave shear stress occurs at water depths of 0.6 m (τ_{wave}=0.11), 1.2m (τ_{wave}=0.56), and 1.6m (τ_{wave}=1.02) for the low, medium, and high wind speed scenarios, respectively.

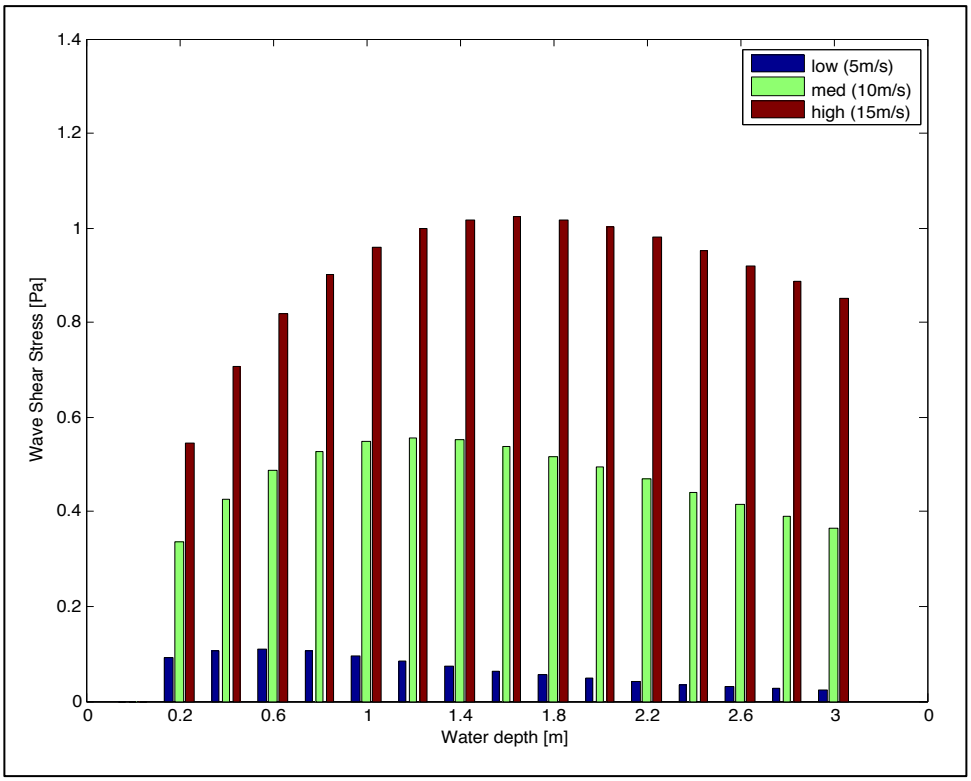

Figure 4.7: Wave shear stress (Pa) at various depths (m) calculated using a full wave spectrum. A fetch of 10km and 3 wind speeds (5 m/s, 10m/s, and 15m/s) were inputted into the Young-Verhagen model to estimate H_s and T.

Effect of Water Depth on Potential Deposition

Given the relationship between depth and wave shear stress shown in figure 4.7, changes in SSC (fig 4.8) and sediment mass (fig 4.9) were estimated for water depths greater than the marsh height. No results are shown for water depths of 1.0

m and below because this is less than the elevation of the marsh (assuming a mean water depth below MSL of -0.5 m and a marsh elevation above MSL of 0.5 m). Maximum SSC during medium and high wind speeds occurs at depths of 1.2 and 1.8 m, respectively, following the trends found in wave-generated bottom shear stresses (fig 4.8). SSC for the low wind speed group is essentially equal to the background concentration (~65 mg L^{-1}).

Assuming the marsh remains at its current elevation, sediment mass in the upper water column increases at depths higher than the depth associated with maximum bed shear stress due to increased depth of the water flooding the marsh, despite slightly lower SSC (fig 4.9).

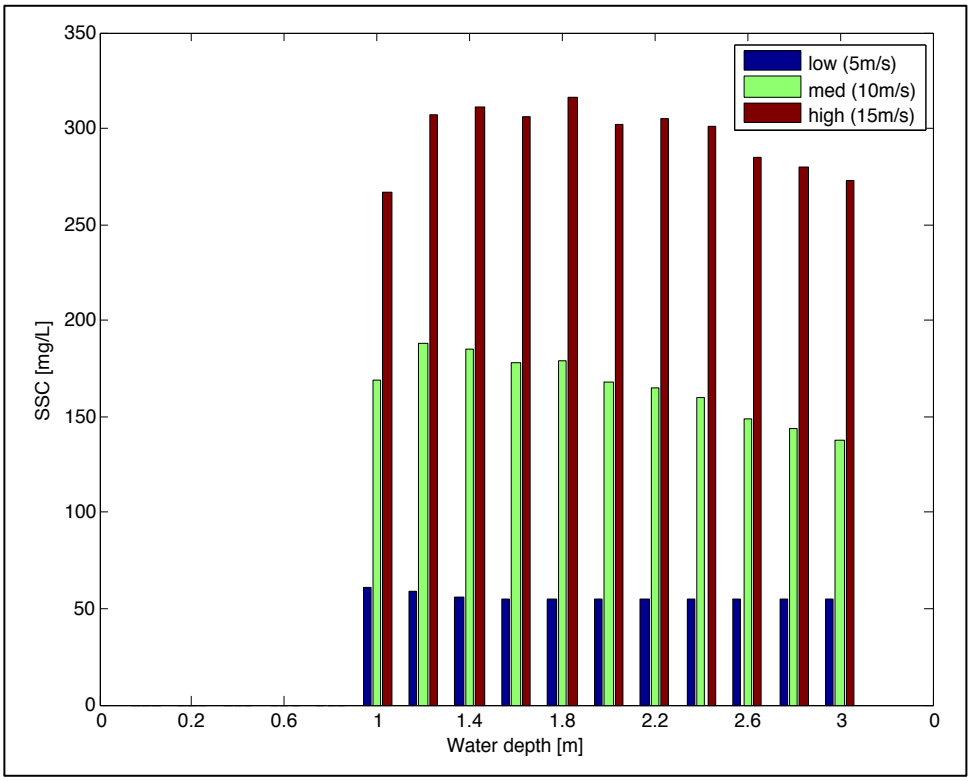

Figure 4.8: Change in SSC (mg L^{-1}) at elevations above the marsh platform height

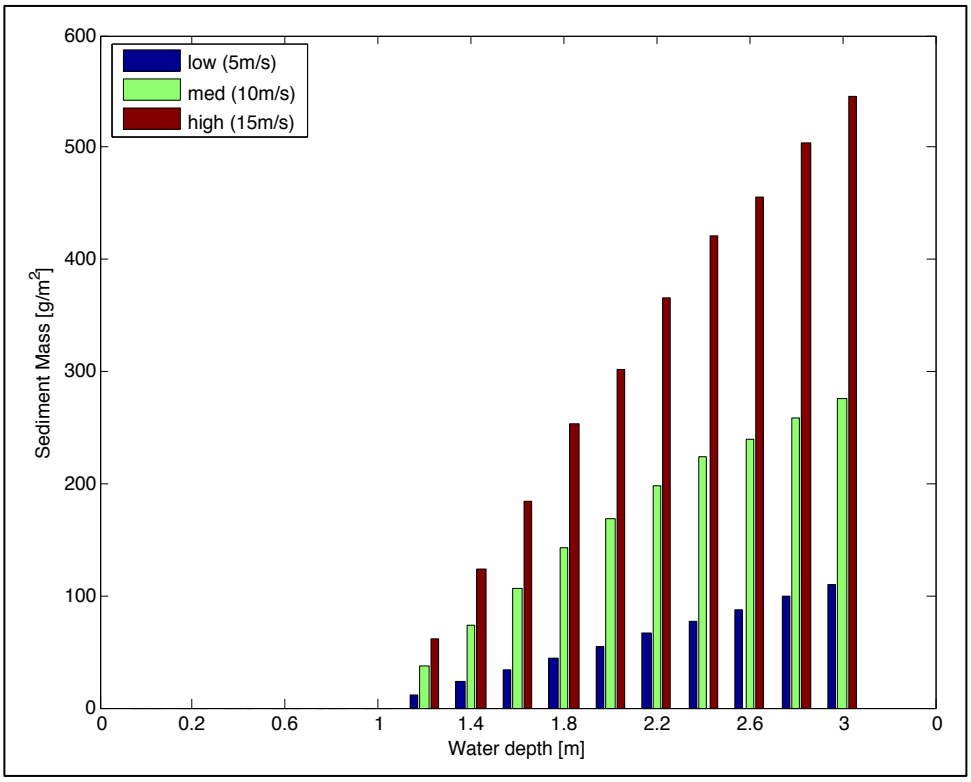

Figure 4.9: Change in sediment mass (g m^{-2}) with depth for water flooding the marsh platform. Assumes the marsh platform height remains at its current elevation (1.0 m)

4.4 Discussion

Wave Conditions

Overall, the Young-Verhagen wave model provides a good estimate of significant wave height at our Chimney Pole sites. The correlation is poorer during times when there were no waves at the sites (day 336 to 339), likely due to the model's overestimation of peak wave period. The model slightly overestimates waves when the wind blows from the west and north (225°-360° & 0°-45°) and underestimates waves when the wind blows from the east and south (90°-225°). This could be attributable to our calculation of fetch, which varies with wind direction. Despite overestimated wave heights during the large resuspension event

that occurred around day 328, measured SSC was still 20% higher than estimated SSC due to higher wave shear stress. Higher recorded wave shear stress recorded on the tidal flat, despite smaller recorded wave heights, is likely attributable to longer observed wave periods relative to modeled wave periods. For November-December 2013, average recorded wave period was 1.65 seconds whereas average modeled wave period was 0.96 seconds.

Effect of Water Depth on Wave-Generated Bed Shear Stress.

Given a fetch of 10 km and high wind speed conditions, maximum wave stress occurs at a depth of 1.6 m. For comparison, during March 2014, depth at TBF only exceeded 1.4 m for 25% of tidal cycles, which almost exclusively occurred when storm surge coincided with spring tide (see fig 2.3). In the Virginia coastal bays, high storm surge is typically associated with winds blowing from the northeast (Fagherazzi & Wiberg 2009, Mariotti et al. 2010).

During May-June 2013, a time of limited northerly winds (see fig 2.18) and storm surge, depth at TBF only exceeded 1.4 m for 3% of tidal cycles. A northeast wind direction is associated with low fetch at our Chimney Pole sites. For example, mean fetch calculated for northeast winds (0°-90°) when water depth exceeded the marsh elevation was 0.29 km for site A and 0.37 km for site B in November 2013 (tbl 4.1). Therefore, maximum wave shear stress for high wind speed conditions will not likely be reached via storm surge because fetch will be much less than 10 km.

Moderate increases in sea level will force water levels to more frequently exceed 1.4-1.8 m, depths associated with the highest wave shear stress. Increased

depth due to SLR would not depend on wind direction, thereby allowing for both large fetch and depth when winds blow from a westerly direction (tbl 4.1). Based on the model, large increases in RSLR will decrease wave shear stress for all wind speed groups, thereby decreasing SSC on the tidal flat.

Although high wind speed conditions generate the largest wave shear stress, the moderate wind speed scenario may be more likely. Wind speeds of 10 m s^{-1} occur more frequently than wind speeds of 15 m s^{-1}. Observations from 2013 indicate that wind speeds exceeded 10 m s^{-1} 3.5% of the year (fig 4.10), whereas wind speeds exceeded 15 m s^{-1} less than 1% of the year. Maximum wave shear stress under moderate wind speeds is much more likely to be met given that the maximum occurs at a depth of 1.2 m, and the current marsh height is approximately 1 m above the tidal flat.

In comparison, for the high wind speed scenario maximum wave shear stress occurs at a depth of 1.6 m. It is less likely that this maximum will be reached in the next few decades. At a SLR rate of 4 mm yr^{-1}, a 0.4 m change in water depth would take 100 years to occur. Over this time scale, dramatic landscape change would likely take place, especially considering that some sections of the edge are eroding laterally at rates greater than 2 m yr^{-1} (McLoughlin et al. 2014). Even if wind speeds increase by 2 m s^{-1} within the next half-century (Young et al. 2011), wind speeds of 15 m s^{-1} will still be uncommon. Interestingly, 91% of the time when wind speed exceeded 15 m s^{-1} in 2013, wind direction was between 270-360° (W-NW), indicating that a long fetch often accompanies high wind speeds at the study site.

Wind direction	Mean Fetch (km) at site A (h>=0.65)	Mean Fetch (km) at site B (h>=0.55)
NE (0° - 90°)	0.29	0.37
SE (90° - 180°)	0.19	0.39
SW (180° - 270°)	6.4	7.9
NW (270° - 360°)	5.4	4.6

Table 4.1: Mean fetch (km) by wind direction (degrees) for times when water elevation exceeds the platform height at sites A and B calculated for the November-December 2013 deployment.

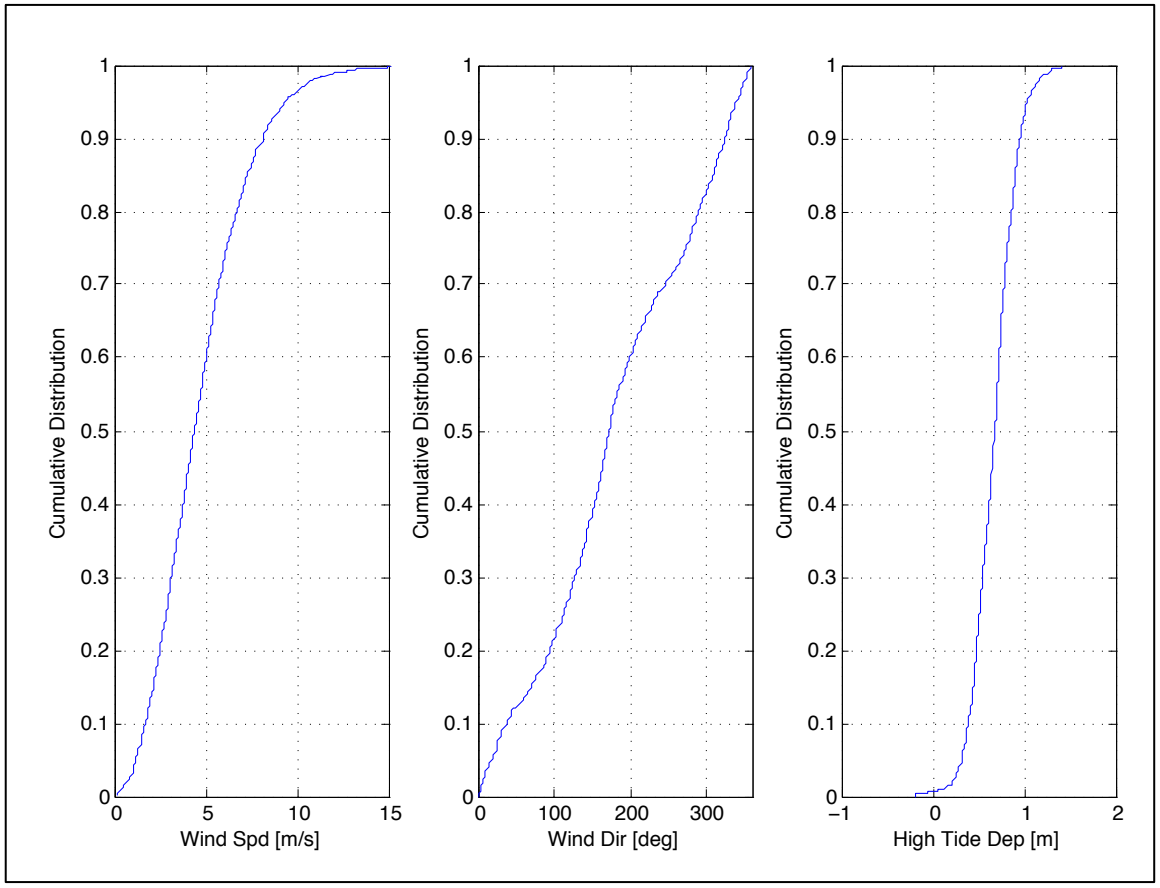

Figure 4.10: From left to right: Cumulative distribution of wind speed (m s^{-1}) and wind direction (degrees) recorded in South Bay, and depth at high tide (m) relative to MSL recorded at Wachapreague for the year of 2013.

Effect of Water Depth on Potential Deposition

Changes in near-surface SSC as water depth increases roughly parallel changes in wave shear stress. Given that wave shear stress primarily determines SSC, it is expected that maximum SSC will occur at water depths corresponding to maximum bottom shear stress.

If the marsh elevation remains constant, increased water depth on the marsh surface increases the sediment mass in the water column, thus increasing potential deposition. However, this is highly dependent on the elevation of the marsh, which would increase if the marsh keeps pace with sea-level rise. If this happens then the depth of the water flooding the marsh would remain constant as total depth increases and SSC decreases. This would result in decreased sediment mass at elevations higher than the depth associated with maximum bed shear stress. In this case, changes in sediment mass as water depth increases would parallel changes in wave shear stress and SSC.

For storm surge conditions, it is assumed that the elevation of the marsh does not change with depth. Therefore, as total depth increases the depth of the water flooding the marsh also increases. Based on our observations, near surface SSC during storm surge likely mirrors the background concentration due to little wave activity, regardless of total water depth. Constant SSC and increased depth of water flooding the marsh would increase sediment mass as storm surge increases. While storm surge could augment water elevation above typical spring tide levels (~0.8-1 m above MSL), thereby increasing potential deposition, the effects of storm

surge versus peak spring tide on SSC are uncertain because they were not separated in our analysis of the observations.

Conclusion

The results from this study indicate a strong correlation between wind direction and wave formation, whereby the largest waves form when westerly winds blow across Hog Island Bay at relatively high speeds (> 8 m s^{-1}). During this study, large waves at our sites on Chimney Pole did not coincide with storm surge conditions, likely due to the fact that storm surge in the Virginia coastal bays generally occurs when winds blow from the northeast, a direction associated with very short fetch at our sites.

As waves propagated from Hog Island Bay onto the tidal flat, wave height increased. The combination of higher waves and shallower depths increased wave shear stress on the tidal flat relative to the lagoon. Given strong westerly winds, maximum bed shear stress on the tidal flat occurred at water elevations between MSL and MHHW, the range associated with stable marsh platforms. Above MHHW, bottom shear stress declined. The wave events that generated the greatest bottom shear stress and SSC occurred during neap tide cycle when the marsh flooded infrequently. This is significant given that SSC at the top of the water column was much higher during times of westerly winds exceeding 8 m s^{-1} than during all other times.

Like waves, current patterns on the tidal flat are also correlated with wind conditions. More typical southerly winds are associated with a northward flood, southward ebb current pattern. On the other hand, stronger northerly winds push currents southward regardless of tidal phase. In addition to winds, the marsh edge

influences current direction by steering currents along the scarp at water elevations below the marsh platform height.

On the marsh, tidal creeks complicate current patterns. At 3 of the 4 marsh stations, data indicated that the marsh flooded from Hog Island Bay and ebbed into the tidal creeks backing the sites. This may be attributable to quicker draining of the tidal creeks relative to the bay, as well as the steep downward slope of the marsh behind the interior stations. Given dominant current direction, it is unlikely that the tidal creeks provide sediment to our sites. For sediment transported onto the marsh, high bed shear stress likely prevented sediment from depositing near the marsh edge, resulting in maximum deposition further into the interior.

To predict future changes in SSC due to RSLR and increased coastal storminess, wave shear stress was estimated for various depth and wind conditions. For a fetch of 10 km (consistent with winds from the west) and moderate wind speeds (> 10 m s^{-1}), maximum wave shear stress occurs at a depth of 1.2 m. This maximum can be reached under present-day conditions, but would occur more frequently with moderate SLR and would be less sensitive to wind direction. If the marsh keeps pace with SLR, potential deposition, estimated as the mass of sediment in water flooding the marsh, will also be maximized at a depth of 1.2 m. However, if marsh elevation remains constant, water depths above 1.2 m have the potential to increase marsh deposition rates because while SSC in the water flooding the marsh would be below maximum values, the mass of sediment in suspension increases with increasing water depth above the marsh platform.

The two primary factors that influence sediment deposition on marshes proximal to bay-marsh boundaries, but do not impact tidal creek marshes, are waves and current direction. SSC on the tidal flat is highly correlated with wave shear stress, and minimally correlated with current shear stress, the primary control of SSC in tidal creeks (Christiansen et al. 2000). However, the impact of large wave events on sediment deposition at Chimney Pole is limited by the fact that these events typically occur when the marsh is not flooded. Unconstrained flow limits sediment deposition on marsh islands, because currents can carry sediment towards, but also away from, the marsh during flooding conditions.

Sediment transported onto the marsh was not deposited near the marsh edge. At our edge stations, high bed shear stresses likely prevent sediment from settling, or rework it if it is temporarily deposited. Maximum deposition occurred further into the marsh interior. Unlike tidal creek marshes (Christiansen et al. 2000), bed shear stress may at times be high enough to mobilize sediment on the marsh surface at our sites. Our observations indicate that deposition occurs during flooding tides at rates (0.028 (meas) and 0.025 (calc) g cm^{-2} per four weeks) that are consistent with Christensen's (1998) estimates for the low marsh adjacent to Phillips Creek.

Works Cited

Cahoon, D.R. & D.J. Reed. (1995). Relationships among Marsh Surface Topography, Hydroperiod, and Soil Accretion in a Deteriorating Louisiana Salt Marsh. *Journal of Coastal Research,* 11(2): 357-69.

Carniello, L., D'Alpaos, A. & A. Defina. (2011). Modeling wind waves and tidal flows in shallow micro-tidal basins. *Estuarine, Coastal and Shelf Science,* 92: 263-276.

Carniello, L., Defina, A. & A. D'Alpaos. (2012). Modeling sand-mud transport induced by tidal currents and wind-waves in shallow microtidal basins: Application to the Venice Lagoon (Italy). *Estuarine, Coastal & Shelf Science,* 102-3: 105-15.

Christiansen, T. (1998). Sediment Deposition on a Tidal Salt Marsh. (Unpublished PhD Dissertation). University of Virginia, Charlottesville, VA.

Christiansen, T., Wiberg, P.L. & T.G. Mulligan. (2000). Flow and Sediment Transport on a Tidal Salt Marsh Surface. *Estuarine, Coastal and Shelf Science,* 50: 315-31.

D'Alpaos, A., Lanzoni, S., Mudd, S.M., & S. Fagherazzi. (2006). Modeling the influence of hydroperiod and vegetation on the cross-sectional formation of tidal channels. *Estuarine, Coastal and Shelf Science*, 69 (3–4): 311–24.

Day Jr., J.W., Hall, C.S., Kemp, W.M. & A. Yánez-Arancibia. (1989). *Estuarine Ecology*. Hoboken: John Wiley and Sons.

Day Jr., J.W., Scarton, F., Rismondo, A. & D. Are. (1998). Rapid deterioration of a salt marsh in Venice Lagoon, Italy. *Journal of Coastal Research,* 14: 583-90.

Defina, A., Carniello, L., Fagherazzi, S. & L. D'Alpaos. (2007). Self- organization of shallow basins in tidal flats and salt marshes, *Journal of Geophysical Research,* 112: F03001.

Donelan, M.A., Hamilton, J., & W.H. Hui. (1985). Directional spectra for wind-generated waves. *Philosophical Transactions of the Royal Society of London*, A 315L: 509–62.

Drake, D.E. & D.A. Cacchione. (1989) Estimates of the suspended sediment reference concentration (C_a) and resuspension coefficient (γ_0) from near-bottom observations on the California shelf. *Continental Shelf Research*, 9: 51-64.

Fagherazzi, S., Carniello, L. & A. Defina. (2006). Critical bifurcation of shallow microtidal landforms in tidal flats and salt marshes, *Proceedings of the National Academy of Sciences USA,* 103(22): 8337–41.

Fagherazzi, S., & P. L. Wiberg. (2009). Importance of wind conditions, fetch, and water levels on wave- generated shear stresses in shallow intertidal basins. *Journal of Geophysical Research,* 114: F03022.

Fagherazzi, S., Mariotti, G., Porter, J.H., McGlathery, K.J., & P.L. Wiberg. (2010). Wave energy asymmetry in shallow bays. *Geophysical Research Letters,* 37(24): L24601.

Fagherazzi, S., Wiberg, P.L., Temmerman, S., Struyf, E., Zhao, Y. & P.A. Raymond. (2013). Fluxes of water, sediment, and biogeochemical compounds in salt marshes. *Ecological Processes,* 2:3.

Feagin, R. A., Lozanda-Bernard, S.M., Ravens, T.M., Möller, I., Yeager, K.M. & A. H. Baird. (2009). Does vegetation prevent wave erosion of salt marsh edges? *Proceedings of the National Academy of Sciences USA,* 106: 10109-13.

Fredsoe, J., & R. Deigaard. (1992). *Mechanics of Coastal Sediment Transport*. Advanced Series on Ocean Engineering Vol. 3. Singapore: World Science.

French, J.R., Spencer, T., Murray, A.L., & N.S. Arnold. (1995). Geostatistical analysis of sediment deposition in two small tidal wetlands, Norfolk, United Kingdom. *Journal of Coastal Research,* 11: 308–21.

Friedrichs, C.T., & J.E. Perry. (2001). Tidal salt marsh morphodynamics, *Journal of Coastal Res*earch, 27: 6–36.

Guy, H.P. (1969). *Laboratory theory and methods for sediment analysis*. U.S. Geological Survey Techniques of Water-Resources Investigations, book 5, chap. C1. Washington, DC: U.S. Government Printing Office.

Hill, P.S., Nowell, A.R.M., & P.A. Jumars. (1988) Flume evaluation of the relationship between suspended sediment concentration and excess boundary shear stress*. Journal of Geophysical Research*, 93: 12499-510.

Hornberger, G.M., Raffensperger, J.P, Wiberg, P.L., & K.N. Eshleman. (1998). *Elements of Physical Hydrology.* Baltimore, MD: Johns Hopkins Press.

Kirwan, M.L., Guntensperger, G.R., D'Alpaos, A., Morris, J.T., Mudd, S.M., & S. Temmerman. (2010). Limits on the adaptability of coastal marshes to rising sea level. *Geophysical Research Letters,* 37: L23401.

Kirwan, M.L. & Guntenspergen, G.R. (2012). Feedbacks between inundation, root production, and shoot growth in a rapidly submerging brackish marsh. *Journal of Ecology,* 100(3): 764-70.

Law, B.A., Milligan, T.G., Hill, P.S., Newgard, J., Wheatcroft, R.A., & P.L. Wiberg. (2013). Bed Flocculation on a muddy intertidal flat in Willapa Bay, Washington, Part I: A regional survey of the grain size of surficial sediments. *Continental Shelf Research*, 60: S136-44.

Lawson, S. E. (2004). Sediment Suspension as a Control on Light Availability in a Coastal Lagoon. (Unpublished Master's Thesis). University of Virginia, Charlottesville, VA.

Lawson, S.E., Wiberg, P.L., McGlathery, K.J., & D.C. Fugate. (2007). Wind-driven sediment suspension controls light availability in shallow coastal lagoon. *Estuaries and Coasts*, 30(1): 102-12.

Mariotti, G., & S. Fagherazzi. (2010). A numerical model for the coupled long-term evolution of salt marshes and tidal flats, *Journal of Geophysical Research,* 115: F01004.

Mariotti, G., Fagherazzi, S., Wiberg, P.L., McGlathery, K.J., Carniello, L. & A. Defina. (2010). Influence of storm surges and sea level on shallow tidal basin erosive processes. *Journal of Geophysical Research,* 115: C11012.

Mariotti, G. & S. Fagherazzi. (2013). Critical width of tidal flats triggers marsh collapse in the absence of sea-level rise. *Proceedings of the National Academy of Sciences USA*, 110(14): 5353–56.

Mariotti, G. & J. Carr. (2014). Dual role of salt marsh retreat: long term loss and short term resilience. *Water Resources Research*, 50(4): 2963-74.

McLoughlin, S.M. (2010). Erosional Processes along Salt Marsh Edges on the Eastern Shore of Virginia. (Unpublished Master's Thesis). University of Virginia, Charlottesville, VA.

McLoughlin, S.M., Wiberg, P.L., Safak, I., & K.J. McGlathery. (2014). Rates and forcing of marsh-edge erosion in a shallow coastal bay: Virginia. *Estuaries and Coasts,* DOI 10.1007/s12237-014-9841-2

Mehta, A.J. (1988). Laboratory Studies on Cohesive Sediment Deposition and Erosion. Dronkers, J. & van Leussen, W. (Eds): *Physical Processes in Estuaries* (427-45). London: Springer-Verlag.

Miller, M.C., McCave, I.N., & P.D. Komar. (1977). Threshold of sediment motion under unidirectional currents. *Sedimentology*, 24: 507-27.

Mitchener, H. and Torfs, H. (1996). Erosion of mud/sand mixtures. *Journal of Coastal Engineering,* 29: 1-25.

Möller, I., Spencer, T. & J. R. French. (1996). Wind wave attenuation over saltmarsh surfaces: Preliminary results from Norfolk, England. *Journal of Coastal Research,* 12(4): 1009–16.

Möller, I., Spencer, T., French, J.R., Leggett, D.J. & M. Dixon. (1999). Wave transformation over salt marshes: A field and numerical modeling study from North Norfolk, England. *Estuarine, Coastal & Shelf Sci*ence, 49(3): 411–26.

Möller, I. (2006). Quantifying saltmarsh vegetation and its effect on wave height dissipation: Results from a UK East coast saltmarsh. *Estuarine, Coastal and Shelf Science,* 69:337-51.

Morris, J.T., Sundareshwar, P.V., Nietch, C.T., Kjerfve, B. & D.R. Cahoon. (2002). Responses of coastal wetlands to rising sea level. *Ecology,* 83:2869-77.

Mudd, S.M., Fagherazzi, S., Morris, J.T. & D.J. Furbish. (2004). Flow, sedimentation, and biomass production on a vegetated salt marsh in South Carolina: toward a predictive model of marsh morphologic and ecologic evolution. In Fagherazzi, S., Marani, A., Blum, L.K. (Eds.), *The Ecogeomorphology of Tidal Marshes* (pp. 165–87). Washington, D.C.: American Geophysical Union.

Mudd, S.M., Howell, S.M., & J.T. Morris. (2009). Impact of dynamic feedbacks between sedimentation, sea-level rise, and biomass production on near-surface marsh stratigraphy and carbon accumulation. *Estuarine, Coastal & Shelf Science,* 82: 377-89.

Mudd, S.M., D'Alpaos, A. & J.T. Morris. (2010). How does vegetation affect sedimentation on tidal marshes? Investigating particle capture and hydrodynamic controls on biologically mediated sedimentation. *Journal of Geophysical Research*, 115(F3): F03029.

Oertel, G. F. (2001). Hypsographic, hydro-hypsographic, and hydrological analysis of coastal bay environments, Great Machipongo Bay, Virginia. *Journal of Coastal Research,* 17:775-83.

Parchure, T.M. & A.J. Mehta. (1985). Erosion of soft cohesive sediment deposits. *Journal of Hydraulic Engineering,* 111 (10): 1308-26.

Pestrong, R. (1969). The shear stress of tidal marsh sediments. *Journal of Sedimentary Petrology,* 39:322-26.

Rinaldi, M., Casagli, N., Dapporto, S. & A. Gargini. (2004). Monitoring and modeling of pore water pressure changes and riverbank stability during flow events. *Earth Surface Processes & Landforms*, 29: 237–54.

Rouse, H. (1937). Modern conceptions of the mechanics of turbulence. *Transactions of the American Society of Civil Engineers,* 102: 436-505.

Rubin, D.M. & D.J. Topping. (2001). Quantifying the relative importance of flow regulation and grain size regulation of suspended sediment transport α and tracking changes in grain size of bed sediment. *Water Resources Research*, 37(1): 133-46.

Shields, A.F.(1936). Application of similarity principles and turbulence research to bed-load movement, vol 26. Mitteilungen der Preussischen Versuchsanstalt für Wasserbau und Schiffbau, Berlin, Germany, pp 5–24.

Smith, J. D. & S.R. Mclean. (1977). Spatially averaged flow over a wavy surface. *Journal of Geophysical Research*, 82: 1735–46.

Sternberg, R.W., Cacchione, D.A., Drake, D.E., & K. Kranck. (1986) Suspended sediment dynamics in an estuarine tidal channel within San Francisco Bay, California. *Marine Geology,* 71: 237-58.

Stumpf, R.P. (1983). The process of sedimentation on the surface of a salt marsh. *Estuarine, Coastal and Shelf Science,* 17(5): 495-508

Temmerman, S., Bouma, T.J., Govers, G., & D. Lauwaet. (2005). Flow paths of water and sediment in a tidal marsh: relations with marsh developmental stage and tidal inundation height. *Estuaries,* 28(3): 338–52.

Tonelli, M., Fagherazzi, S. & M. Petti. (2010). Modeling wave impact on salt marsh boundaries. *Journal of Geophysical Research,* 115: C09028.

van Ledden, M., van Kesteren, W.G.M., & J.C. Winterwerp. (2004). A Conceptual Framework for the Erosion Behaviour of sand-mud mixtures. *Continental Shelf Research,* 24(1): 1-11.

Wiberg, P.L. & C.R. Sherwood. (2008). Calculating wave-generated bottom orbital velocities from surface-wave parameters. *Computers & Geosciences*, 34: 1243–62.

Wiberg, P.L. & J.D. Smith. (1983) A comparison of field data and theoretical models for wave-current interactions at the bed on the continental shelf. *Continental Shelf Research,* 2: 147-62.

World Health Organization. (2005). *Millennium Ecosystem Assessment: Ecosystems and Human Well-Being—Health Synthesis Report.* Geneva: WHO Press.

Young, I.R., & L.A. Verhagen. (1996a). The growth of fetch limited waves in water of finite depth. 1. Total energy and peak frequency. *Coastal Engineering,* 29(1–2): 47–78.

Young, I.R., & L.A. Verhagen. (1996b). The growth of fetch limited waves in water of finite depth. 2. Spectral evolution. *Coastal Engineering,* 29(1 – 2): 79–99.

Young, I.R., Zieger, S. & A.V. Babanin. (2011). Global Trends in Wind Speed and Wave Height. *Science*, 332(6028): 451-55.

Zervas, C.E. (2001) *Sea level variations of the United States, 1854-1999.* (NOAA Technical Report NOS CO-OPS 36). Silver Spring, MD: National Oceanic and Atmospheric Administration.

Appendix 1

Sensor Serial Number	Calibration Curve
S8671	y= 2.1319x +23.821
T8397	y=2.0123x +2.2602
S9284	y=2.4272x +0.7863
54076	y=0.7786x +81.087
54075	y=1.024x +48.189
54077	y=0.8989x +67.533
S9346	y=1.4624x +39.054

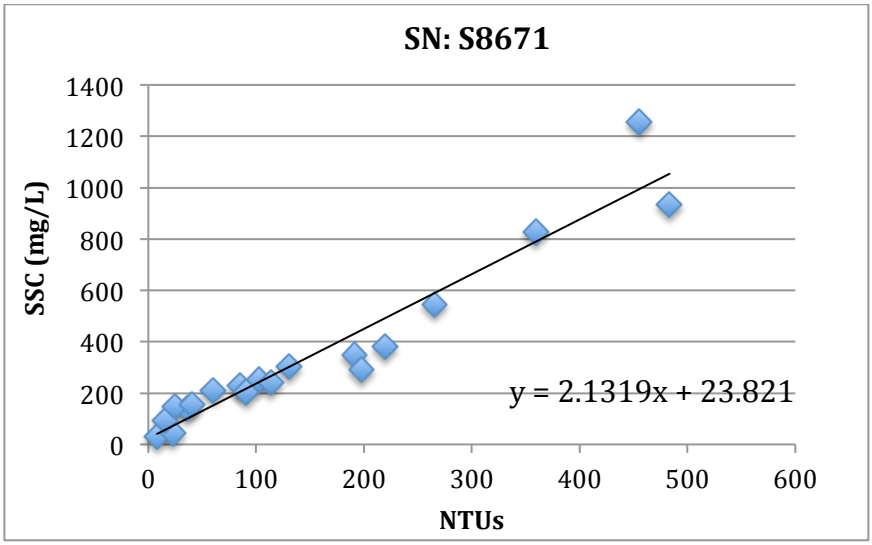

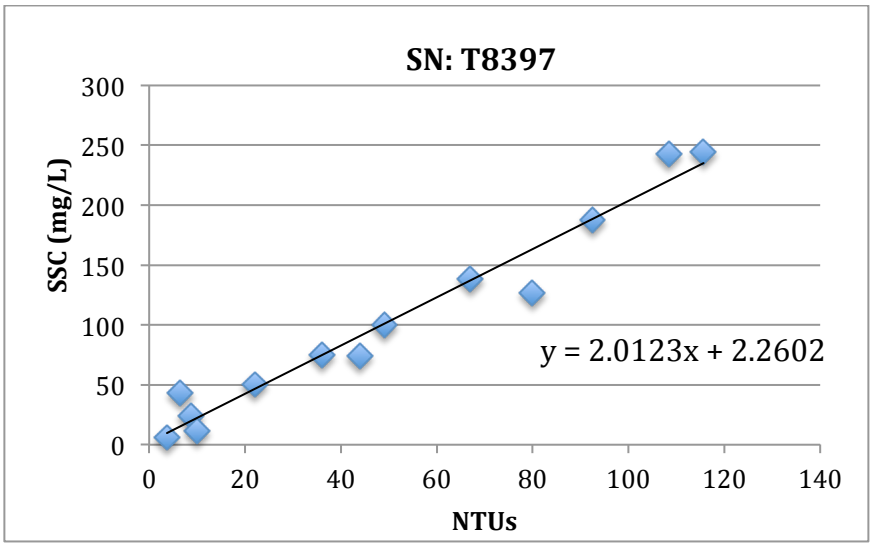

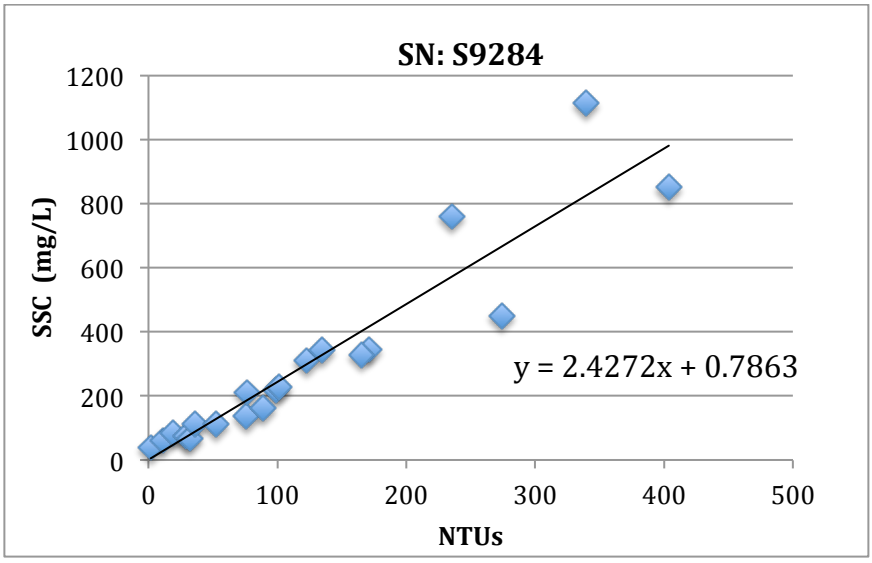
SN: S9284
SSC (mg/L)
NTUs
y = 2.4272x + 0.7863
0
200
400
600
800
1000
1200
0
100
200
300
400
500

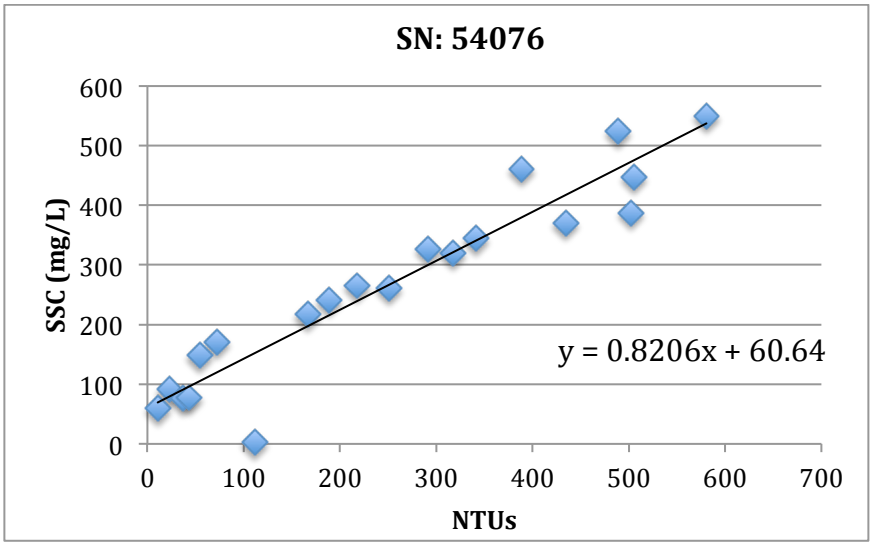
SN: 54076
SSC (mg/L)
NTUs
y = 0.8206x + 60.64
0
100
200
300
400
500
600
0
100
200
300
400
500
600
700

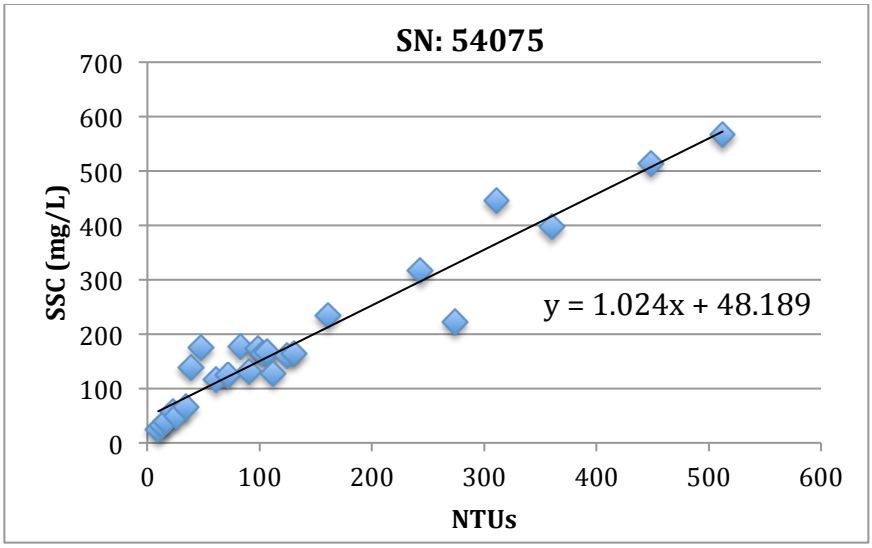
SN: 54075
SSC (mg/L)
NTUs
y = 1.024x + 48.189
0
100
200
300
400
500
600
700
0
100
200
300
400
500
600

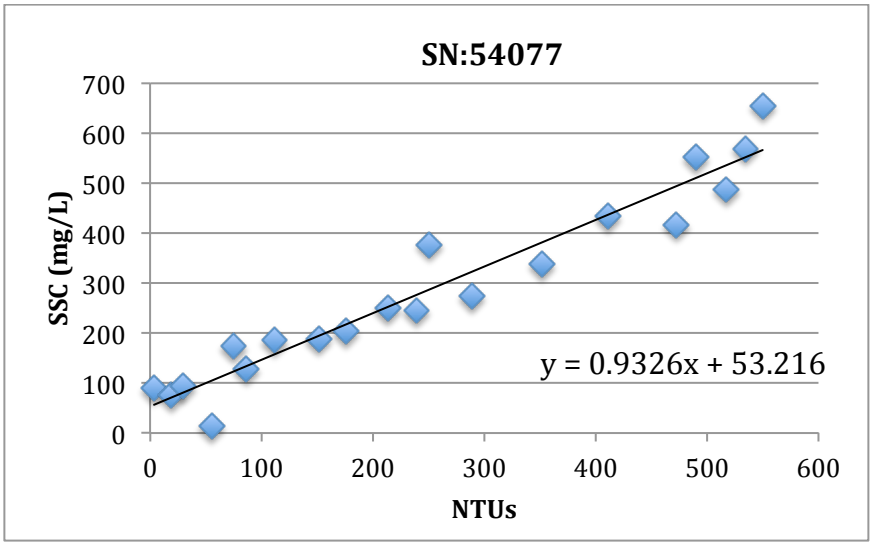
SN:54077
SSC (mg/L)
NTUs
y = 0.9326x + 53.216
0
100
200
300
400
500
600
700

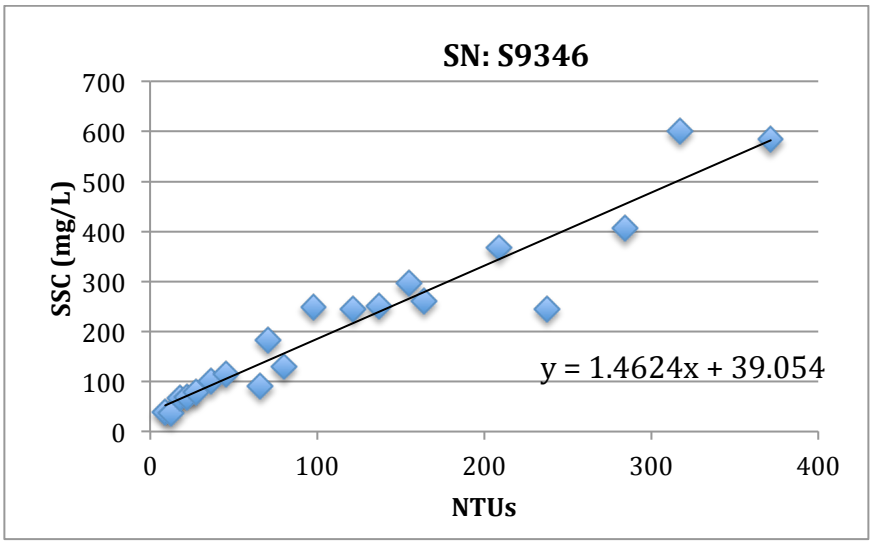
SN: S9346
SSC (mg/L)
NTUs
y = 1.4624x + 39.054
0
100
200
300
400
500
600
700

Appendix 2: Grain Size Distribution

**Tables below show cumulative distribution (%) of grain size for each sample taken at each site. Distributions are averages of the 3 subsamples taken for each sample. Standard deviation of the distribution is also given.

Grain Size (μm)	TAE Sample 1		TAE Sample 2	
	Cum Dist	Std Dev	Cum Dist	Std Dev
0.41	0.34	0.01	0.29	0.01
0.45	0.66	0.02	0.55	0.01
0.50	1.11	0.03	0.94	0.02
0.54	1.67	0.05	1.41	0.03
0.60	2.33	0.07	1.96	0.04
0.66	3.07	0.09	2.59	0.05
0.72	3.89	0.11	3.27	0.06
0.79	4.77	0.14	4.02	0.07
0.87	5.70	0.16	4.79	0.08
0.95	6.66	0.19	5.60	0.09
1.05	7.63	0.22	6.41	0.10
1.15	8.62	0.26	7.23	0.11
1.26	9.61	0.29	8.05	0.11
1.38	10.58	0.32	8.87	0.12
1.52	11.55	0.36	9.67	0.12
1.67	12.51	0.39	10.47	0.12
1.83	13.47	0.43	11.27	0.11
2.01	14.43	0.46	12.07	0.11
2.21	15.40	0.50	12.88	0.10
2.42	16.39	0.54	13.71	0.10
2.66	17.42	0.58	14.56	0.09
2.92	18.50	0.62	15.46	0.08
3.21	19.64	0.66	16.41	0.09
3.52	20.86	0.71	17.42	0.10
3.86	22.16	0.76	18.49	0.12
4.24	23.56	0.81	19.63	0.15
4.66	25.05	0.87	20.85	0.18
5.11	26.63	0.93	22.13	0.23
5.61	28.31	1.00	23.47	0.28
6.16	30.08	1.08	24.88	0.33
6.76	31.92	1.15	26.33	0.39
7.42	33.85	1.24	27.82	0.45
8.15	35.84	1.33	29.35	0.51
8.94	37.90	1.42	30.92	0.58

9.82	40.02	1.52	32.52	0.65
10.78	42.20	1.62	34.16	0.71
11.83	44.44	1.73	35.84	0.77
12.99	46.74	1.84	37.58	0.82
14.26	49.13	1.96	39.39	0.85
15.65	51.62	2.07	41.29	0.87
17.18	54.20	2.19	43.30	0.88
18.86	56.89	2.31	45.43	0.88
20.71	59.68	2.44	47.67	0.88
22.73	62.56	2.57	50.05	0.88
24.95	65.56	2.71	52.59	0.88
27.39	68.66	2.87	55.33	0.88
30.07	71.88	3.02	58.29	0.88
33.01	75.16	3.17	61.48	0.88
36.24	78.47	3.29	64.89	0.89
39.78	81.70	3.38	68.47	0.90
43.67	84.80	3.45	72.16	0.92
47.94	87.69	3.51	75.86	0.93
52.63	90.33	3.56	79.48	0.92
57.77	92.64	3.61	82.94	0.92
63.42	94.59	3.63	86.12	0.93
69.62	96.10	3.59	88.94	0.96
76.43	97.18	3.45	91.38	1.03
83.90	97.87	3.19	93.42	1.11
92.10	98.29	2.84	95.11	1.19
101.10	98.59	2.43	96.51	1.23
110.99	98.87	1.96	97.66	1.15
121.84	98.73	1.79	98.57	0.95
133.75	99.16	1.19	99.23	0.65
146.82	99.53	0.66	99.66	0.35
161.18	99.80	0.29	99.89	0.14
176.93	99.94	0.09	99.97	0.04
194.23	99.99	0.01	100.00	0.01
213.22	100.00	0.00		

Grain Size (μm)	TBE Sample 1		TBE Sample 2		TBE Sample 3	
	Cum Dist	Std Dev	Cum Dist	Std Dev	Cum Dist	Std Dev
0.41	0.36	0.01	0.34	0.01	0.38	0.02
0.45	0.69	0.02	0.66	0.01	0.74	0.03
0.50	1.17	0.03	1.11	0.02	1.24	0.05
0.54	1.77	0.05	1.67	0.03	1.87	0.08
0.60	2.46	0.07	2.32	0.04	2.61	0.11
0.66	3.25	0.10	3.06	0.05	3.44	0.14
0.72	4.12	0.12	3.88	0.06	4.36	0.18
0.79	5.06	0.15	4.75	0.08	5.35	0.22
0.87	6.05	0.18	5.68	0.09	6.39	0.27
0.95	7.07	0.21	6.62	0.11	7.46	0.32
1.05	8.11	0.24	7.59	0.13	8.55	0.37
1.15	9.17	0.27	8.56	0.15	9.65	0.42
1.26	10.22	0.30	9.52	0.17	10.75	0.47
1.38	11.27	0.32	10.47	0.19	11.85	0.53
1.52	12.31	0.34	11.41	0.21	12.93	0.58
1.67	13.34	0.35	12.34	0.24	14.00	0.64
1.83	14.37	0.36	13.26	0.26	15.07	0.71
2.01	15.40	0.36	14.17	0.29	16.14	0.77
2.21	16.44	0.36	15.10	0.31	17.22	0.84
2.42	17.51	0.35	16.03	0.34	18.33	0.91
2.66	18.61	0.34	17.00	0.37	19.48	0.98
2.92	19.76	0.33	18.01	0.41	20.69	1.06
3.21	20.97	0.33	19.08	0.45	21.96	1.14
3.52	22.26	0.34	20.21	0.49	23.32	1.23
3.86	23.64	0.37	21.42	0.53	24.76	1.32
4.24	25.11	0.41	22.71	0.58	26.31	1.40
4.66	26.68	0.46	24.09	0.63	27.95	1.49
5.11	28.35	0.51	25.54	0.68	29.70	1.58
5.61	30.11	0.57	27.08	0.74	31.54	1.66
6.16	31.96	0.62	28.70	0.79	33.46	1.74
6.76	33.90	0.66	30.38	0.85	35.47	1.82
7.42	35.92	0.68	32.13	0.91	37.54	1.89
8.15	38.02	0.69	33.94	0.97	39.67	1.95
8.94	40.19	0.68	35.81	1.02	41.87	2.01
9.82	42.44	0.64	37.73	1.07	44.11	2.06
10.78	44.75	0.60	39.71	1.12	46.40	2.10
11.83	47.15	0.56	41.75	1.17	48.73	2.14
12.99	49.62	0.55	43.87	1.21	51.12	2.18
14.26	52.19	0.60	46.07	1.24	53.58	2.22

15.65	54.87	0.72	48.38	1.27	56.12	2.26
17.18	57.64	0.88	50.79	1.30	58.75	2.31
18.86	60.50	1.08	53.32	1.32	61.46	2.36
20.71	63.43	1.29	55.95	1.33	64.24	2.41
22.73	66.39	1.50	58.68	1.33	67.07	2.43
24.95	69.37	1.69	61.50	1.31	69.96	2.43
27.39	72.37	1.85	64.43	1.27	72.89	2.40
30.07	75.36	1.96	67.47	1.22	75.86	2.36
33.01	78.31	2.02	70.59	1.16	78.83	2.29
36.24	81.18	2.03	73.76	1.11	81.74	2.23
39.78	83.89	1.97	76.92	1.06	84.53	2.17
43.67	86.40	1.86	79.99	1.01	87.11	2.11
47.94	88.66	1.70	82.91	0.94	89.45	2.05
52.63	90.64	1.52	85.62	0.87	91.51	1.98
57.77	92.36	1.31	88.08	0.77	93.29	1.88
63.42	93.82	1.11	90.27	0.66	94.80	1.74
69.62	95.06	0.94	92.16	0.56	96.05	1.58
76.43	96.09	0.81	93.78	0.48	97.07	1.41
83.90	96.96	0.72	95.16	0.44	97.89	1.22
92.10	97.69	0.67	96.35	0.44	98.54	1.03
101.10	98.33	0.61	97.38	0.45	99.04	0.83
110.99	98.88	0.52	98.28	0.43	99.41	0.61
121.84	99.33	0.39	99.00	0.36	99.68	0.39
133.75	99.66	0.24	99.52	0.25	99.85	0.20
146.82	99.87	0.11	99.83	0.13	99.95	0.08
161.18	99.96	0.03	99.96	0.05	99.99	0.02
176.93	99.99	0.00	99.99	0.01	100.00	0.00
194.23	100.00	0.00	100.00	0.00		

Grain Size (μm)	TAI Sample 1		TAI Sample 2		TAI Sample 3	
	Cum Dist	Std Dev	Cum Dist	Std Dev	Cum Dist	Std Dev
0.41	0.51	0.06	0.50	0.03	0.36	0.00
0.45	0.98	0.11	0.97	0.05	0.69	0.01
0.50	1.66	0.19	1.64	0.09	1.17	0.02
0.54	2.51	0.28	2.46	0.13	1.76	0.03
0.60	3.49	0.39	3.43	0.18	2.45	0.04
0.66	4.61	0.50	4.52	0.23	3.23	0.05
0.72	5.85	0.62	5.71	0.29	4.09	0.07
0.79	7.20	0.74	7.00	0.35	5.02	0.09
0.87	8.62	0.85	8.35	0.41	5.99	0.11
0.95	10.10	0.95	9.73	0.48	7.00	0.13
1.05	11.63	1.03	11.14	0.53	8.02	0.15
1.15	13.19	1.10	12.55	0.59	9.06	0.18
1.26	14.79	1.14	13.94	0.64	10.09	0.20
1.38	16.41	1.16	15.33	0.69	11.12	0.22
1.52	18.06	1.15	16.68	0.73	12.13	0.24
1.67	19.75	1.11	18.02	0.76	13.14	0.26
1.83	21.49	1.05	19.34	0.79	14.15	0.27
2.01	23.29	0.97	20.67	0.81	15.16	0.28
2.21	25.16	0.87	22.00	0.83	16.19	0.28
2.42	27.14	0.77	23.37	0.85	17.24	0.27
2.66	29.22	0.70	24.78	0.86	18.33	0.25
2.92	31.43	0.67	26.25	0.87	19.48	0.23
3.21	33.79	0.70	27.81	0.87	20.68	0.20
3.52	36.29	0.79	29.48	0.87	21.97	0.16
3.86	38.94	0.93	31.25	0.87	23.34	0.12
4.24	41.72	1.08	33.14	0.87	24.79	0.08
4.66	44.63	1.24	35.16	0.87	26.34	0.06
5.11	47.64	1.38	37.29	0.86	27.96	0.10
5.61	50.71	1.51	39.52	0.86	29.67	0.16
6.16	53.81	1.62	41.84	0.85	31.44	0.23
6.76	56.91	1.70	44.23	0.84	33.26	0.31
7.42	59.96	1.76	46.69	0.83	35.13	0.38
8.15	62.93	1.80	49.20	0.82	37.05	0.46
8.94	65.80	1.83	51.74	0.81	38.99	0.53
9.82	68.52	1.84	54.31	0.80	40.96	0.60
10.78	71.07	1.86	56.90	0.80	42.96	0.67
11.83	73.45	1.89	59.51	0.81	44.98	0.72
12.99	75.67	1.93	62.14	0.82	47.05	0.77
14.26	77.75	1.98	64.82	0.84	49.18	0.81

15.65	79.73	2.05	67.55	0.86	51.39	0.84
17.18	81.62	2.13	70.33	0.88	53.69	0.86
18.86	83.43	2.22	73.13	0.91	56.09	0.87
20.71	85.12	2.31	75.92	0.93	58.56	0.86
22.73	86.69	2.37	78.68	0.96	61.12	0.84
24.95	88.14	2.40	81.38	0.99	63.77	0.81
27.39	89.49	2.39	84.00	1.01	66.52	0.78
30.07	90.75	2.37	86.54	1.02	69.39	0.73
33.01	91.96	2.37	88.94	1.02	72.35	0.67
36.24	93.11	2.43	91.16	1.00	75.35	0.59
39.78	94.18	2.53	93.13	0.98	78.32	0.49
43.67	95.14	2.63	94.80	0.98	81.18	0.38
47.94	95.98	2.68	96.15	0.99	83.84	0.25
52.63	96.70	2.61	97.20	1.01	86.26	0.14
57.77	97.33	2.43	97.98	1.01	88.40	0.04
63.42	97.88	2.21	98.57	0.95	90.25	0.04
69.62	98.35	2.02	99.00	0.83	91.82	0.07
76.43	98.72	1.85	99.32	0.66	93.12	0.07
83.90	98.99	1.65	99.56	0.49	94.17	0.05
92.10	99.18	1.41	99.74	0.33	95.01	0.04
101.10	99.33	1.15	99.86	0.20	95.71	0.07
110.99	99.49	0.89	99.94	0.10	96.36	0.09
121.84	99.64	0.62	99.98	0.04	97.01	0.09
133.75	99.78	0.37	99.99	0.01	97.71	0.07
146.82	99.90	0.18	100.00	0.00	98.42	0.07
161.18	99.97	0.06			99.06	0.07
176.93	99.99	0.01			99.56	0.07
194.23	100.00	0.00			99.85	0.04
213.22					99.97	0.02
234.07					100.00	0.00

Grain Size (μm)	TBI Sample 1		TBI Sample 2		TBI Sample 3	
	Cum Dist	Std Dev	Cum Dist	Std Dev	Cum Dist	Std Dev
0.41	0.32	0.00	0.24	0.01	0.28	0.01
0.45	0.62	0.01	0.47	0.03	0.55	0.02
0.50	1.05	0.01	0.80	0.04	0.94	0.03
0.54	1.58	0.02	1.21	0.06	1.41	0.05
0.60	2.20	0.02	1.69	0.09	1.97	0.07
0.66	2.89	0.03	2.23	0.11	2.59	0.10
0.72	3.66	0.03	2.83	0.14	3.29	0.12
0.79	4.48	0.03	3.48	0.17	4.04	0.15
0.87	5.33	0.03	4.16	0.20	4.83	0.19
0.95	6.21	0.03	4.87	0.22	5.64	0.22
1.05	7.10	0.03	5.60	0.25	6.48	0.26
1.15	7.99	0.03	6.34	0.27	7.32	0.29
1.26	8.87	0.04	7.08	0.30	8.17	0.33
1.38	9.74	0.05	7.82	0.32	9.01	0.38
1.52	10.60	0.06	8.55	0.34	9.85	0.42
1.67	11.44	0.07	9.28	0.37	10.68	0.46
1.83	12.28	0.08	10.00	0.39	11.51	0.51
2.01	13.13	0.09	10.73	0.42	12.34	0.56
2.21	13.98	0.10	11.46	0.45	13.18	0.61
2.42	14.85	0.11	12.20	0.48	14.04	0.66
2.66	15.75	0.11	12.96	0.52	14.93	0.72
2.92	16.70	0.12	13.74	0.57	15.85	0.79
3.21	17.70	0.13	14.56	0.62	16.81	0.86
3.52	18.76	0.14	15.41	0.68	17.82	0.93
3.86	19.89	0.14	16.32	0.75	18.89	1.01
4.24	21.10	0.15	17.27	0.82	20.01	1.10
4.66	22.38	0.17	18.28	0.91	21.20	1.19
5.11	23.73	0.18	19.34	1.01	22.45	1.29
5.61	25.14	0.20	20.46	1.12	23.75	1.39
6.16	26.60	0.21	21.63	1.24	25.11	1.49
6.76	28.11	0.23	22.85	1.38	26.51	1.60
7.42	29.65	0.25	24.13	1.52	27.96	1.70
8.15	31.22	0.27	25.45	1.68	29.45	1.80
8.94	32.82	0.28	26.83	1.85	30.98	1.90
9.82	34.45	0.30	28.27	2.03	32.56	1.99
10.78	36.10	0.30	29.77	2.22	34.19	2.07
11.83	37.79	0.30	31.34	2.41	35.88	2.14
12.99	39.53	0.29	33.00	2.59	37.64	2.20
14.26	41.35	0.28	34.76	2.78	39.50	2.25

15.65	43.26	0.25	36.65	2.95	41.49	2.29
17.18	45.29	0.23	38.68	3.11	43.62	2.31
18.86	47.42	0.22	40.89	3.27	45.91	2.33
20.71	49.68	0.21	43.26	3.41	48.35	2.34
22.73	52.08	0.20	45.83	3.54	50.97	2.34
24.95	54.66	0.18	48.61	3.65	53.78	2.34
27.39	57.46	0.16	51.62	3.73	56.80	2.32
30.07	60.50	0.17	54.86	3.76	60.03	2.29
33.01	63.77	0.20	58.33	3.75	63.45	2.24
36.24	67.21	0.26	62.02	3.67	67.00	2.17
39.78	70.74	0.32	65.85	3.54	70.61	2.06
43.67	74.27	0.37	69.78	3.34	74.19	1.93
47.94	77.71	0.40	73.72	3.10	77.66	1.78
52.63	81.01	0.42	77.57	2.79	80.95	1.59
57.77	84.10	0.44	81.25	2.45	83.99	1.39
63.42	86.96	0.46	84.66	2.07	86.74	1.19
69.62	89.52	0.48	87.71	1.70	89.15	0.99
76.43	91.73	0.50	90.33	1.36	91.19	0.80
83.90	93.55	0.48	92.53	1.07	92.87	0.64
92.10	94.97	0.43	94.34	0.85	94.25	0.50
101.10	96.08	0.36	95.86	0.68	95.41	0.39
110.99	96.98	0.30	97.14	0.55	96.45	0.30
121.84	97.77	0.23	98.20	0.42	97.41	0.23
133.75	98.48	0.17	99.03	0.29	98.30	0.17
146.82	99.11	0.12	99.59	0.16	99.05	0.11
161.18	99.59	0.07	99.88	0.06	99.59	0.06
176.93	99.87	0.03	99.98	0.01	99.88	0.02
194.23	99.98	0.01	100.00	0.00	99.98	0.00
213.22	100.00	0.00			100.00	0.00

Grain Size (μm)	TA-middle Sample 1		TA-middle Sample 2		TA-middle Sample 3	
	Cum Dist	Std Dev	Cum Dist	Std Dev	Cum Dist	Std Dev
0.41	0.25	0.02	0.29	0.08	0.32	0.00
0.45	0.49	0.03	0.56	0.15	0.62	0.01
0.50	0.83	0.06	0.94	0.24	1.06	0.02
0.54	1.25	0.09	1.40	0.33	1.59	0.03
0.60	1.75	0.13	1.92	0.41	2.22	0.04
0.66	2.31	0.17	2.48	0.47	2.92	0.05
0.72	2.94	0.22	3.09	0.51	3.71	0.06
0.79	3.63	0.28	3.71	0.51	4.55	0.08
0.87	4.35	0.34	4.35	0.48	5.44	0.09
0.95	5.12	0.42	4.99	0.44	6.35	0.11
1.05	5.90	0.49	5.63	0.39	7.29	0.12
1.15	6.71	0.58	6.28	0.37	8.24	0.14
1.26	7.53	0.67	6.94	0.38	9.19	0.16
1.38	8.35	0.77	7.62	0.40	10.13	0.17
1.52	9.17	0.87	8.34	0.44	11.07	0.18
1.67	10.00	0.98	9.11	0.51	12.01	0.19
1.83	10.84	1.10	9.93	0.65	12.95	0.20
2.01	11.68	1.22	10.81	0.89	13.89	0.21
2.21	12.54	1.34	11.75	1.23	14.85	0.21
2.42	13.41	1.47	12.74	1.64	15.83	0.22
2.66	14.30	1.60	13.77	2.07	16.85	0.22
2.92	15.23	1.73	14.83	2.49	17.92	0.22
3.21	16.21	1.87	15.92	2.88	19.05	0.22
3.52	17.23	2.00	17.03	3.20	20.26	0.23
3.86	18.30	2.13	18.17	3.48	21.54	0.23
4.24	19.43	2.27	19.35	3.70	22.90	0.24
4.66	20.62	2.40	20.58	3.90	24.35	0.25
5.11	21.87	2.53	21.87	4.10	25.89	0.27
5.61	23.18	2.66	23.23	4.29	27.50	0.29
6.16	24.54	2.79	24.64	4.49	29.17	0.32
6.76	25.95	2.92	26.09	4.68	30.91	0.35
7.42	27.41	3.04	27.57	4.82	32.70	0.38
8.15	28.91	3.17	29.06	4.90	34.53	0.41
8.94	30.46	3.29	30.54	4.91	36.40	0.44
9.82	32.05	3.41	32.04	4.86	38.31	0.47
10.78	33.69	3.53	33.57	4.80	40.24	0.50
11.83	35.38	3.64	35.18	4.76	42.22	0.52
12.99	37.13	3.75	36.88	4.77	44.24	0.55
14.26	38.97	3.86	38.72	4.86	46.32	0.57

15.65	40.91	3.97	40.69	4.99	48.49	0.59
17.18	42.98	4.07	42.76	5.11	50.75	0.62
18.86	45.18	4.18	44.90	5.15	53.11	0.67
20.71	47.51	4.30	47.09	5.07	55.56	0.73
22.73	49.99	4.42	49.34	4.90	58.11	0.79
24.95	52.62	4.55	51.72	4.68	60.78	0.85
27.39	55.43	4.71	54.32	4.49	63.57	0.89
30.07	58.43	4.88	57.22	4.40	66.52	0.92
33.01	61.61	5.09	60.45	4.44	69.60	0.95
36.24	64.95	5.32	64.00	4.60	72.79	0.99
39.78	68.38	5.56	67.77	4.79	76.03	1.06
43.67	71.86	5.77	71.63	4.93	79.25	1.14
47.94	75.32	5.92	75.47	4.95	82.36	1.23
52.63	78.69	5.98	79.16	4.82	85.27	1.30
57.77	81.90	5.95	82.65	4.56	87.92	1.33
63.42	84.87	5.86	85.87	4.25	90.26	1.31
69.62	87.54	5.74	88.81	3.94	92.27	1.26
76.43	89.86	5.61	91.44	3.64	93.97	1.19
83.90	91.83	5.46	93.72	3.32	95.41	1.13
92.10	93.48	5.25	95.62	2.90	96.63	1.06
101.10	94.89	4.91	97.13	2.33	97.67	0.97
110.99	96.12	4.36	98.24	1.62	98.53	0.85
121.84	97.20	3.60	99.04	0.97	99.17	0.66
133.75	98.12	2.69	99.56	0.51	99.60	0.43
146.82	98.87	1.78	99.85	0.22	99.84	0.22
161.18	99.42	0.98	99.96	0.06	99.95	0.07
176.93	99.76	0.42	99.99	0.01	99.99	0.01
194.23	99.93	0.12	100.00	0.00	100.00	0.00
213.22	99.99	0.02				
234.07	100.00	0.00				

Grain Size (μm)	TB-middle Sample 1		TB-middle Sample 2		TB-middle Sample 3	
	Cum Dist	Std Dev	Cum Dist	Std Dev	Cum Dist	Std Dev
0.41	0.28	0.01	0.38	0.03	0.25	0.02
0.45	0.55	0.02	0.74	0.05	0.48	0.03
0.50	0.93	0.03	1.25	0.09	0.82	0.05
0.54	1.40	0.05	1.88	0.14	1.24	0.08
0.60	1.95	0.07	2.62	0.19	1.74	0.11
0.66	2.57	0.09	3.44	0.25	2.30	0.14
0.72	3.25	0.11	4.35	0.31	2.93	0.18
0.79	3.99	0.13	5.33	0.38	3.61	0.23
0.87	4.77	0.16	6.35	0.45	4.34	0.28
0.95	5.57	0.19	7.39	0.52	5.10	0.33
1.05	6.39	0.21	8.45	0.59	5.88	0.38
1.15	7.22	0.24	9.51	0.66	6.69	0.44
1.26	8.04	0.27	10.56	0.73	7.51	0.50
1.38	8.86	0.29	11.59	0.79	8.33	0.57
1.52	9.67	0.32	12.60	0.86	9.16	0.65
1.67	10.47	0.34	13.60	0.93	9.99	0.73
1.83	11.27	0.37	14.59	1.00	10.83	0.82
2.01	12.07	0.39	15.57	1.08	11.66	0.91
2.21	12.88	0.41	16.56	1.15	12.51	1.02
2.42	13.70	0.43	17.57	1.23	13.37	1.13
2.66	14.56	0.46	18.61	1.32	14.25	1.25
2.92	15.45	0.48	19.69	1.41	15.16	1.38
3.21	16.39	0.50	20.84	1.50	16.10	1.51
3.52	17.38	0.52	22.05	1.61	17.08	1.65
3.86	18.43	0.55	23.34	1.71	18.10	1.80
4.24	19.55	0.57	24.71	1.82	19.18	1.96
4.66	20.74	0.59	26.15	1.94	20.30	2.12
5.11	21.99	0.62	27.66	2.05	21.48	2.28
5.61	23.31	0.64	29.24	2.16	22.72	2.44
6.16	24.68	0.67	30.85	2.27	24.01	2.60
6.76	26.10	0.69	32.50	2.37	25.35	2.75
7.42	27.57	0.72	34.18	2.46	26.74	2.90
8.15	29.09	0.74	35.87	2.54	28.18	3.04
8.94	30.64	0.76	37.57	2.61	29.67	3.16
9.82	32.24	0.78	39.27	2.67	31.21	3.27
10.78	33.88	0.80	40.97	2.72	32.80	3.36
11.83	35.57	0.82	42.66	2.76	34.44	3.43
12.99	37.32	0.84	44.35	2.80	36.14	3.48
14.26	39.16	0.86	46.06	2.84	37.91	3.49

15.65	41.11	0.88	47.81	2.88	39.76	3.48
17.18	43.19	0.91	49.59	2.91	41.71	3.44
18.86	45.39	0.94	51.40	2.93	43.79	3.38
20.71	47.74	0.98	53.23	2.94	46.00	3.30
22.73	50.24	1.03	55.08	2.94	48.35	3.20
24.95	52.90	1.08	56.94	2.93	50.87	3.08
27.39	55.75	1.14	58.83	2.92	53.56	2.95
30.07	58.80	1.21	60.76	2.92	56.42	2.81
33.01	62.06	1.30	62.73	2.92	59.45	2.66
36.24	65.48	1.39	64.77	2.92	62.61	2.50
39.78	69.02	1.48	66.89	2.90	65.87	2.33
43.67	72.61	1.56	69.09	2.86	69.19	2.15
47.94	76.18	1.61	71.37	2.76	72.51	1.98
52.63	79.65	1.61	73.73	2.62	75.80	1.80
57.77	82.95	1.58	76.15	2.44	78.99	1.61
63.42	86.02	1.51	78.62	2.25	82.05	1.42
69.62	88.80	1.44	81.11	2.06	84.91	1.22
76.43	91.25	1.39	83.61	1.91	87.56	1.02
83.90	93.34	1.38	86.14	1.79	89.96	0.84
92.10	95.10	1.37	88.71	1.67	92.13	0.70
101.10	96.55	1.32	91.28	1.52	94.10	0.62
110.99	97.73	1.17	93.76	1.30	95.86	0.58
121.84	98.64	0.91	96.00	1.00	97.37	0.52
133.75	99.29	0.58	97.80	0.66	98.57	0.41
146.82	99.71	0.28	99.04	0.34	99.38	0.25
161.18	99.91	0.09	99.70	0.13	99.81	0.11
176.93	99.99	0.02	99.95	0.03	99.97	0.03
194.23	100.00	0.00	100.00	0.00	100.00	0.00

Grain Size (μm)	TAF Sample 1		TAF Sample 2		TAF Sample 3	
	Cum Dist	Std Dev	Cum Dist	Std Dev	Cum Dist	Std Dev
0.41	0.33	0.01	0.37	0.02	0.38	0.03
0.45	0.64	0.02	0.73	0.03	0.74	0.06
0.50	1.08	0.03	1.23	0.05	1.26	0.09
0.54	1.63	0.04	1.85	0.08	1.89	0.14
0.60	2.26	0.06	2.58	0.11	2.63	0.20
0.66	2.98	0.07	3.41	0.14	3.47	0.26
0.72	3.78	0.09	4.32	0.18	4.39	0.33
0.79	4.64	0.10	5.30	0.22	5.38	0.40
0.87	5.53	0.12	6.34	0.26	6.42	0.47
0.95	6.46	0.13	7.41	0.31	7.49	0.55
1.05	7.40	0.14	8.51	0.35	8.58	0.62
1.15	8.35	0.15	9.62	0.40	9.68	0.70
1.26	9.30	0.15	10.73	0.45	10.78	0.77
1.38	10.24	0.16	11.84	0.50	11.87	0.83
1.52	11.18	0.17	12.95	0.55	12.95	0.90
1.67	12.10	0.18	14.05	0.61	14.04	0.96
1.83	13.03	0.20	15.16	0.67	15.13	1.03
2.01	13.96	0.23	16.28	0.73	16.24	1.11
2.21	14.90	0.26	17.42	0.80	17.38	1.20
2.42	15.87	0.30	18.61	0.87	18.57	1.32
2.66	16.89	0.35	19.84	0.95	19.82	1.47
2.92	17.95	0.40	21.15	1.04	21.15	1.66
3.21	19.08	0.45	22.54	1.12	22.58	1.90
3.52	20.29	0.51	24.04	1.21	24.12	2.19
3.86	21.58	0.56	25.65	1.30	25.78	2.54
4.24	22.96	0.62	27.38	1.39	27.56	2.94
4.66	24.44	0.67	29.25	1.48	29.47	3.38
5.11	26.01	0.72	31.25	1.56	31.49	3.88
5.61	27.67	0.77	33.37	1.64	33.62	4.42
6.16	29.42	0.81	35.62	1.70	35.84	4.99
6.76	31.24	0.84	37.98	1.76	38.14	5.60
7.42	33.13	0.87	40.46	1.80	40.50	6.22
8.15	35.09	0.90	43.04	1.82	42.91	6.86
8.94	37.11	0.91	45.71	1.84	45.34	7.50
9.82	39.19	0.92	48.47	1.83	47.79	8.12
10.78	41.34	0.92	51.30	1.81	50.23	8.73
11.83	43.54	0.90	54.20	1.77	52.66	9.29
12.99	45.82	0.88	57.16	1.72	55.08	9.80
14.26	48.20	0.85	60.19	1.67	57.51	10.27

15.65	50.69	0.81	63.29	1.61	59.96	10.69
17.18	53.30	0.76	66.45	1.54	62.45	11.05
18.86	56.04	0.71	69.65	1.48	64.95	11.32
20.71	58.90	0.67	72.88	1.43	67.44	11.48
22.73	61.88	0.65	76.09	1.38	69.90	11.52
24.95	64.98	0.66	79.25	1.33	72.37	11.48
27.39	68.23	0.69	82.33	1.28	74.88	11.42
30.07	71.61	0.73	85.30	1.23	77.49	11.39
33.01	75.08	0.75	88.09	1.19	80.23	11.41
36.24	78.58	0.75	90.66	1.15	83.05	11.40
39.78	82.02	0.72	92.94	1.14	85.85	11.26
43.67	85.28	0.65	94.89	1.15	88.47	10.91
47.94	88.26	0.57	96.47	1.18	90.74	10.33
52.63	90.88	0.47	97.68	1.19	92.59	9.62
57.77	93.10	0.37	98.53	1.15	94.02	8.88
63.42	94.92	0.30	99.07	1.05	95.04	8.10
69.62	96.37	0.30	99.38	0.91	95.73	7.31
76.43	97.49	0.36	99.55	0.75	96.20	6.57
83.90	98.33	0.41	99.65	0.61	96.57	5.94
92.10	98.96	0.42	99.72	0.48	96.89	5.38
101.10	99.41	0.36	99.79	0.36	97.21	4.83
110.99	99.70	0.25	99.86	0.24	97.57	4.21
121.84	99.88	0.14	99.92	0.14	97.98	3.50
133.75	99.96	0.06	99.96	0.06	98.44	2.70
146.82	99.99	0.01	99.99	0.02	98.91	1.89
161.18	100.00	0.00	100.00	0.00	99.33	1.17
176.93					99.65	0.60
194.23					99.86	0.24
213.22					99.96	0.07
234.07					99.99	0.01
256.95					100.00	0.00

Grain Size (μm)	TBF Sample 1		TBF Sample 2		TBF Sample 3	
	Cum Dist	Std Dev	Cum Dist	Std Dev	Cum Dist	Std Dev
0.41	0.35	0.07	0.37	0.01	0.34	0.00
0.45	0.69	0.14	0.71	0.03	0.66	0.01
0.50	1.16	0.23	1.21	0.05	1.12	0.01
0.54	1.76	0.34	1.82	0.07	1.69	0.02
0.60	2.45	0.45	2.54	0.10	2.36	0.03
0.66	3.23	0.57	3.36	0.13	3.11	0.03
0.72	4.09	0.69	4.27	0.16	3.95	0.04
0.79	5.02	0.79	5.26	0.20	4.84	0.05
0.87	6.01	0.88	6.30	0.24	5.79	0.06
0.95	7.02	0.95	7.39	0.28	6.76	0.08
1.05	8.07	0.99	8.51	0.32	7.76	0.09
1.15	9.13	1.01	9.65	0.36	8.77	0.10
1.26	10.21	0.99	10.82	0.40	9.78	0.12
1.38	11.29	0.95	11.99	0.45	10.79	0.14
1.52	12.37	0.89	13.16	0.49	11.78	0.16
1.67	13.47	0.81	14.35	0.54	12.78	0.18
1.83	14.58	0.72	15.55	0.58	13.78	0.20
2.01	15.72	0.63	16.78	0.63	14.79	0.22
2.21	16.88	0.54	18.03	0.68	15.82	0.25
2.42	18.10	0.46	19.33	0.73	16.87	0.28
2.66	19.37	0.41	20.68	0.78	17.98	0.31
2.92	20.71	0.39	22.10	0.83	19.14	0.35
3.21	22.12	0.39	23.60	0.89	20.37	0.39
3.52	23.63	0.42	25.19	0.95	21.69	0.43
3.86	25.24	0.47	26.88	1.02	23.10	0.47
4.24	26.95	0.53	28.68	1.09	24.62	0.51
4.66	28.75	0.61	30.59	1.17	26.24	0.56
5.11	30.66	0.68	32.61	1.25	27.98	0.60
5.61	32.65	0.76	34.74	1.34	29.82	0.65
6.16	34.73	0.82	36.97	1.44	31.76	0.69
6.76	36.89	0.86	39.30	1.54	33.80	0.74
7.42	39.10	0.87	41.72	1.64	35.94	0.79
8.15	41.38	0.85	44.24	1.75	38.17	0.83
8.94	43.71	0.81	46.86	1.86	40.49	0.88
9.82	46.09	0.75	49.57	1.97	42.89	0.94
10.78	48.52	0.68	52.38	2.08	45.38	0.99
11.83	50.99	0.60	55.30	2.19	47.96	1.04
12.99	53.52	0.54	58.34	2.30	50.63	1.10
14.26	56.11	0.51	61.51	2.40	53.40	1.15

15.65	58.77	0.50	64.80	2.49	56.27	1.19
17.18	61.49	0.54	68.19	2.57	59.24	1.22
18.86	64.26	0.59	71.65	2.63	62.29	1.25
20.71	67.04	0.64	75.10	2.67	65.38	1.28
22.73	69.79	0.65	78.47	2.66	68.50	1.29
24.95	72.52	0.62	81.69	2.59	71.63	1.29
27.39	75.21	0.57	84.70	2.46	74.73	1.27
30.07	77.87	0.55	87.47	2.28	77.76	1.22
33.01	80.50	0.57	89.95	2.09	80.69	1.14
36.24	83.08	0.66	92.11	1.91	83.45	1.04
39.78	85.56	0.77	93.92	1.79	85.99	0.92
43.67	87.89	0.87	95.38	1.72	88.25	0.81
47.94	90.00	0.92	96.52	1.70	90.23	0.70
52.63	91.87	0.90	97.37	1.67	91.93	0.59
57.77	93.47	0.82	98.01	1.60	93.38	0.50
63.42	94.81	0.70	98.48	1.48	94.61	0.42
69.62	95.90	0.58	98.85	1.31	95.66	0.36
76.43	96.79	0.49	99.13	1.12	96.53	0.34
83.90	97.52	0.45	99.35	0.95	97.22	0.34
92.10	98.13	0.44	99.50	0.80	97.78	0.33
101.10	98.65	0.43	99.61	0.66	98.23	0.31
110.99	99.10	0.40	99.70	0.51	98.63	0.27
121.84	99.46	0.31	99.79	0.37	99.01	0.23
133.75	99.73	0.19	99.87	0.22	99.37	0.17
146.82	99.90	0.08	99.94	0.11	99.67	0.11
161.18	99.97	0.02	99.98	0.04	99.87	0.05
176.93	100.00	0.00	100.00	0.01	99.97	0.02
194.23					100.00	0.00